Dynamics of Riverbeds and Sandbody Formation

Guido Barzini

Clare College
Cambridge

A dissertation submitted for the degree of Doctor of Philosophy at the University of Cambridge.

August 1994

Dynamics of Riverbeds and Sandbody Formation

G.N.Barzini

This dissertation starts with an introduction to the subject matter and an overview of some of the existing work in this field, followed by an explanation of the motives for developing a highly simplistic model of a river system, and a more detailed summary of the work done on it. The second chapter contains a description of the model developed, along with an explanation the choices made, and an overview of both the ways in which the result might be expected to resemble a real system, and how it might differ. This is followed by a description of the behaviour of this model in the region of linear behaviour, where it can be studied analytically, and then of the development of a simulation designed to extend the research into the non-linear regime. The fifth and sixth chapters go over the results obtained from this simulation, making comparisons where possible with physical systems. The fifth chapter covers naturally occurring examples: beaches and braided rivers, while the second is devoted entirely to a more detailed comparison with one specific experiment whose conditions are in some ways close to the simulation's. This reveals a number of resemblances.

The chapter after this covers an alteration of the model that attempts to remedy the limitations imposed by the initial use of periodic boundary conditions, by allowing sediment to be created or destroyed in a controlled manner. It also describes the new aspects of linear behaviour resulting from this change, particularly the sharp transition that exists between erosional and depositional behaviour. Chapter eight extends this discussion to the non-linear behaviour, and the extent to which the two are similar.

The last chapter summarises the ground covered, and outlines a number of possibilities for future use and improvement of the model.

Preface

This Dissertation is the result of work carried out in the Theory of Condensed Matter Group at the Cavendish Laboratory, Cambridge, between October 1990 and August 1994.

I would like to thank the following for their contributions towards the completion of this work. Firstly, my supervisor, Dr. Robin Ball, for his guidance and advice, encouragement, and apparently limitless patience. Secondly my BP contacts, Drs Martin Blunt and Peter King, for their support and useful discussion and advice. Also Hans-Henrick Stoehlum who for providing references to some useful data, and Prof. Elpidio Caroni for providing details of his experimental work for comparison. Also to the occupants of my house, and all my friends for their support during this time, as well as contributing image-processing expertise in the case of Ian Robinson and Jon Williams.

The financial support of a C.A.S.E award from the S.E.R.C., in conjunction with BP, is gratefully acknowledged.

This dissertation, except where otherwise stated, is the result of my own work, and includes nothing which is the outcome of collaboration. No part of this dissertation has been previously submitted for a degree, diploma, or other qualification at this or any other University.

Guido Barzini

Guido Barzini

August 1994

Contents

Chapter 1: Introductory material

1.1 Overview

Historically, interest in river behaviour is long-standing, and much effort has gone into understanding, and where possible predicting it. One of the earliest such attempts to be properly recorded is the effort that went into the prediction of the annual floods of the Nile [1], providing amongst other things a strong incentive for the development of solar calendars. Today research continues into many aspects of rivers, including their sedimentology. This is unsurprising given the extensive impact of rivers on economic development at all levels of technology from basic agriculture to the oil industry. However, attempts to achieve quantitative accuracy have always been hampered by the complexity of the systems involved, and the number of dependent and independent variables to be considered (not to mention the difficulty of distinguishing between them [2]): except in a small number of cases, the only way to proceed is numerically. Hence, detailed studies really came into their own with the advent of the digital computer.

Since numerical simulation became feasible, work on rivers has tended to fall into four main categories:

(a) Models that incorporate a set of empirically determined equations to describe aspects of the flood-plain evolution (e.g. [3]): these aim primarily at producing realistic flood-plain strata and less at determining variable interdependence. They have the advantage of drawing on extensive observations, and can be tuned to reproduce many features of real systems but there is a price to be paid in that inferences as to causal connections between changes of input and output may not have any correspondence with reality. Indeed, the choice of control variables may differ deliberately from those that would be expected on physical ground, if this offers the possibility of a more readily tuneable model (reference [3] contains a good example of this).

(b) Detailed physical models that attempt to solve the fluid flow and sediment transport realistically [4]. These produce highly realistic results, but are limited to fairly small grids by the high computational cost. As with the first category, they tend to require detailed initial conditions and to exhibit a degree

of complexity that can make understanding of individual aspects difficult. The first of these objections is clearly becoming less important given that the price of computer power (measured in dollars/Mflops or any comparable ratio) has been dropping steadily for the last forty-five years and shows no sign of stopping. This approach is probably the way forward for much geological work: if the object is to predict the possible evolution of an existing system, or to determine which out of a number of past situations is most likely to have given rise to it, these models are highly successful. However they are not always the best for understanding some of the simpler underlying mechanisms, since attempting to understand the interdependence of various effects requires large amounts of data to be generated and then analysed for possible correlation.

(c) Simplistic physical models. These make important assumptions about the basic underlying processes such as water flow and erosion in order to gain simplicity at the expense of realism. While they were popular at a time when computer power was more limited, they were to some extent eclipsed as more detailed simulation became possible. There has however been a recent revival of interest in such models [5-9] due to the comparative ease with which many features of their behaviour can be understood, and also to suggestions that some aspects of system behaviour may be comparatively independent of the details of the model. For example in [6 the authors found that the system as modelled exhibited self-organised criticality, a form of behaviour generally robust with respect to small changes of the model [10]. Other workers have also found that fine-tuning many details of their models has little or no effect on the statistical nature of the output [8]. Clearly, behaviour of this type has implications as to which aspects of river behaviour can be usefully modelled, and also has the attraction of suggesting that one can do away with large numbers of free parameters. In summary, while they do not currently produce entirely realistic river simulations such models combine insight into some aspects of hydrology with comparatively easily understood physics in an appealing way : an analogy can be drawn with the way the basic Ising model is not a complete description of magnetism, but reproduces many of its important phenomena (particularly in the area of phase transitions, in issue that arises in chapters 7 and 8 of this work), and continues to attract interest because it is amenable to being understood analytically.

In addition to these, mention should be made of the use of scale modelling to study rivers on scales ranging from single channels to entire drainage networks. This approach ties in with (a) above in that while not greatly reducing the complexity of the problem (although a number of factors such as

vegetation are removed) it allows the effects of carefully controlled changes of known conditions to be assessed on time-scales usefully shorter than geological. Much work in this area has originated from a large and quite complex flume bed built at Leeds University in collaboration with BP [11] , but a large number of other experiments, often smaller and simpler also exist [12,13]. One of these is considered at some length in chapter 6 [13], being in some ways directly comparable to the simulation work that makes up much of this thesis.

1.2 Motivation

The model developed in this work falls into category (c); its purpose was to develop a simple description of water-flow and sediment transport, incorporating only as much detail as was needed to satisfy some basic physical constraints, and to use this to see how water flow over an initially flat plane of erodible sediment might lead to a non-uniform time evolution and to see what features might result from such a model. This had the advantage of side-stepping the choice of realistic initial conditions that would otherwise be needed to set up a river channel in order to follow its evolution: ideally the model would be then proceed to evolve its own river channel towards a form whose statistical properties would be independent of the initial conditions (although the detailed topography, of course, would not).

The long term goal was to gain some understanding of flood-plain sedimentology: the general pattern is that most of the coarser sediments carried by a river remain in the river channel, which ultimately results in a sandbody, while part of the silt carried ends up distributed over the surrounding plain during floods, producing much finer shales. This is of economic importance [14,15] since the sandstone is frequently (i.e. unless it included too high a concentration of mud) oil-permeable, while the shale is not. As a result much work has gone into understanding the occurrence and distribution of sandbodies, both statistically [16,17] and through modelling their formation and the river channels that give rise to them. Clearly in this context a model of how rivers develop channels, and become distinct features of a landscape would be of interest.

Since model was intended to be applicable specifically to flood-plains it could incorporate a number of helpful assumptions even before its form was finalised. These included that of the river-bed having a shallow slope, and a central assumption that the evolution of the landscape itself is by far the slowest process involved, and thus that the water-flow can be calculated, as a reasonable approximation, as though the landscape were static. There are clearly examples

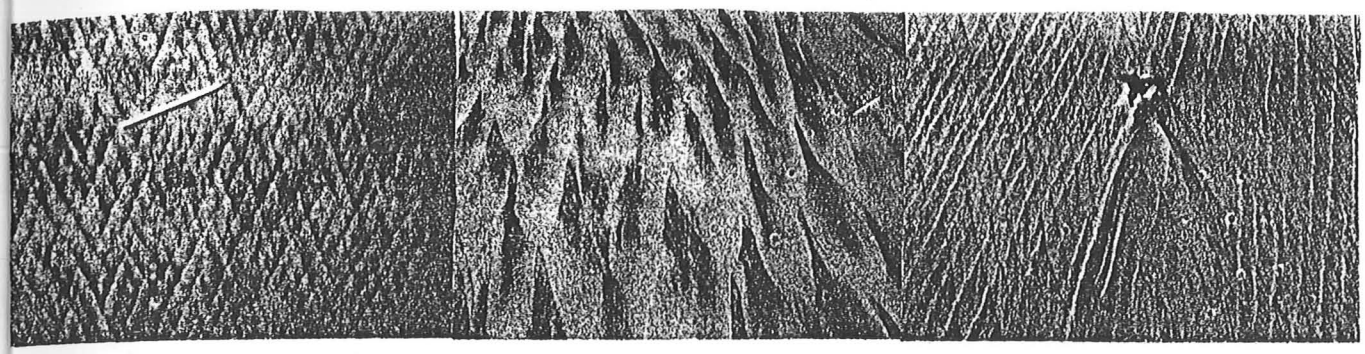

Fig.1.1: A variety of rhomboid rill patterns found on beaches
(reproduced from reference 20)

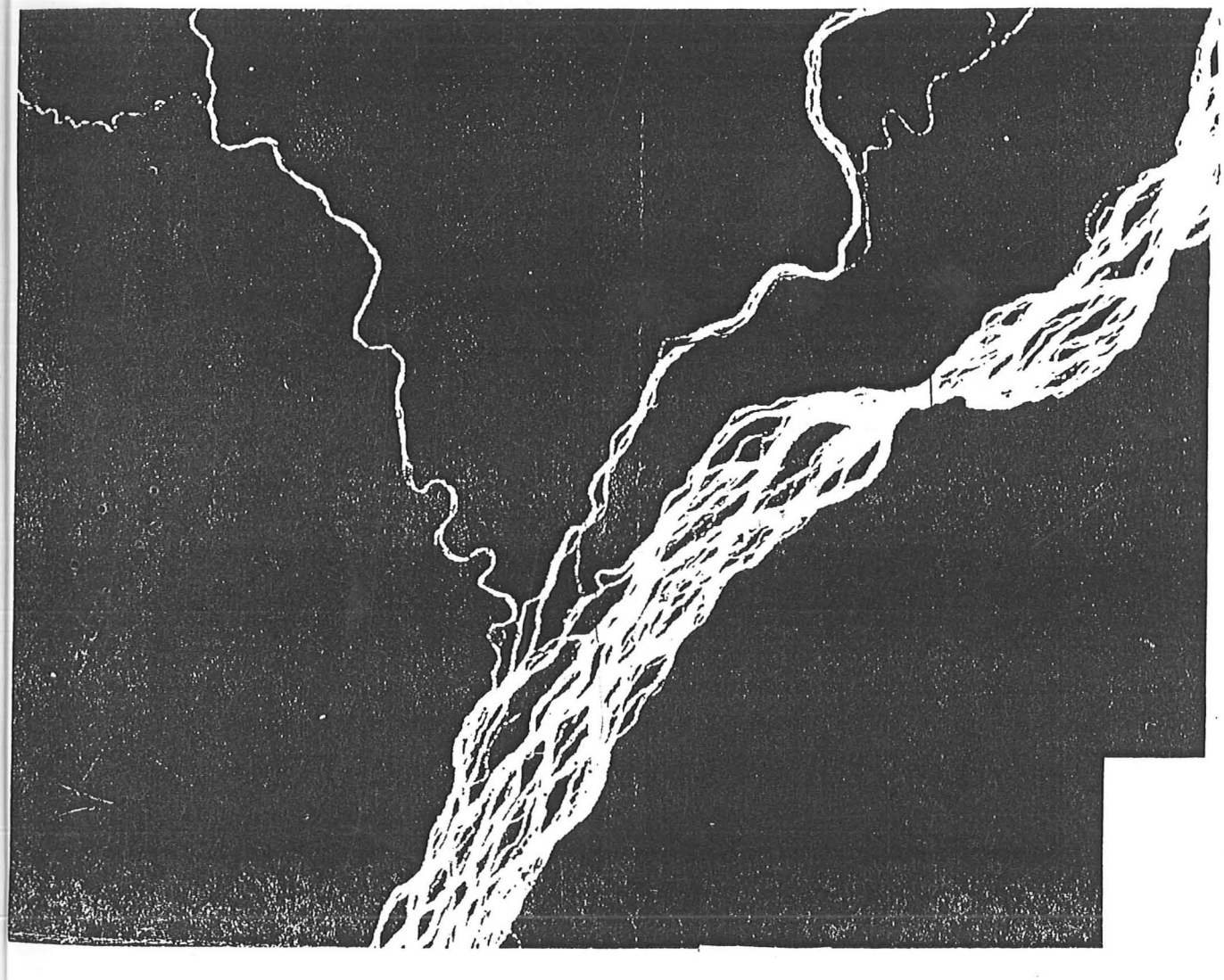

Fig. 1.2: Satellite photograph of the Zaire river (from reference 21). The distribution of islands exhibits self-similarity, and remains constant both along and across the river.

where this is inapplicable, the most obvious and spectacular being such events as flash-floods and mud-slides but for a flood-plain it is a reasonable approach. This has the attraction that the whole problem can be separated conceptually (and if this seems desirable in actual implementation) into two parts: that of calculating the water-flow over a static landscape, and that of then using this result tò calculate the sediment transport, and hence the landscape evolution. In practice this not necessarily the most efficient approach, but it provides a clear and simple basis on which to develop the model.

1.3 Summary of Contents

The contents fall quite naturally into three main parts, plus chapter 9 which contains a summing up of the ground covered and a discussion, detailed in places, of what else could be done with the model, and how it could be refined to capture other aspects of the systems it aims to simulate.

The first part, consisting of chapters 1 to 3, covers the work up to the point when use of computer simulation became necessary. Having established here the motivation behind this work, and hence the general lines along which it was intended to develop, chapter 2 goes on to introduce more details and to establish the equations that describe the model used, along with references to the relevant empirical models. The next chapter is a study of the time-dependent behaviour of the model in the regime where it is open to analytic solution: the limit of small perturbations to a stationary solution, where the equations can be treated as linear. This reveals that the model exhibits non-trivial behaviour in that the stationary solution studied (a planar surface of sediment) is actually unstable (in line with experimental evidence [18]) and develops structure. Details of the time-evolution are included although they cover only the linear regime. Consideration is also given to what simplifications can be made that do not destroy the essentials of this behaviour (with particular regard to possible gains in ease of simulation resulting from such changes).

The second part, chapters 4 to 6, covers the first phase of the numerical work, from simulation through to analysis of the results. Chapter 4 describes the work of writing a numerical simulation to allow study of the model to be extended into the non-linear regime, along with a discussion of the various design considerations and compromises involved, and the testing applied to ensure that its behaviour is a reflection of the original equations. This is followed by a description in chapter 5 of the results of these simulations. After a discussion of the time-dependent behaviour of a simulation run, the patterns of topography that result once the simulation has reached statistical steady-state illustrated.

Resemblances to a various real systems are noted, including the formation of rill-patterns on beaches (as illustrated in fig. 1.1 [20]) and, on a much larger scale, the channels of certain braided rivers such as fig. 1.2 [21]). In the latter case an attempt at quantitative comparison is made, which although not conclusive does show an encouraging degree of agreement between simulation and reality.

The following chapter focuses on one particular experiment, performed at the University of Trieste by Prof. Caroni, which involved a scale model in which water was made to flow over an initially flat plane of sediment of uniform composition. This is considered in some detail, as it bears a notable resemblance to the conditions being simulated, and offers the possibility of making direct comparisons. Attention is drawn to the significant differences that do exist between the two cases, and then the comparison of the real and simulated terrains is made. This includes consideration of the relation between flow-depth and topography, and comparison of terrain cross-sections.

The final part, consisting of chapters 7 and 8, follows a new line of approach designed to remove some of the limitations imposed by the original design of the simulation. Chapter 7 outlines the problems associated with the periodic boundary conditions chosen for the program, and considers two possible ways of solving them. It then follows through in detail one of these (the adjustment of the sediment transport equations produced in chapter 2 to produce net erosion or deposition) considering the way it affects the analysis performed in chapter 3 and what new features of behaviour emerge from this. The most important being a division of the results into two phases, characterised by different terrain features. The next chapter describes the carrying over of these alterations to the numerical simulation, along with a description of the results obtained and the various measurements and analyses performed on the terrain data in order to describe the transition and the two phases, along with a discussion of what they might correspond to in real systems, and the applicability of this aspect of the model.

References

[1] A.Pannekoek, *A History of Astronomy* , (Gore Allen & Unwin, 1961)

[2] S.A.Schumm, *The Fluvial System,* (Wiley-Interscience 1977)

[3] R.C.Crane, PhD thesis, Department of Geology, University of Reading (1982)

[4] D.M.Tetzlaff and J.W.Harbaugh, *Simulating Clastic Sedimentation* , (Van Nostrand Reinhold 1989)

[5] S.Cramer & M.Marder, Phys. Rev. Lett. **68**, 205 (1992)

[6] H.Takayasu and H.Inaoka, Phys. Rev. Lett. **68**, 966 (1992)

[7] R.Leheny and S.Nagel, Phys. Rev. Lett. **71**, 1470 (1993)

[8] A.B.Murray and C.Paula, *A Cellular Model of Braided Rivers*, to be published in Nature

[9] A. Rinaldo, I.Rodriguez-Iturbe, R.Rigon, E.Ijjasz-Vasquez and R.Bras, Phys. Rev. Lett. **70**, 822 (1993)

[10] P.Bak, C.Tang and K.Weisenfeld, Phys. Rev. Lett. **59**, 381 (1987)

[11] P.J.Ashworth and J.L.Best, B.P. Internal Reports (Jan. 1989, Dec. 1989, Feb. 1991 and Aug. 1991)

[12] S.A.Schumm and H.R.Khan, Geol. Soc. Amer. Bull. **83**, 1755 (1972)

[13] E.Caroni, Preprint, Hydrofractals '93 conference, Ischia

[14] R.Chapman, *Petroleum Technology*, (Elsevier, 1973)

[15] D.C.Swanson, J. Petrol. Tech. **45**, 368 (1993)

[16] P.R.King, *The Connectivity and Conductivity of Overlapping Sandbodies* In: *North Sea Oil and Gas Reservoirs II* (Graham & Trotman 1990)

[17] H.H.Haldorsen, P.J.Brand and C.J.MacDonald, *Review of the Stochastic Nature of Reservoirs* In: *Mathematics in Oil Production* (Oxford, 1988)

[18] K.Richards, *Rivers: Form and Process in Alluvial Channels*, (Methuen 1982)

[19] L.B.Hong, T.R.H.Davies, Geol. Soc. Amer. Bull. II **90**, 1839 (1979)

[20] P.D.Komar, *Beach Processes and Sedimentation*, (Prentice-Hall 1976)

[21] M.A.Summerfield, *Global Geomorphology*, (Longman Scientific, 1991)

Chapter 2: The Model

2.1: General

As outlined in the previous chapter, the model was intended to be as simple as was possibly compatible with obtaining realistic information about the behaviour of the systems it was intended to model. This required, first of all, putting together a set of simplified equations to describe the water flow: while in principle the Navier-Stokes equations are as good a description of the problem as could be needed for this purpose, their solution would hardly be practical on a problem this size. Solution of Navier-Stokes, usually by finite element methods, has been used in hydrology problems, but is usually reserved for modelling water flow over (geologically) small features such as weirs where fine detail is required.

Similarly modelling the sediment transport by the water flow involves deciding on a set of approximate equations. The difference in this case in is that there is no longer any one model encompassing all aspects of the problem to provide a comparison with the simplified version, due to the number of different mechanisms involved in real sediment movement and the difficulty of quantifying their respective importance (which will vary depending on the details of the river in question)[1-3].

2.2: Water Flow

The first decision made regarding the water flow is widespread in work of this sort: the flow velocity is averaged vertically so as to have a single value v(x,y) everywhere in the x-y plane [4,5]. This is of course most important if the model is being developed with an eye to numerical solution, as the move from three to two dimensions will cut the computational work involved drastically.

Within the set of two-dimensional water-flow equations the models that have been show widely different of degrees of sophistication : varying from those in which a unit of water is simply moved down the steepest neighbour-neighbour bond at each timestep[6] , to those which use a vertical integration of the Navier-Stokes equations to obtain a flow velocity in the plane[4] , each applicable to modelling a different aspect of river behaviour. Here again this model was designed as a compromise: it seemed clear that to produce any realistic structure within the river-channel, flow

velocity would have to reflect such factors as slope and water depth. At the same time, it seemed desirable to make the flow velocity a purely local function of slope and depth only, since this would ensure that the equations were purely differential in form, greatly simplifying their solution. This is basically equivalent to saying that the momentum of a unit of water would adjust in response to a change in slope over a distance negligible compared to the smallest length-scale of interest in the model, and hence that an integral to 'remember' the course the water had come down was unnecessary, or more specifically, that the limit $l \to 0$ in the equation $v(x) = \int a(x)e^{-x/l}dx$ could be taken, l being some (not necessarily constant) relaxation length (v represents the flow velocity, and a(x) a function of the terrain)..

This is known not to be true in general: a fast-moving stream, flowing over a smooth rock bed can in fact flow up a gentle gradient over a distance of some metres. However, it seemed applicable enough to the cases being considered here of rivers flowing over flood-plains whose slope only changes very gradually, typically over miles [2,3]. Geological factors that could cause the angle or direction of slope to change suddenly, such as faulting, are being consciously ignored here. They are known to produce quite dramatic changes in the behaviour of some real systems. This decision also has implications for other aspects of the work such as the details of numerical implementation: a set of equations that did conserve the momentum of the water from one time-step to the next would strongly suggest the use of , for example, a marker-in-box method rather than finite difference methods as greatly simplifying the task of keeping track of momenta (the two approaches are discussed in more detail in Chapter 4).

Given these decisions about what the equations should incorporate, a dimensional argument suggested that the velocity take the form

$$\mathbf{v} = -ad^{1/2}\,\mathbf{g}_{eff}/\,(g_{eff})^{1/2} \qquad (2.1)$$

with d(x,y) being the water depth and a some dimensionless constant which would incorporate such factors as viscosity, density and coefficient of roughness. Such coefficients have been calculated empirically as equations of this from were widely used in early work modelling flow down a straight channel [7,8], and the variation of velocity as the square root of slope has been incorporated into a number of models [9,10]. The effective gravitational acceleration acting on the water, $\mathbf{g}_{eff}$, simply represents the component of gravity acting along the slope.

There is an ambiguity here as to the definition of slope: either that of the terrain over which the water flows, or that of the water surface(in the

sorts of problems for which equations like this were originally used the problem does not arise since clearly if the slope is constant and the flow uniform the two definitions will be identical). The most obvious choice would tend to be that of the underlying land but here are problems to this: the most obvious is that water will tend to accumulate indefinitely in any depression in the ground, building up into a clearly unphysical 'hill'. One of the common ways of overcoming this is to have a momentum-like term allowing the water to travel some distance uphill, so that as the water in the hollow gets deeper water entering it moves faster and travels further up the far side, until at some point it is able to get over the exit lip, and so an equilibrium is reached. This, however, is already ruled out if the previous arguments about avoiding the details of conserving momentum are to kept to. The approach used here is different: the slope is taken to be that of the water surface itself. Thus the hollow simply fills until the water level has risen above the exit, and then spills over (fig.s 2.1a and 2.1b outline the two approaches) . These two methods are both based on real aspects of water flow, but would be expected to be applicable to different conditions. The latter approach would seem more realistic for, e.g. deep, wide lakes where the flow velocity alone would be insufficient to carry water out of the lake, but there are certainly cases where the former would be closer to the true picture (one could in fact distinguish the cases by the predicted of the water surface: the two methods clearly lead to different expectations).

Given that the model is intended for modelling rivers in their lower stages ,where slopes of less than 1 in 100 are common[2-3], the assumption seemed justified that the small angle approximations apply, and the component of g down the slope of the water surface therefore approximates to

$$\mathbf{g}_{\text{eff}} = g \nabla (h+d) \qquad (2.2)$$

where h(x,y) is the height profile of the underlying land.

Finally, there is conservation of water to be built in. If the water flux is defined as $\mathbf{q} = d\,\mathbf{v}$ then this is simply:

$$\partial d/\partial t = - \nabla.\mathbf{q} \, . \qquad (2.3)$$

This may of course be broken in places by the addition of terms on the RHS corresponding to sources or sinks of water (e.g. rainfall).

These equations complete a (simplistic) model of the water flow. They are in broad agreement with certain empirical models of dissipative water flow , and while they miss some aspects of real water flow they are complete in the sense of allowing solution forwards in time given a set of initial conditions and a description of the underlying landscape.

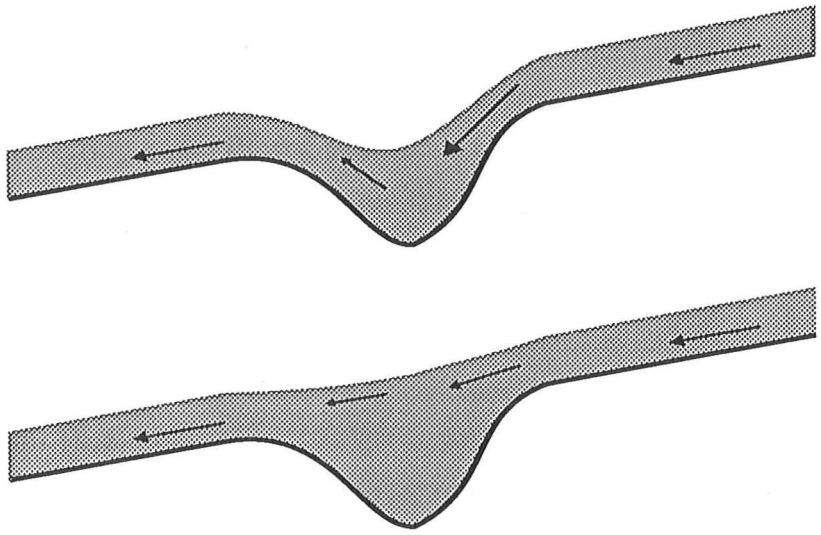

Fig.2.1 : Dealing with hollows
(a) The momentum gained by the water on the downslope carries it up the other side
(b) The water fills the hollow until the surface slope ,and hence the flow velocity, are downhill at all points.
(Arrows representing flow velocity are purely diagrammatic.)

2.3: Sediment Transport

Given this model of the fluid dynamics, further assumptions are now needed to produce a description of the processes of erosion, transport and deposition that will cause the landscape in question to evolve. The complication here is that in reality a wide range of transport mechanisms are known to apply to different sediment types [1-4]: material may move in solution, suspension, or simply rolled along the bottom as bedload in the case of coarser sediments, and the relation between the rate of transport by these mechanisms and such factors as flow rate and degree of turbulence does not appear fully understood. Furthermore, it will vary according to the form of transport being considered: while the first of these can actually be quite important in some cases (e.g. limestone landscapes) it is far more dependent on the composition of the bedrock and

the pH and ion contents of the water than on flow details. The other two are at least both driven by energy dissipation within the flow, and might be expected to show similar responses to variables such as depth and flow velocity (both can and have been studied in some detail at the level of the forces acting on an individual element of sediment in order to quantify their behaviour). A number of simplifications are therefore needed.

The first is that there is only one sediment type : clearly there are interesting generalisations if more sediment types are included, particularly if the load of one type of sediment is allowed to affect the quantity of another type that may be transported. Multiple sediment types give rise in real systems to a wide variety of mixing and segregation effect, e.g. in channel bars[10] , and an extension to at least two types would be needed to address sedimentological issues, but for development of the model removing these issues is a great simplification, particularly that of how transport of one sediment type would interact with that of another (some discussion of this is attempted in Chap.9) .

If the load (volume fraction) of sediment borne by the water is denoted L(x,y), then the flux of sediment is assumed to be

$$q_S = L\,q \ . \qquad (2.4)$$

(this is true simply by definition of L: if it is the volume of sediment suspended in dV of water then the flux of sediment past any point must be given by the above equation). Along with this is the assumption that there is a maximum amount of sediment that the water can support at any given point, and that it is possible to define this as the capacity C, which can be described as a homogenous function of the depth and flow velocity:

$$C=Kd^{\alpha}v^{2\beta} \qquad (2.5)$$

for some constants K, α, and β. Noting that C can readily be re-written as a function of any two not linearly related flow variables, this is again consistent with many of the empirical formulae describing sediment transport[4,11,12] . This is in line with the physical expectation that the river's capacity to move sediment about is directly related to its rate of energy dissipation, but there are problems as to what assumptions should be made about the flow type and causes of power dissipation (namely the relative importances bed friction and internal turbulence) in an attempt to calculate the values of α and β from scratch using the flow equations. Furthermore the actual balance is likely to depend on local details and indeed the values in the literature vary by more than can easily be accounted for by measurement errors. This is to be expected since any such equation is an attempt to roll into one the various transport mechanisms

outlined previously, and this could not realistically be done in a way consistent across widely different river systems.

The last assumption built into the model is that where there is a discrepancy between the load L and capacity C, sediment is eroded or deposited from the river bottom at a rate linear in the difference, with some time constant τ, leading to a rate of change in the landscape height , h, given by :

$$\partial h/\partial t = d\,(L-C)/\tau \qquad (2.6)$$

This is probably the most troublesome aspect (but one way of resolving it is discussed below): it is not obvious that the rate need be linear (but one could hope that it would be for small discrepancies, i.e. that the linear term in the expansion of the real rate of change would be non-vanishing), and it is equally unclear that in general τ is a constant (it could include, for example, geometrical factors such as the depth of water, or have its own dependence on the flow velocity, possibilities which are not considered further here) , or that it would be the same in erosion and deposition. Finally, there is plenty of empirical evidence that most, though not all, sediments have some degree of cohesion with the result that below a certain threshold value of shear-force (and hence flow-rate) no erosion at all can occur[4,11]. Making τ a constant and using the same value in both erosion and deposition therefore has no clear physical basis, but was adopted because of the attraction of making the rate of erosion/deposition an analytic function of the load/capacity imbalance. For these reasons , the use of τ is the least satisfactory aspect of the model, and there is a strong incentive to consider behaviour in the limit of $\tau \to 0$. This limit is physically plausible since it only where C is changing rapidly (spatially) that a non-zero value of τ would be expected to have a serious impact and the assumption that the effect sudden changes in terrain profile need not be captured realistically is already built into the water-flow equations. In Chapter 3 the implications of taking this limit are considered in more detail, and it is seen that most of the interesting behaviour of the model does survive.

The model is completed, in principle, by adding conservation of sediment

$$-\partial h/\partial t = \nabla.(\mathbf{q}L) + d\partial L/\partial t \qquad (2.7)$$

, but in fact one further simplifying assumption is made that the relaxation time of the water depth is negligible on the timescale over which the underlying terrain changes (again it is possible to come up with counter-examples: a mud-slide, or as a less extreme example a river breaking its banks are clear cases in which the terrain over which the

water flows is being remodelled by the water-flow fast enough that no steady-state approximation is likely to hold). Then for a given state of the landscape the water will effectively be in steady-state and equation (2.3) can be replaced by $\nabla.\mathbf{q} = 0$. This simplifies the model both conceptually and (very much) computationally since it means rather than dealing with the two coupled systems, the steady-state solution of the water-flow can (in principle) be written down as a function of the landscape and its spatial (but not temporal) derivatives, and then substituted into the landscape evolution, reducing the problem from 2nd to 1st order in time.

References

[1] J.R.L.Allen, *Sedimentary Structures*, (Elsevier Scientific 1982)

[2] K.Richards, *Rivers: Form and Process in Alluvial Channels*, (Methuen 1982)

[3] S.A.Schumm, *The Fluvial System*, (Wiley-Interscience 1977)

[4] D.M.Tetzlaff and J.W.Harbaugh, *Simulating Clastic Sedimentation*, (Van Nostrand Reinhold 1989)

[5] S.Cramer and M.Marder, Phys. Rev. Lett. **68**, 205 (1992)

[6] H.Takayasu and H.Inaoka, Phys. Rev. Lett **68**, 966 (1992)

[7] Equation 2.1 is essentially Chezy's equation in vector form.

[8] R.Manning, Trans. Inst. Civil. Eng. Ireland **20**, 161 (1891)

[9] A.B.Murray and C.Paula, *A cellular Model of Braided Rivers*, to be published, Nature

[10] R.C.Crane, PhD Thesis, Department of Geology, University of Reading (1982)

[11] M.P. DuBoys, Annales des Ponts et Chausses **18**, 141 (1879)

[12] E.Meyers-Peter and R.Muller, *Formulas for Bedload Transport*, In: *Proceedings of the Third Meeting of Intern. Assoc. Hydr. Res.* , 39 (1948)

Chapter 3 : Linear Analysis

3.1 Outline

Having come up with the basic model, it was clearly important to see whether it had any potentially interesting behaviour before investing time in a simulation. For example, it seems from physical intuition that a flat surface of sediment, with an initially uniform flow of water over it should spontaneously start to generate structure seeded by noise present in the initial conditions, an effect which can actually be observed in real systems [1-3], as well as being commonly predicted in models of this sort [4,5]. The presence or absence of such behaviour is easy to verify using linear stability analysis to investigate the response of a stationary solution to perturbations so small that only the linear terms of the equations need be considered.

3.2 Analysis

By inspection, one such stationary solution of the model equations is a flat surface of sediment with constant slope, represented by $h_0=\theta.\mathbf{r}$ (or simply $h_0=\theta x$), initially set up with uniform depth d_0 and sediment load at saturation everywhere : $L=C_0$. Since the flow equations are local, the water flux will be uniform. In such a set-up the flux of sediment will have no divergence and hence there will be no net erosion or deposition , provided that there are no sources or sinks at the edge of the surface (a condition that can be met in a simulation by using periodic boundary conditions, and for the purpose of this analysis simply by not having any edges).

The perturbation to be considered is sinusoidal: this simplifies the analysis by making all the non-constant terms exponential, and since we are only considering the linear case, any other form could be obtained from these results by Fourier analysis. A small perturbation of the initially flat bottom profile is introduced such that the land surface h can be written as the sum of the stationary solution h_0 and the perturbation, Δh :

$$h = h_0+\Delta h = h_0 + h_1 e^{i\mathbf{k}.\mathbf{r}} \qquad (3.1)$$

This will result in changes of depth and capacity which can be written as

$$\Delta d = A\,\Delta h, \text{ and } \Delta C = B\,\Delta h.$$

where A and B are (complex) amplitudes which can be found by expanding $\mathbf{q}$ to 1st order in h_1 using the equations 2.1 and 2.2 and then imposing $\nabla.\mathbf{q}=0$ to find the equilibrium response. This gives

$$A = - (1/2k_x^2 + k_y^2) /(1/2k_x^2 + k_y^2 - 3/2\theta ik_x/d_0) \quad (3.2)$$

There is also useful information to be gained by considering a simple case of the time-dependent form (i.e. not setting $\partial(\Delta d)/\partial t=0$) : this shows that (3.2) is stable, with small deviations from this response, d_1, decaying exponentially as :

$$\frac{\partial d_1}{\partial t} = [-d_0^{3/2}\theta^{1/2}(1/2k_x^2 + k_y^2) + i3/2d_0^{1/2}\theta^{-1/2}k_x]d_1$$

Now expanding C using this result for Δd gives

$$B = -K(g\theta)^{\beta}d_0^{\alpha+\beta-1}\{ \beta(ik_x(1+A)d_0/\theta + A) + \alpha A\} \quad (3.3)$$

$$=K(g\theta)^{\beta}d_0^{\alpha+\beta-1}\{ (\alpha+\beta)k_y^2 + (\alpha/2-\beta)k_x^2\}/(1/2k_x^2+k_y^2 - 3/2\theta ik_x/d_0)$$

Since the equations are to first order linear with constant coefficients, h_1 will have a time dependence which can be represented as e^{pt}. Equating (2.6) with (2.7) and rearranging gives

$$\Delta L = \Delta C/(d_0+\tau(i\mathbf{k}.\mathbf{q}+pd_0). \quad (3.4)$$

Substituting this back into (2.6) gives a quadratic in p with solutions

$$p_{\pm} = [-(d_0+Bd_0^2+i\tau\mathbf{k}.\mathbf{q}) \pm \sqrt{(d_0+Bd_0^2+i\tau\mathbf{k}.\mathbf{q})^2 -4i\tau\mathbf{k}.\mathbf{q}Bd_0^2}] / 2d_0\tau$$

Of these roots, p- has a real negative part for all **k** using any plausible ranges of α, β to be found in the literature (2-3 and 1.5-2 respectively)[6], corresponding to perturbations dying away exponentially with time, and so can be expected to have no significant effect on the behaviour of the system. P_+, on the other hand, has regions of **k** in which it has a positive real part, indicating an instability of the initial state (fig.3.1).

In more detail, fig.3.2 shows a contour plot of $Re(p_+)$ as a function of **k** in the plane for the values of α, β finally used. This shows that if **k** is written as $k(\cos\phi,\sin\phi)$ then $Re(p_+)>0$, giving exponential growth, for ϕ greater than a critical angle ϕ_c, and also that $Re(p_+)$ has a maximum as a function of ϕ and tends to 0 as ϕ reaches $\pi/2$. This physically corresponds to the fact that this model conserves sediment and that if there is no sink at the lower boundary, the only way for a channel to deepen is by there being a cross-channel component of water flow that transports sediment from troughs to crests. This clearly requires that **k** have a component parallel to **q**, and hence, since **q** remains down-slope to 0th order, channels running directly down-slope do not grow. (Growth could also be possible in principle by the increased flow down a channel, and hence increased capacity, outweighing the amount of sediment erosion needed to deepen the channel, but that does not apply here.)

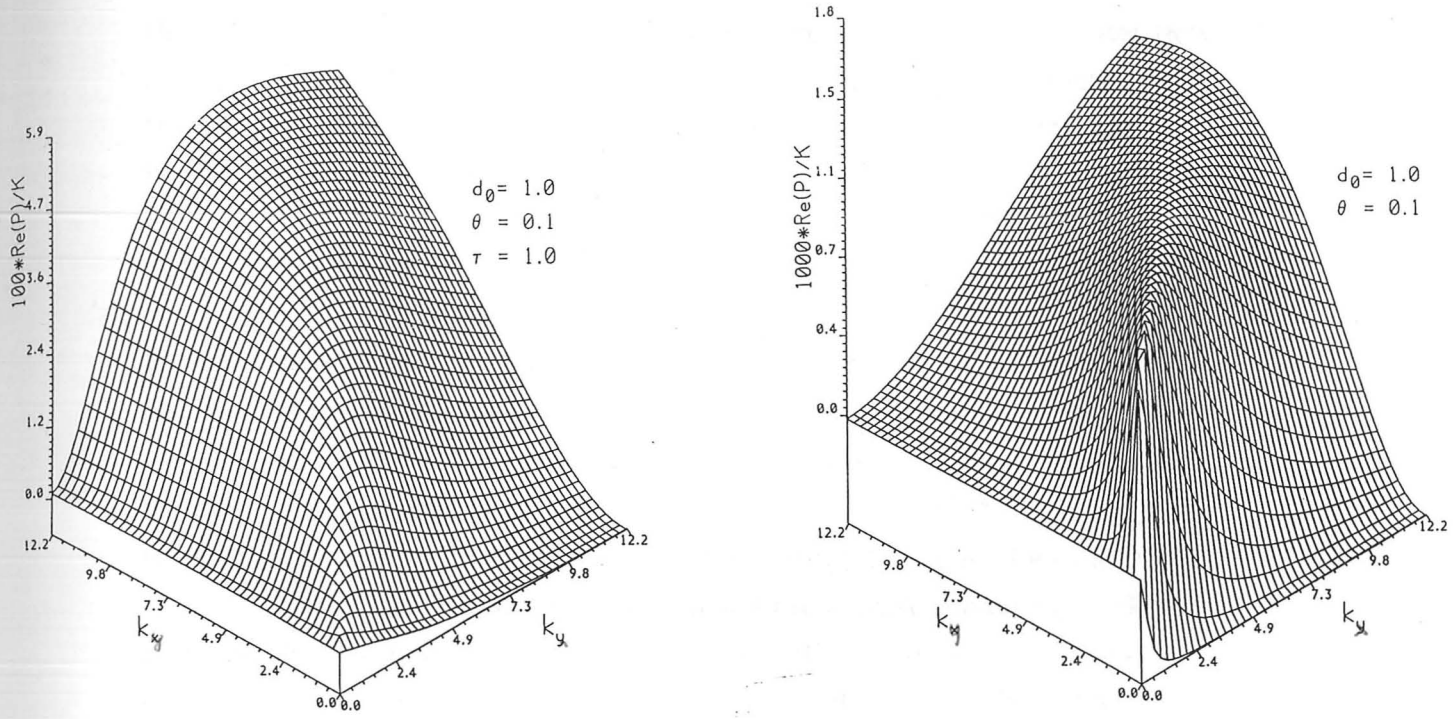

(a) (b)

Fig. 3.1: Relief plot of the real part of p_+ as a function of **k** with (a) showing the original form from eqn. 3.4, and (b) the simplified form in 3.5.

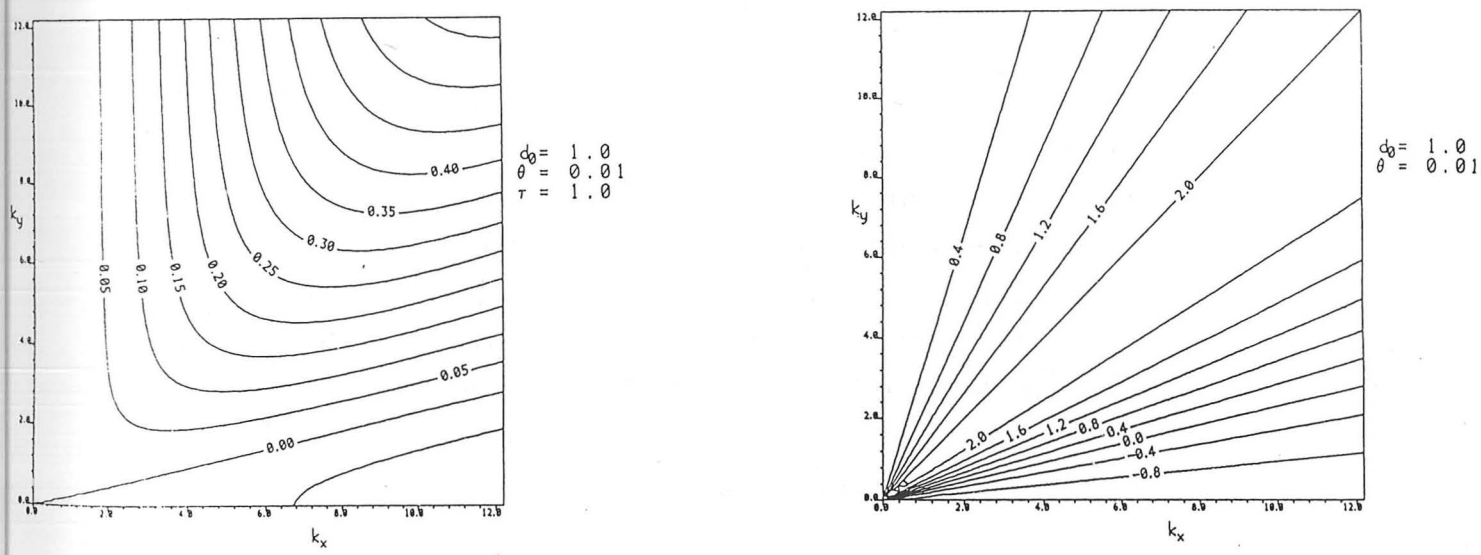

Fig. 3.2: The same data displayed as a contour plot to highlight the fact that the ridge curves towards the k_y axis in (a) but not in (b).

However, the closer to downstream a channel runs, the faster the water flow along it will be. The balance between increasing flow speed and increasing the angle between channels and flow to give the maximal cross-stream value is what dictates the value of ϕ_m.

3.3 Limiting Cases

It can be seen in fig.3.2 that the angle of fastest growth, ϕ_m , is nearly constant at low k, but tends to $\pi/2$ as k increases and examination of the equation show that this happens for $|\tau \mathbf{k}.\mathbf{q}| >> d_0$, where τ is an equilibration time for sediment load w.r.t. carrying capacity (eqn. 2.6). This results from the fact that for significant deepening of a channel to occur, the time taken for sediment to be transported from a trough to a crest, given by $1/(\mathbf{k}.\mathbf{v})$ must exceed τ otherwise sediment picked up will tend to become spread uniformly over crests and troughs. Hence the angle between $\mathbf{k}$ and $\mathbf{v}$ increases with k, as the shallower angle between channels and flow increases the time for flow from trough to crest. However in a real system there must also be some competing cut-off at high k due to effects such as turbulent mixing, so that we would not expect this to hold above some limit. Furthermore, the form of τ is also uncertain, making attempts to judge where the effect would become important pretty well impossible..

We are thus motivated to focus on the case where $\tau < 1/ kv < 1/p$ holds, meaning physically that the time for sediment to be scoured/deposited is smaller than that for either the landscape or the water-flow to alter significantly or for waterflow to carry sediment across one wave-length. This has the advantages that the problem of an unknown and probably variable τ does not affect this regime, and the system no longer contains any time-scale beyond that defined by the initial conditions (q/d_0^2). The rate of evolution simply scales with the size and slope of the system and the instability reduces to $p_+ = (-i\mathbf{k}.\mathbf{q}B)/ (d_0 + d_0^2 B)$.

One further approximation can be made that $|\bar{B}d_0| \ll 1$ in cases to which this model is applicable, equivalent to saying that $d\partial L/\partial t \ll \mathbf{q}.\nabla L$, i.e. that the sediment load is in steady-state. This can be justified by the following argument: if the water is taken to be in equilibrium the rate of change of L is dependent on the rate of change of the underlying landscape (which is small) while the divergence of the flux depends only on the shape of the landscape. In this limit, p_+ becomes simply $-i\mathbf{k}.\mathbf{q}B/d_0$, with real part

$$3/2Kd_0^{\alpha+\beta 1/2}\theta^{\beta+3/2}g^{\beta+1/2}\frac{k^2\cos^2\phi((\alpha+\beta)\sin^2\phi+(\alpha/2\beta)\cos^2\phi)}{[k^2(1/2\cos^2\phi+\sin^2\phi)^2+9/4\theta^2\cos^2\phi/d_0^2]} \qquad (3.5)$$

which clearly has a maximum at a definite value of ϕ (fig.3.1b) which is a function of α, β and k resulting in well-defined channels at a definite angle to the downstream direction, the angle for the onset of instability being given by

$$\phi_c=\text{Tan}^{-1}\,[(\beta-\alpha/2)/(\beta+\alpha)]^{1/2}. \qquad (3.6)$$

Also the angle of maximum growth no longer goes to $\pi/2$ as k increases, as expected since the explanation of this effect was dependent on a non-zero value of τ.

There is also the k-dependence to consider. Here the main criterion is the value of k compared to θ/d. When significantly larger, the value of $Re(p_+)$ reaches an asymptotic limit (approached significantly faster than in the case of $\tau=1$), while for smaller values, it is quadratic in k resulting in behaviour that is diffusion-like or anti-diffusion-like depending on ϕ. While high wavenumber perturbations grow fastest, it seems possible that the length-scale d/θ plays a significant part in the behaviour of the system, determining a length for large-scale structure.

3.4 Overview.

The linear analysis clearly leaves important questions about the behaviour of the model, such as long term behaviour, unanswered. However it does reveal some potentially interesting features. In summary, these are:

(i) That while the obvious planar solutions are indeed stationary, they are unstable and can be expected to develop structure spontaneously given any non-zero level of noise.

(ii) That this structure would be expected to take the form of sinusoidal ripples running at a definite direction to the downstream direction : the assumption from this analysis is that whatever the form of the noise added, the result would be dominated by the Fourier components with the highest rate of growth. In a simulation of course an upper limit to this behaviour is provided by the limits of the spatial resolution. The fact that the most unstable ripples do not run directly downstream, but at a preferred angle, is a non-trivial point, and suggests possible comparisons to certain real systems such as rills on beaches [7] (this is discussed further in chapter 5).

(iii) That at least qualitatively this behaviour survives simplifications to the model which have the advantage of removing a rather arbitrary and intractable parameter, and hence that the simplified equations are those to investigate in more detail numerically.

References

[1] L.B.Hong and T.R.H.Davies, Geol. Soc. Amer. Bull. II **90**, 1839 (1979)

[2] P.E.Ashmore, *Process and Form in Gravel Braided Streams: Laboratory Modelling and Field Observations* (University of Alberta 1985)

[3] E.Caroni, Preprint, Hydrofractals '93 conference, Ischia

[4] S.Cramer and M.Marder, Phys. Rev. Lett. **68** , 205 (1992)

[5] G.Parker, J. Fluid Mech. **76** , 457 (1976)

[6] D.M.Tetzlaff and J.W.Harbaugh, *Simulating Clastic Sedimentation* , (Van Nostrand Reinhold 1989)

[7] P.D.Komar, *Beach Processes and Sedimentation*, (Prentice-Hall 1976)

Chapter 4: simulation

4.1. Introduction

A number of design issues had to be resolved before any start could be made on writing the simulator. These included considerations unrelated to the physics, such as the choice of language, the importance or otherwise of portability, and the platform(s) on which the simulator was to be developed and run. Other issues involve the way in which the physical problem is to be approximated: boundary conditions and method of solution. .

4.2. Computational details

The choice of language for the simulation, and most of the subsidiary programming for data-processing, was FORTRAN77 : while not particularly sophisticated for application programming (it is hard to provide a usable, system-independent interface) , it is well suited to numerical work: it provides a wide range of mathematical facilities, and is very widely available in a standard form with highly efficient optimising compilers. Although the original expectation was that the entire project would be carried out on the university's IBM mainframe, it seemed prudent to keep to the language standards (most vendors provide compilers which allow for a number of useful and desirable extensions. Unfortunately these can not always be relied on to be the same in different brands) This turned out to be very fortunate, allowing the simulation code to be ported half-way through the project from the IBM mainframe to a DEC workstation running VMS, and subsequently to another running Unix with minimal loss of time in each case.

4.3. Design

The major design questions were the choice of boundary conditions, and the implementation of the differential equations. Three major approaches have dominated flow simulations: finite difference methods, finite-element methods and marker-in-cell.

4.3.1 The choice between F.D, F.E, and M.i.C.

Finite-difference is the most widely taught approach at undergraduate level, and hence the one most people immediately think of when first asked to write a differential equation solver. In outline it involves dividing up the area (or volume) under consideration into a grid (usually regular) and assigning the variables values at each grid-point. These values can be used to calculate local approximations to spatial derivatives to the required order in the lattice-spacing (using a Taylor series) [1]. The derivatives are then used to calculate the rates of change, with which the variable values over the entire grid are updated and the entire process iterated. This approach is popular because it is conceptually attractively simple, and this simplicity is reflected in the ease with which a basic finite difference scheme such as the Euler method (1st order approximations in space and time, explicit update i.e. $y(t+dt) = y(t) + y'(t)dt$, with ' denoting a time-derivative) can be implemented. Unfortunately, such a scheme can readily be shown to be numerically unstable unless the ratio of time-step to spatial separation is kept within certain bounds, leading to very slow solution for fine grids [1-3]. This is true of the majority of explicit schemes [4]. For linear differential equations this can be overcome by going over to an implicit scheme (one where $y(t+dt) = y(t) + y'(t+dt)$: $y'(t+dt)$ can be written in terms of $y(t+dt)$ and the problem of update is reduced to a matrix inversion), such schemes being stable [1,4]. While an analogous procedure would work in the non-linear case, the fact that the relation between the values of y and y' can no longer be written as a matrix makes such an approach vastly more expensive. In general, efficient solution of non-linear equations by finite-difference schemes is a large and quite specialist area of work.

Finite element schemes involve dividing the region of solution into sub-regions (the finite elements) within each of which a series using a suitable set of basis functions is used to approximate the required solutions, the coefficients being found by minimising the deviations from the equation to be solved [4] (there is also a requirement of continuity between elements).

Marker-in-cell schemes exist in a variety of forms, but a typical implementation for a flow-solver would be as follows. A number of elements of water are set up: each has a fixed volume, a position in two or three dimensions and various other attributes (e.g. velocity, density), the whole being readily represented by a set of arrays. At the start of the run, the positions of all the

water elements are initialised (typically so as to spread them uniformly over the area being simulated). The distribution of water elements is used to calculate the depth at points on a lattice (by counting the number of water-elements in the 'unit cell' belonging to each lattice point: essentially a binning procedure), which is then interpolated two-dimensionally to give a depth at the position of each element. This and the slope at that position (the slope being the spatial derivative of the interpolation function), are used to calculate the velocity of each element. The velocities are then used to move all the elements to new positions, updating the simulation by one time-step, and the process iterated. (This is an outline of a scheme that can be found in more detail in reference [5]).

Compared with finite-difference, marker-in-cell schemes have a number of advantages: most stability-related problems are removed at a go, by the way the water is represented. Trivially, it is no longer possible for oscillations to build up without limit since the depth can not go negative at any point, being a count of the actual number of water elements in a bin, and in general behaviour is more obviously constrained towards being physically realistic. Another attraction is that finite-difference methods tend to produce results containing strong anisotropies introduced by the lattice used (a problem discussed further in Chap.5), an effect greatly mitigated in marker-in-cell schemes where the positions variables of the water elements are allowed to be continuous. On the debit side, a large number of elements are typically needed to reduce the effect of the depth being quantised, result in greater use of both memory and processor time.

The final decision was to go with finite-difference on the basis of more straightforward implementation, and to attempt to mitigate its disadvantages (in the case of lattice anisotropy by trying different lattices, in the case of instability by using an adaptive time-step scheme), although it is not obvious in retrospect that was the most desirable course: the problems of estimating the effect of the lattice on the geometry of the results resulted in a noticeable amount of extra work.

4.3.2 Boundary Conditions.

Choice of boundary conditions is central to what aspects of the model the simulation is being used to study. For example, it would be possible to set up a low-resolution simulation that covered an entire flood-plain from mountains (an inerodible upper boundary) down to the sea (some suitably contrived

sink)[5,6]. This is ideal for the study of large-scale features such as drainage networks [7,8], but the edge-effects and the continually varying slope are a disadvantage when looking at more local features (this is covered further in chapter 7 when looking at the effects of erosion).One early consideration was to set the simulation up to produce results directly comparable with those of the linear analysis. As chosen, the boundary conditions were essentially periodic, but adjusted for the slope: the 'left' and 'right' edges of the simulation array were identified in the obvious manner, while the 'top' and 'bottom' were identified allowing an offset equal to the total drop down the slope (fig. 4.1). This provides conditions consistent with the stability analysis, except only for the fact that there is now a quantisation condition on the wave-number in both directions of the form $k=2n\pi/Na$ where N is the size of the grid in that direction and a the lattice vector.

One obvious feature of such a set-up is that since the sediment is continually recirculated through the system, no true channels can be formed since the sediment from them cannot be removed. An advantage, however, is that the conditions provide a translational invariance with the result that measurements everywhere on the grid are directly comparable, making a statistical study of the results for an entire grid much simpler.

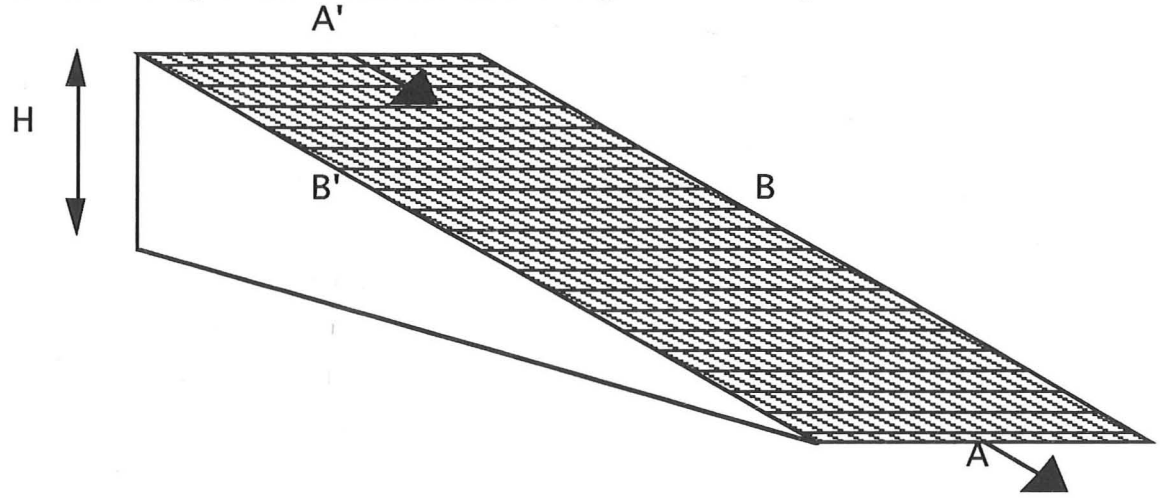

Fig. 4.1: Boundary conditions used in the simulation. Points B and B' are treated as adjacent in the normal way for periodic boundary conditions. Material leaving at A re-enters at A' as though from an identical grid placed at a height H above the one it enters.

4.4. Implementation (1) : water-flow

Initially, the simulation computed the equilibrium water level in the system by forward solution of the equation

$$\partial d/\partial t = - \nabla.\mathbf{q}$$

(which as the previous analysis reveals, will converge to the zero, giving the correct depths), and then updating the entire landscape by one time-step before re-iterating the procedure. While clearly not an ideally efficient approach, this provided a quick way of obtaining code whose output could be tested against the stability analysis.

The first part of the actual programming was development of code to solve for the water-flow alone, so that this could be tested independently. It was at this point that most of the implementation decisions for the model had to be made (although there was some attempt to ensure that the code was modular enough that some of these could later be significantly altered without seriously affecting other parts of the simulation). The approach chosen used a square lattice to approximate the spatial derivatives by the finite-difference scheme shown in Fig. 4.2. The time evolution of the equations used a forward time-step (i.e. explicit) scheme ,a decision based on the non-linearity of the equations to be solved, and consequent desire to avoid the long delays in finding a more suitable method of solution: the literature on efficient solving of non-linear PDEs is extensive, but the schemes used are in general either special-purpose, requiring some expertise to adapt, or heavyweight in implementation. The disadvantage of explicit schemes is, of course, that they all suffer from numerical instability for sufficiently large values of the time-step. The compromise adopted was to use an adaptive time-step which used the fractional change in depth at each point to calculate a suitable time-step: specifically, Δt was chosen at each iteration so that the greatest fraction change in depth of the entire grid did not exceed a specified parameter. Choice of this parameter is clearly crucial to performance and this is something of a problem as it is only readily calculable when the iterated solution is close to its final value: here a Von Neumann stability analysis can be used since the problem can again be treated as effectively linear [1]. Overall, this is not a particularly efficient approach since in the worst case it can result in the entire simulation being bottle-necked by a single badly behaved grid point, but it did prove robust and although it was ultimately dropped for reasons of speed it was extremely useful in developing the sediment transport code: in attempting to graft new code onto an existing program, it is an enormous help if the existing parts are sufficiently reliable that problems arising can all be blamed on the new work.

Having got water-flow code that superficially appeared to work (i.e. one that behaved such that any allowable starting configuration converged to a flat water surface if the underlying bed was flat) the stability analysis provided a good test of its accuracy. While it is clearly not possible to test a numerical algorithm on a truly infinitesimal perturbation, a look at the analysis

suggested that a perturbation amplitude of 1% of the water depth with a slope of 0.01 would be a good compromise between keeping second order effects negligible and not being swamped by numerical noise. As a check on the suitability of the values chosen for the test, values one decade either side of this (i.e. 10% and 0.1%) were also tried: the results are shown in appendix A which gives some tests of accuracy of modulus and argument of the complex amplitude A (Eqn 3.2) both analytical and measured for various values of k.

A number of separate facts emerged from this: the most important ones being that the water surface does indeed converge with fair accuracy to the predicted values, and at the predicted rate (the 0.1% test performed neither noticeably better nor worse than that at 1%, suggesting (a) that 1% is small enough, and (b) that below this accuracy of convergence is limited by other factors, the main one being probably attempting to compare a continuum solution with one on a discrete lattice).

The tests showed that the final accuracy achieved was acceptable, although it varied with wave-number, becoming worse at high |**k**|. This is consistent with the hypothesis that the limitations are in the difference between the correct lattice and continuum solutions, rather than to actual failure of convergence. This issue is addressed further in chapter 8, at a point when it became necessary to look at it in more detail, but the main point here is that the two differ in the latter having $\sin(ak_{x \text{ or } y})/a$ where the former has $k_{x \text{ or } y}$, where a is the lattice spacing, hence the use of one as an approximation to the other becomes worse as k increases.

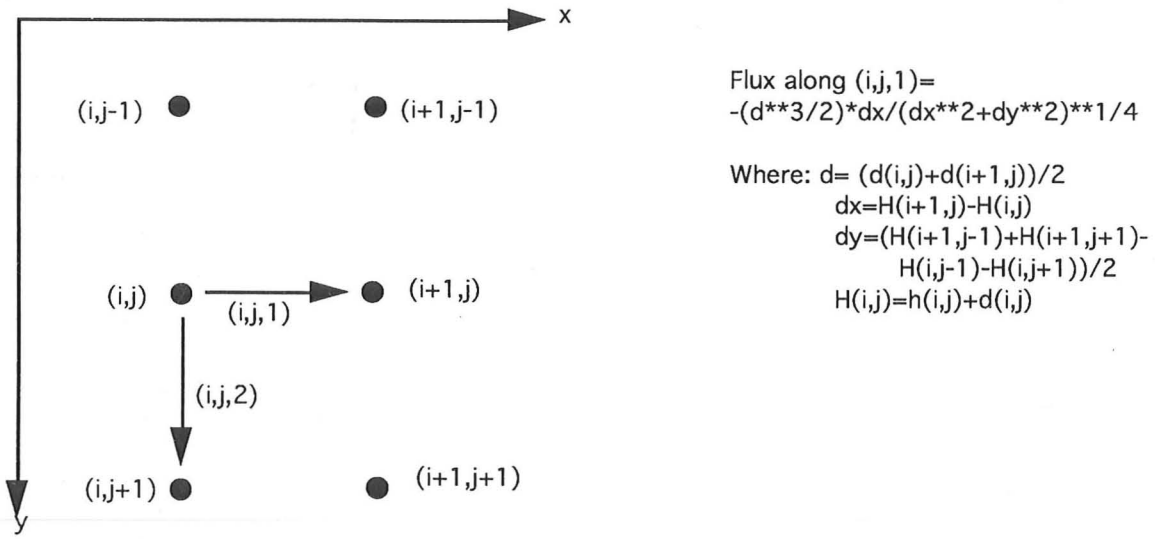

Fig.4.2 Diagram of the difference scheme used in the simulation.

4.5 Implementation (2) sediment transport

The next step was to add the sediment movement routines: at this stage the aim was not to integrate the two as efficiently as possible, but to get them working independently. The simulation in its first form, after setting up the initial conditions, would iterate the flow-solver to convergence, then use the values of water-flux and depth produced by the last step to calculate the sediment capacities at every point, and move corresponding amounts of sediment down each nearest-neighbour bond, again using the values for the water-flux. This part of the code also, therefore, used a forward time-step method.

While not complete yet, this code was now sufficient to allow measurement of the growth exponents for sinusoidal perturbations, and comparison with the linear stability analysis. The results are mentionned in appendix A , and show that the agreement with theory was good. The testing did however illustrate the instability problems associated with the use of an explicit time-step: I was running the programme interactively at this stage for greater ease of debugging, and therefore tended to use larger time-steps than would be the case in the actual simulations, and this tended to cause those runs using perturbations with large positive values of Re(p) to grow at the expected rate up to a certain size, after which they would begin to grow very much faster, as numerical instabilities in the method used took over, finally resulting in overflow. For the actual simulation runs, the time-step used was greatly reduced, solving this problem (reproducing a run at a number of different values of the time step and comparing the results ensured that the problem really had gone away, rather than simply become more subtle).

Given a few more support routines to provide I/O and other practical necessities (including at the time circumventing a 5 minute CPU limit on batch jobs, by saving the results in mid-simulation and re-loading, which was proved a very useful feature in its own right since it ensured that if a run failed for some reason it could always be picked up again at most 5 minutes from where it started) this now provided the simulation programme for the first 'real' runs.

The simulator was subsequently altered in two ways: firstly, experiment showed that interleaving the sediment and water updates more closely (i.e. using a smaller time-step for the sediment update, and updating more often, relaxing the degree of convergence required of the water-solver) provided greater

efficiency (in terms of simulated time : CPU time). Secondly, about two years into the project, the actual method of solution for the water was changed from allowing the water surface to evolve to equilibrium by forward progress of

$$\partial d/\partial t = - \nabla.\mathbf{q}$$

to solving $\nabla.\mathbf{q} = 0$ directly by a relaxation scheme. In this scheme each value of d is updated simultaneously according to

$$d^{n+1} = (1-\Sigma w_i)d^n + \Sigma w_i d_i$$

where the d_i are the values of d at the neighbouring sites and the w_i are a set of weights. This is a conventional relaxation method for solving problems where the divergence of a flux must be set to zero. The weights are recalculated at each iteration since the fluxes are non-linear and hence the weights will be depth-dependent but even so the method provided an appreciable speed-up compared to the original approach. There is however a problem in that the relaxation does not provide exact conservation of water: the approximation is quite good if all the w_i are made small, but there is still a discrepancy. This was corrected by calculating the total gain or loss of water over the entire grid, and spreading a corresponding correction equally over all lattice-points. This correction is made often enough for the adjustment involved to be small compared to the water depth (in practice every ten iterations or so, which does not outweigh the speed gain of using the relaxation method). Making the corresponding change to the stability analysis shows that adding a weak source term to the water flux at every point simply adds a negative (diffusion-like) term to the growth exponent. This results in slower terrain evolution, but provided the term is kept small it will not affect the final result significantly (since form of the water surface is known to be stable to small perturbations).

This completes the description of the methods used in the simulation program. The actual source-code for the simulator can be found in appendix B. All the parameters used are provided to the simulation in a file that is read before run begins. The parameters are in three notional classes (although there is no difference in their actual treatment): those which ought in principle to be fixed, namely K, α, and β, those which determine the physical set-up to be simulated, d_0 and θ, and those which relate purely to the computation: the grid size and time-step. K turns out to be unimportant in that it only affects the overall rate of change and hence any alterations to it can equally be obtained by increasing the time-step (unless one wishes to have a simulation in seconds rather than arbitrary units, which is not really applicable given the difficulty of finding actual values for K), and was set to 1. Similarly, adjustment of the depth , slope, and lattice size makes having a separate parameter for the lattice-

spacing redundant. Although there is a spread of values in the literature, α and β were taken as 1.75 and 3.0 throughout except for a few early tests. Depth and slope were typically 0.1 and 0.01 although these are not typical of real systems (for flood-plains 1.0 and 0.001 would be closer)[6].

References

[1] G.D.Smith , *Numerical Solutions to Partial Differential Equations: Finite Difference Methods* pp.47-72 (Oxford University Press 1985)

[2] C.G.O'Brian, M.A.Hyman and S.Kaplan, J. Math. Phys. **29** , 223 (1951)

[3] R.D.Richtmeyer and K.W.Morton, *Difference Methods for Initial Value Problems* (Interscience Publishers 1967)

[4] L.Lapidus and G.Pinder, *Numerical Solution of Partial Differential Equations in Science and Engineering* (Wiley-Interscience 1982)

[5] D.M.Tetzlaff and J.W.Harbaugh, *Simulating Clastic Sedimentation* , (Van Nostrand Reinhold 1989)

[6] S.A.Schumm, *The Fluvial System,* (Wiley-Interscience 1977)

[7] R.Leheny and S.Nagel, Phys. Rev. Lett. **71**, 1470 (1993)

[8] C.P.Stark, Nature **352** (1991)

Chapter 5 : Results

5.1 Overview

After the necessary code had been developed and tested as described in the previous chapter, it was used to run a number of simulations. These were all set up in the same way (except for two exceptions that will be mentioned below): an initially uniform inclined plane of sediment was set up on a 50x50 grid, and then seeded with noise. This took the form of adding to each grid point a value taken from a uniform distribution in the range 0 to 10^{-4} of the water depth. This grid was then covered in a uniform depth of water and allowed to evolve according to the equations described in chapter 2 until it reached statistical steady-state, this being judged by measuring the activity (see section 5.2 below).

The results were viewed as grey-scale elevation maps (fig. 5.4a). These invited comparison with certain real systems such as beach rills (fig. 5.4b) and braided rivers (fig. 5.6). In the latter case a numerical comparison of certain features was also attempted (section 5.3.2).

5.2 Time-dependent Behaviour

Although the perturbations at first grow exponentially, as suggested by the stability analysis, once the features formed have reached a significant fraction of water depth the rate of evolution peaks and then falls, eventually reaching a plateau level, several orders of magnitude lower than the peak . This is in line with what would qualitatively be expected of such a system: the growth of the Fourier components is driven by a cross-flow moving sediment from trough to crest (in the simulation set-up this is the only mechanism by which features can grow since there are no sources or sinks of sediment), and as the crests grow closer to the water surface, the depth-dependence of the flow model will ensure that transport to them is reduced. More quantitatively, if the activity is defined as $|\Delta h|/\Delta t$ averaged over the entire grid and calculated at the end of an update cycle, then the results are shown in fig.5.1. The plateau region exhibits noise of a largely power-law form: the power spectrum has a large low-frequency part, followed by a section that is to a good approximation power-law with exponent -2, as seen in fig.5.2. Power law behaviour of this sort is widespread in systems that are dissipative and being driven at a steady rate, such as sand-pile automata [1]. This plateau behaviour then persists,

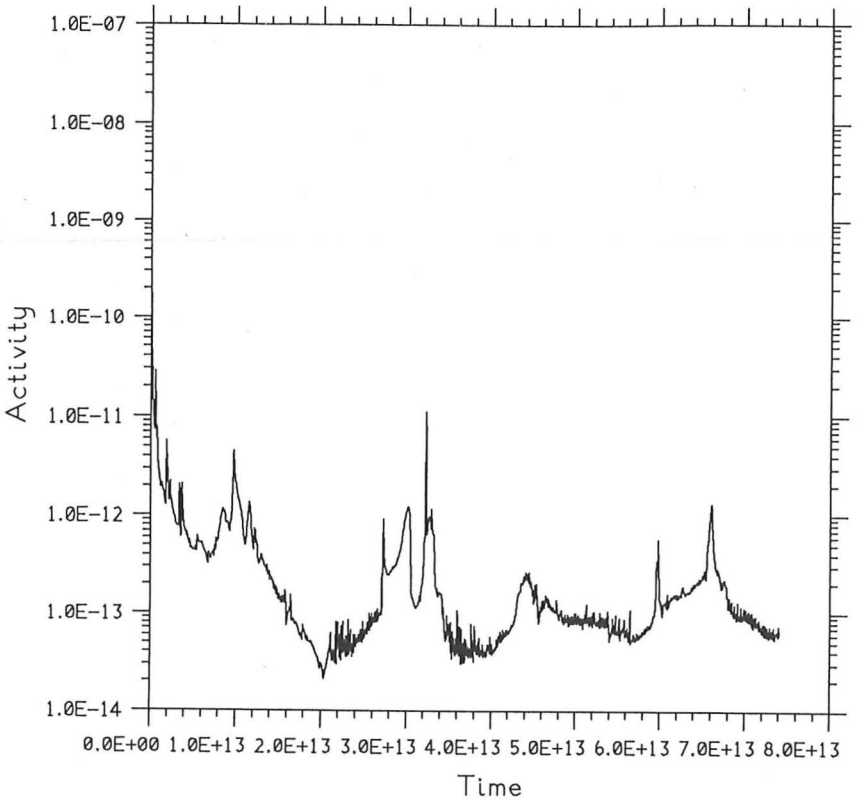

Fig. 5.1: Plot of the activity (as defined in section 5.2) as a function of time (in arbitrary units).

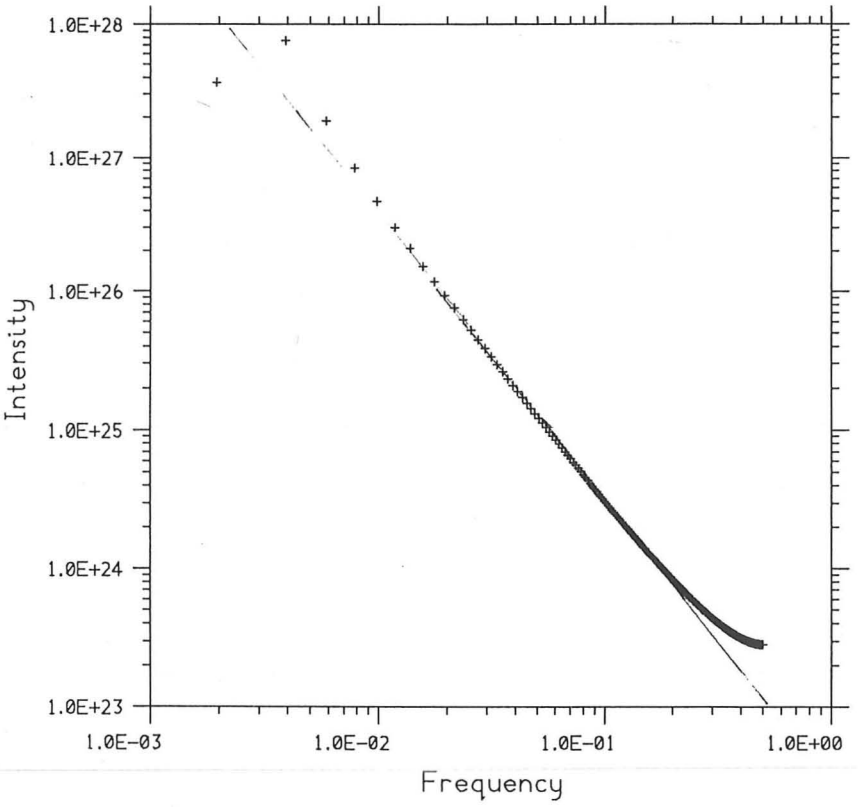

Fig. 5.2: Log-log plot for the power spectrum of a subset of the data in fig.5.1 (taken from t = 3.0E14 until the end of the run) showing clear power-law behavior.

corresponding to a statistical steady-state in which some features fade while others appear and at the same time there is a gradual overall dispersion upstream. While upstream dispersion is not immediately intuitive, is not necessarily inconsistent with real systems: the movement of sediment is downstream, but this does not preclude an upstream group velocity, and such effects have been seen in real systems. This is also consistent with the linear analysis of chapter 3, although the observed rate of dispersion is much slower than that predicted. Indeed, the upstream dispersion is extremely slow compared to the rate at which individual features are being altered. In an attempt to quantify this, I performed a single very long run, using a smaller than typical grid (20x20) to reduce the real time needed for the simulation, and saving the grid at intermediate times: at the end of the run the pattern had shifted upstream by less than on lattice vector . Given the very low speed, inspection is clearly insufficient to determine the actual distance travelled, and a quantitative method was needed. The distance upstream was measured by a least squares fit as follows : if $G_{t1}(i,j)$ is the simulation grid at time t1, $G'_{t1}(i,j)$ is the same grid shifted upstream by one lattice spacing (i.e. such that $G(i,j)=G'(i-1,j)$), and $G_{t2}(i,j)$ is the same grid at some later time t2, then the value of x which minimises

$$([(1-x)G_{t1}+xG'_{t1}] - G_{t2})^2 \qquad (5.1)$$

summed over i,j should define a measure of the upstream displacement, provided that there is a single, clear minimum. A look at fig.5.3 shows that this really is the case: the difference is approximately quadratic in x, with a well-defined minimum, and x therefore seems a useful measure of upstream dispersion. The other fact that emerges, comparing the scales of fig.s 5.3a and b is that, while the best fit is clearly defined, its quality has deteriorated sharply, the minimum difference having increased by a factor of nearly 100. At this rate, the residual for the best possible fit would be expected to approach the maximum feature size over a run only a few times longer. This is leads to the conclusion that even were there no constraints on the length of run possible, it would be impossible to track individual features for more than a few lattice squares before they became unrecognisable, and it is in this sense that the rate of dispersion is small compared to that at which the entire grid is being reworked.

There is however a problem in relating these results to the behaviour of the system: that the power spectrum of the landscape is dominated by features of wave-length close to the lattice spacing (as was predicted by the stability analysis), and wave-numbers close to the Brillouin zone boundary

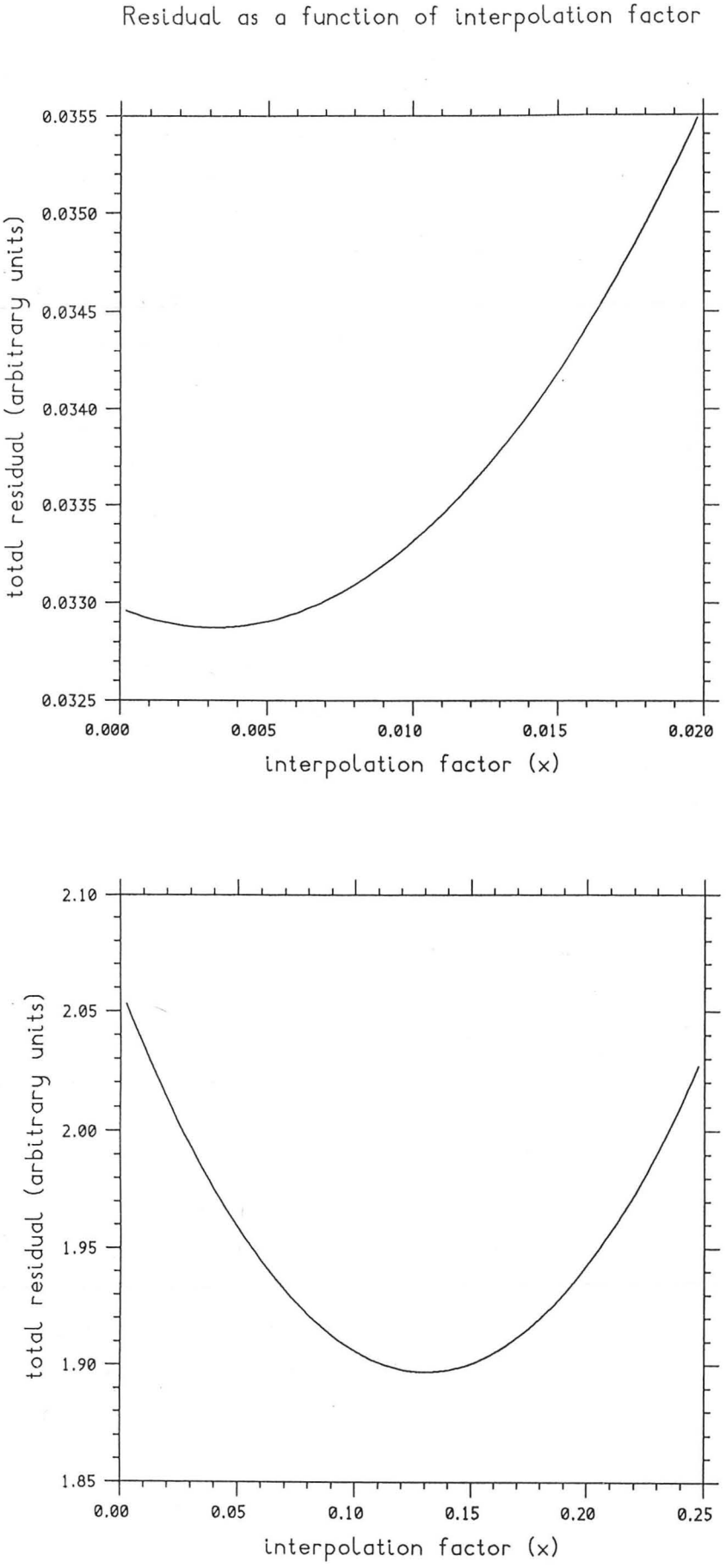

Fig. 5.3: A plot of the residual $([(1-x)G_{t1}+xG'_{t1}] - G_{t2})^2$ against x (as defined in 5.2), with t1 being the start of the run in each case, and t2 being larger for the bottom plot. In both cases there is a minimum, whose position gives the distance moved . This is increasing with time, as is the minimum residual (badness of fit).

would be expected to move slowly if at all anyway. There is therefore the worry that the rate of upstream movement may well be artificially restricted by this, which would also explain why the observed rate of motion is so much less than in the continuum analysis (non-linear effects may also play a part in this). Unfortunately this is not really resolvable without resorting to some drastically different method of simulation.

5.3 Static features.

5.3.1 Overview of results

The results for a run are shown in fig.5.4a as a grey-scale elevation map. The appearance is typical except for the fact that a 100x100 grid was used rather than the usual 50x50 in order to make the pixel size less distracting.

The principal features are sets of ridges and troughs, of wavelength about two lattice-spacings, which run at a clear preferred angle to the downstream direction. This is in line with the results of the stability analysis, although variations (e.g. adapting the simulation to a triangular grid) show that the angle is affected by the lattice vectors of the grid.(A more detailed discussion of the effect on angle can be found in chapter 8.) There is also a definite division on a larger scale into strongly- and weakly-ridged regions. A look at the power spectrum (fig. 5.5) shows that the landscape is indeed dominated by short wavelengths as the stability analysis would lead one to expect, but the disturbance of the water surface is biased towards longer wavelengths (a fact that can be expected since the linear response of the water surface goes as k^{-1} at high k [eqn. 3.2]). This has interesting implications: the processes that form the terrain are controlled by the water depth and by the irregularities in slope of the water surface, rather than of the sediment. Hence the fact that the sediment surface is dominated by wave-vectors at the Brillouin zone boundary is not inconsistent with the appearance of structure at longer wavelengths, such as the division into rough and smooth areas already noted.

5.3.2. Comparison with real systems

Visually there is a noticeable resemblance to features left on beaches by outgoing tides, known as rhomboid rills (fig. 5.4b)[2]. These too show a well-defined angle, and in some (though not all) cases division into smooth and rough areas The resemblance can be explained by the fact that in both

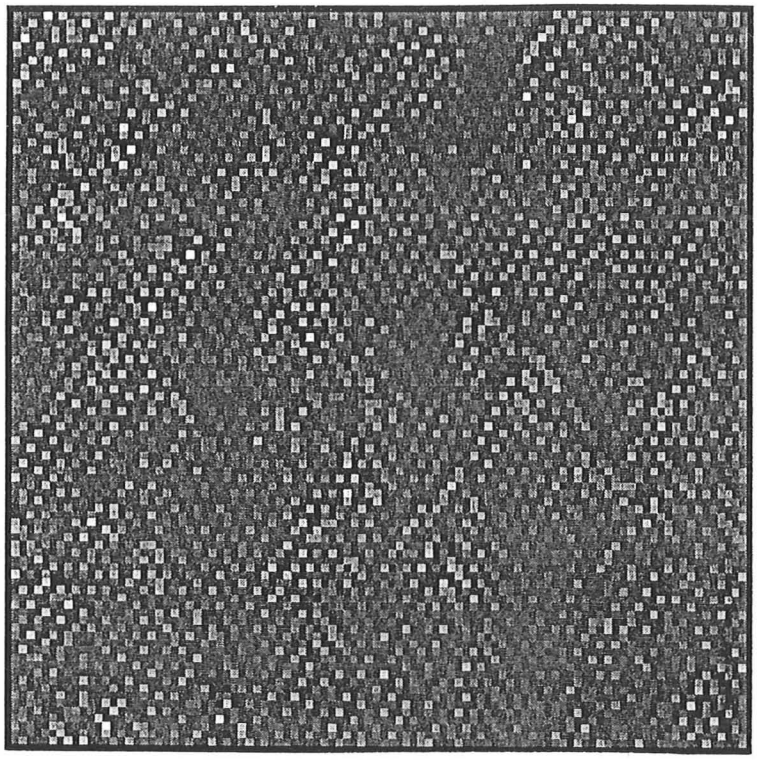

Fig. 5.4a: An elevation map of the terrain produced by a simulation run on a 100x100 grid: black is high, white low, and the mean slope (of 0.02) has been subtracted off for greater clarity (mean depth was 0.1).

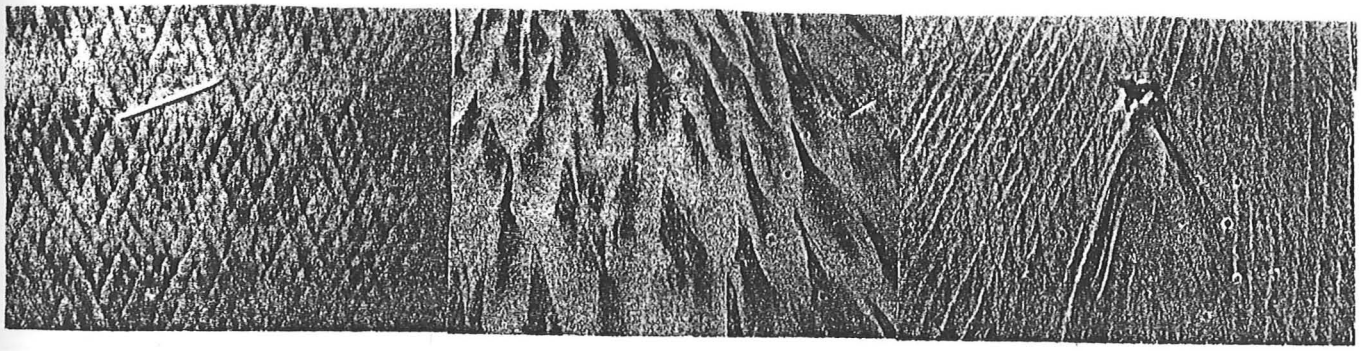

Fig. 5.4b: The rhomboid rill patterns of fig. 1.1, reproduced here for direct comparison with 5.4a.

cases the features are formed on a surface of sediment initially approximately flat, by flow of a small depth of water. The main difference is that in the simulation the boundaries are periodic, while in the case of the beach they are open. However, the flow of water over any one area of sand occurs for a comparatively short time as the tide is going out, so that the effect of the open boundaries can be expected to be small. Unfortunately the data about beach rills needed for a more quantitative comparison was not available at the time, although detailed discussion of a similar experimental set-up can be found in chapter 6.

Of the other water-sediment systems considered for possible comparison with the model, long braided rivers are among the most appropriate: despite the great difference in scale, the resemblance between erosion rills and drainage networks has been noted by others [3]. Such rivers often remain statistically self-similar for long distances both along (tens of km.) and across the stream (up to a few km in the case of some rivers) as a result of which it can again be hoped that boundary effects will be relatively unimportant near the centre. This is well illustrated by the satellite view of the Zaire river in fig. 5.6. The other question that arises regarding the validity of the comparison is that the evolution of a river is driven by a water flow that is largely cyclic from year to year (mainly the level of rainfall) while the total water flow in the model is of course constant. Fortunately , in those cases where the rainfall is heavily seasonal it is normally true that most of the activity occurs at times of high water flow between the start and end of flooding: during the low water season cutting down of channels and reworking of channel-bar sediments occurs [4,5], but these affect aspects of the river (such as channel geometry and sediment sorting) that have no counterpart in the model.

One difficulty in making comparisons with the model is that since the simulation as described here conserves both water and sediment, it cannot produce areas of dry land from the initial conditions given. The solution adopted here was the comparatively crude one of taking a vertical displacement from the initial sediment plane and assigning each point as 'dry' or 'flooded' depending on whether it was higher or lower than the cut-off height. Since most activity was expected to occur in the river system when water levels were high, it was hoped this would not make too serious a difference.

Visual comparison with the photographs of real braided rivers in fig 5.6 [6-8] shows a major difference: that the 'islands' of the simulation feature ragged edges with detail down to the lattice size (as suggested by the

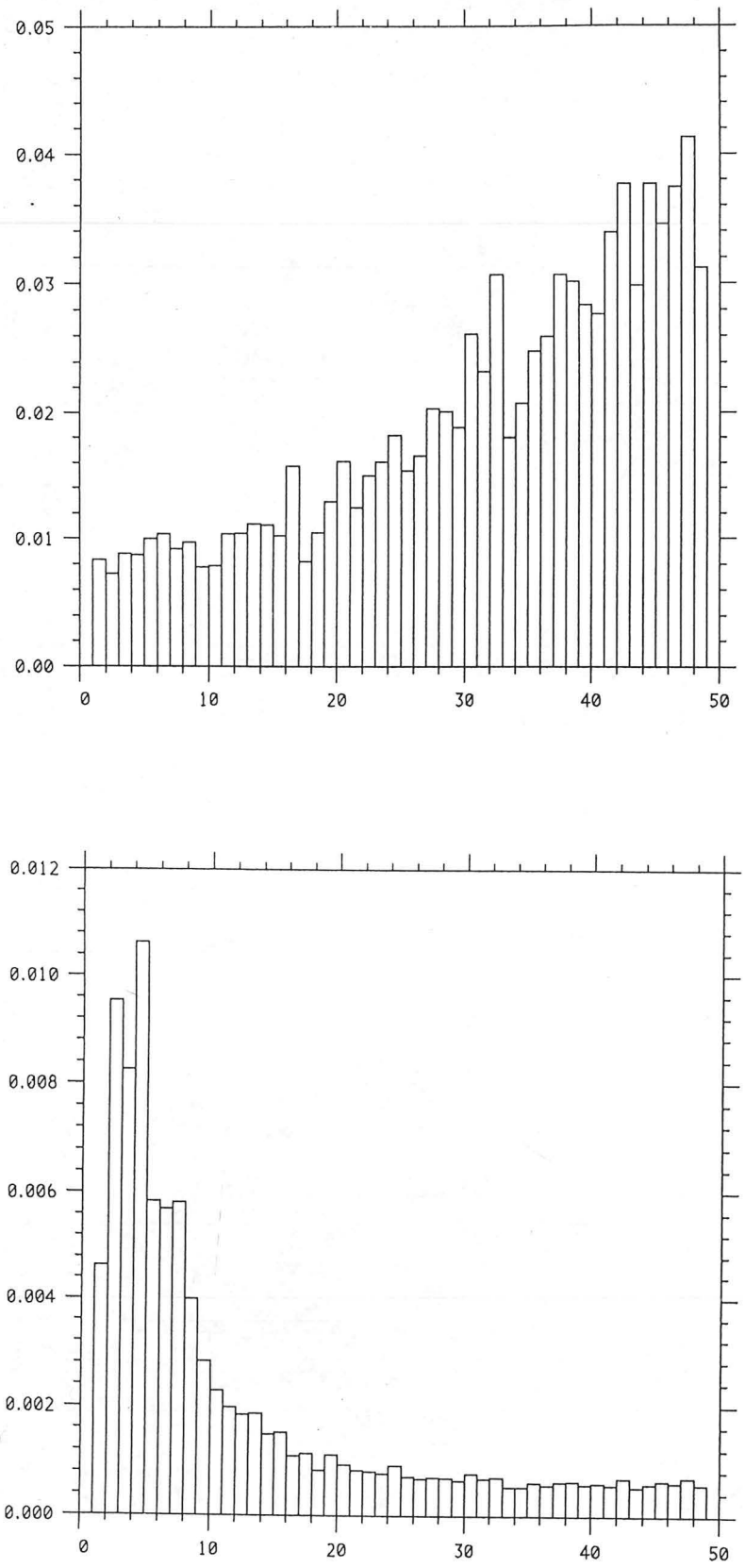

Fig. 5.5: Spatial power spectra for cross-stream sections of the terrain surface (top) and water surface (bottom) of the results shown in fig. 5.4a. The power is in arbitrary units, the wavenumber in repeats to the simulation grid. As the linear analysis in chapter 3 suggests, the water surface shows more long-wavelength power than the land. (Results shown are averages for several sections.)

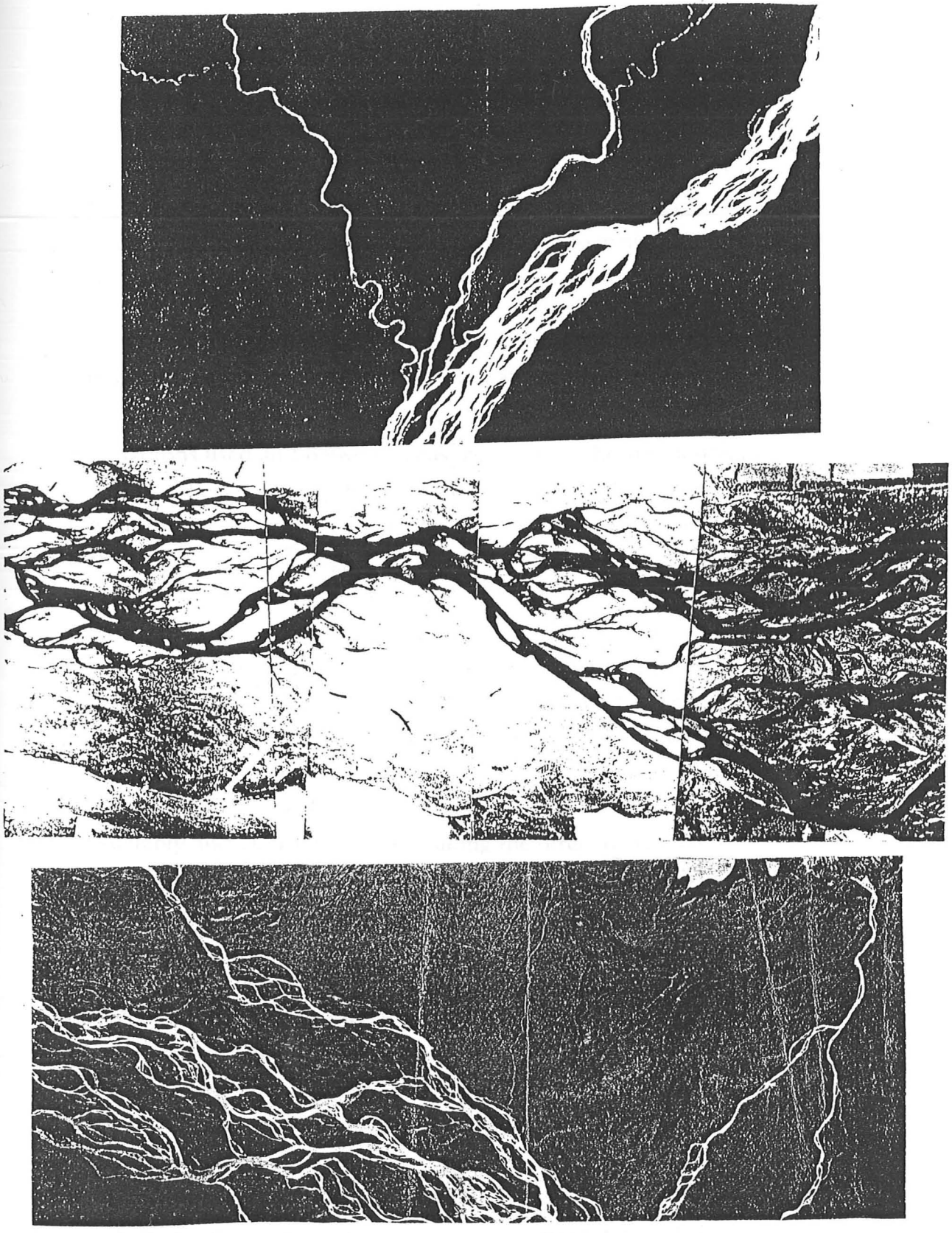

Fig. 5.6: Photographs of the Zaire (top), Rakaia (middle) and Vatnajokull (bottom) rivers in their braided stages (from references 6,7, and 8 respectively). These are the pictures from which the data used in fig.s 5.7 and 5.8 were obtained.

stability analysis) while the real ones are largely compact. In both cases, however, there is a wide range of island sizes from single pixel to most of the width of the river. The range of existing literature on self-similarity in real river systems [9-11] prompted measuring the actual distribution as a quantitative means of comparing the visually somewhat dissimilar systems. Both the simulated and real systems turned out to exhibit a power-law size distribution for the number of islands dN in a given range of area dA,

$$dN/dA \propto A^{-\gamma} \qquad (5.2)$$

Fig. 5.7 shows log-log plots of island size against number both for the photographs used and for the simulation at one value of the depth.

The apparent exponent γ varied by about 30% both between the photographs used and between measurements on the simulation at different values of cut-off depth. Plotting the measured exponent against the cut-off depth for the simulated results revealed a well-defined curve with a large peak. This suggested that converting the cut-off depth to the fraction of the grid covered by water (since water coverage increases monotonically with cut-off depth), and equating this to the fraction of the channel underwater should make a direct comparison of simulation and photographs on the same plot possible . These results of this are shown in fig. 5.8. The measured data too reveal a peak in the value of the exponent. This apparently corresponds to an anisotropic percolation threshold, which was directly measured for the simulation data; the spanning cluster predictably always crosses the grid along the direction of flow.

The considerable x-axis spread of the photographic data is due to the difficulty of defining properly the boundaries of the channel, and distinguishing large islands from part of the mainland. This problem is most noticeable at small water coverage (corresponding to channels near or below the percolation threshold in the model) where such debatable islands are a significant fraction of the exposed land within the channel. Comparison with the simulation also becomes more debatable at low water coverage since as less area is flooded, the approximation of simply 'draining' the simulation by a given amount and considering the exposed land, rather than removing the water as the landscape is evolving becomes cruder . (Clearly the onset of percolation in a real river system is not well-defined, since a truly spanning cluster would result in two separate rivers.) The measurements for the simulation exponents also become less accurate further from the percolation threshold (the error bars are obtained by use of several simulations under the same conditions)

Fig. 5.7: Island size distributions
(simulation results correspond to 57% water cover)

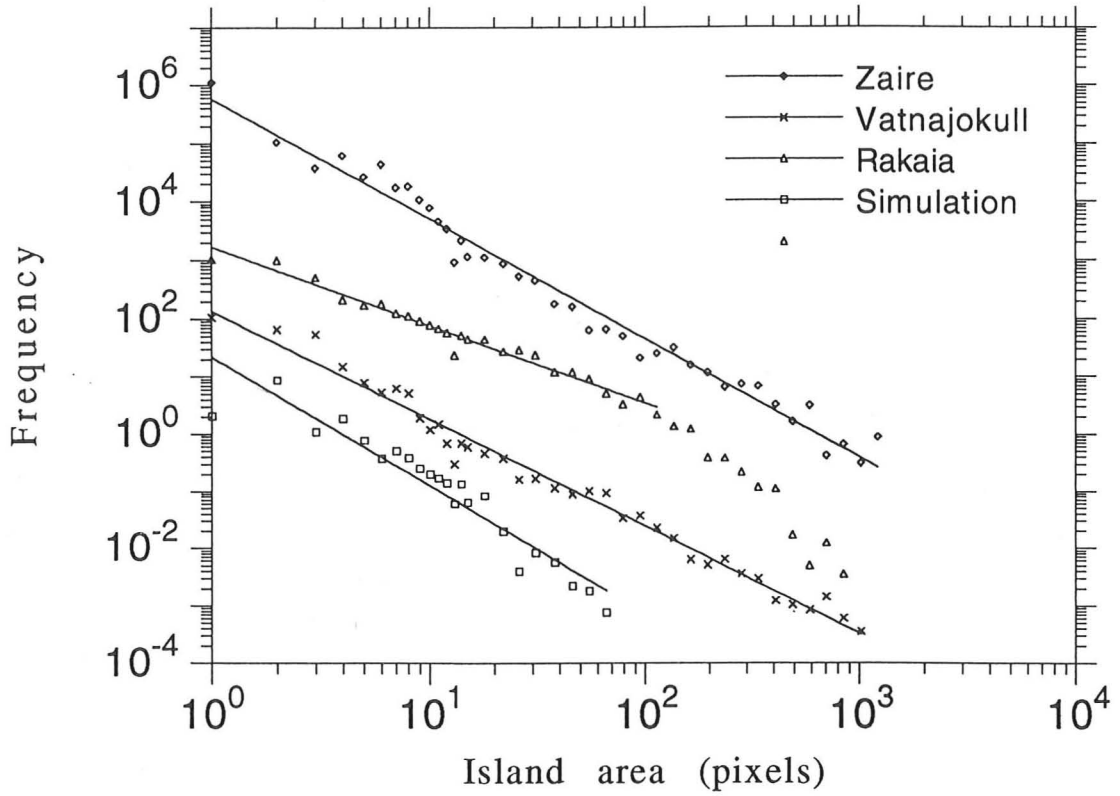

since the range of power-law fit decreases as islands either disappear (deeper water) or are engulfed by the spanning cluster (shallower water).

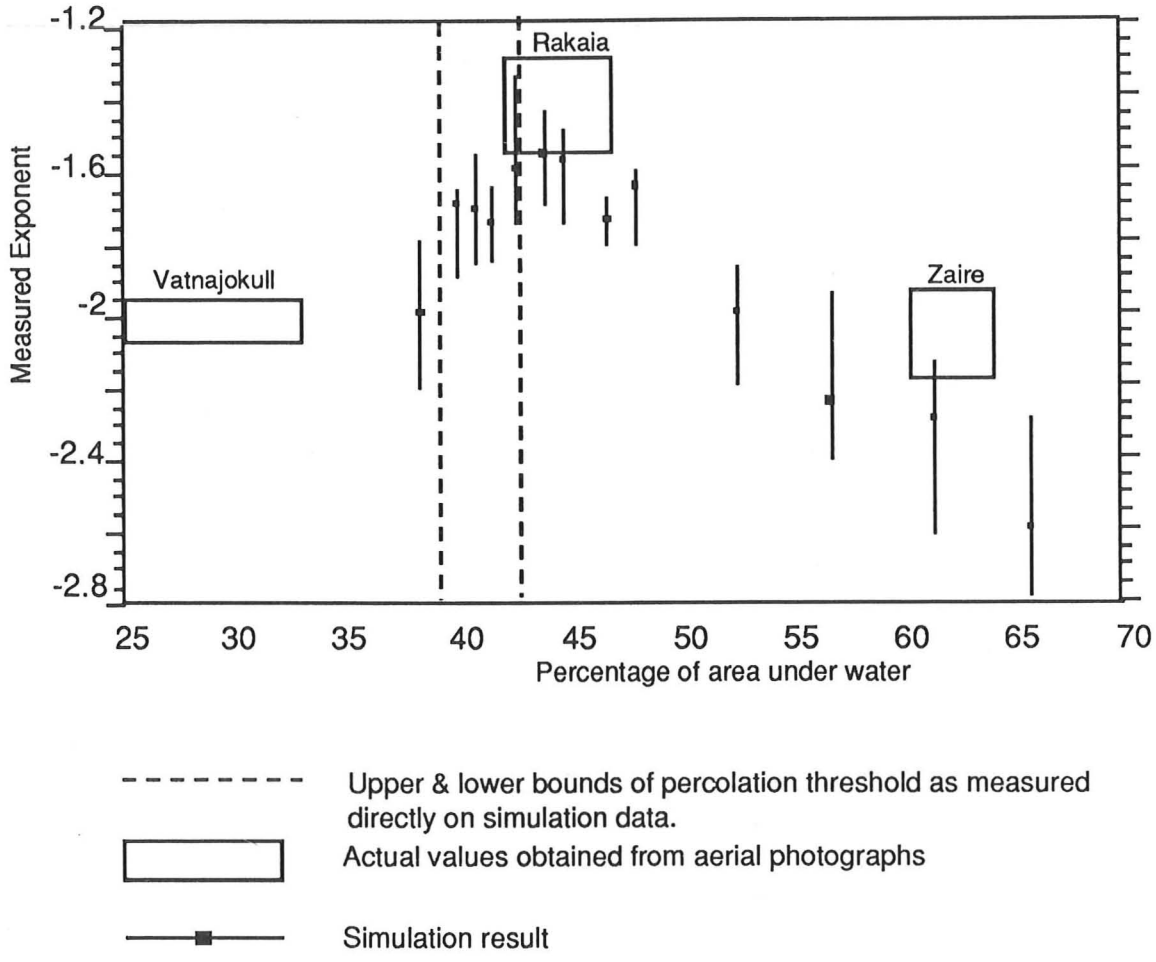

Fig.5.8 : Apparent exponent as a function of water coverage, shown simulations and for the Zaire, Rakaia and Vatnajokull rivers (ref.s [6-8])

Although there is clearly some discrepancy, with the measured exponents being less negative than the simulated ones, both sets of results are consistent with the suggestion of a peak in the exponent at 40-45% water coverage. One other point investigated with regard to the simulation was whether a simple convolution blurring of the deposition function to approximate turbulent mixing, which would remove the extreme small-scale detail of the simulated results can give visually more realistic island patterns (it also seemed possible that this would make the apparent exponent less negative since as the water level is raised the rather loose 'islands' in the simulation will tend to become disconnected into smaller

pieces more readily than the real ones). This was not successful in that the results produced were simply those that would be expected from coarsening the grid: it appears that something more elaborate would be needed (the possible usefulness of adding momentum transport in some form so as to make flow through narrow channels slower is discussed in chapter 9).

References

[1] P.Bak, C.Tang and K.Weisenfeld, Phys. Rev. Lett. **59**, 381 (1987)

[2] P.D.Komar, *Beach Processes and Sedimentation*, (Prentice-Hall 1976)

[3] J.Thorn, Nature **345**, 764 (1990)

[4] R.C.Crane, PhD thesis, Department of Geology, University of Reading (1982)

[5] S.A.Schumm, *The Fluvial System*, (Wiley-Interscience 1977)

[6] M.A.Summerfield, *Global Geomorphology*, (Longman Scientific, 1991)

[7] B.R.Rust, *Fluvial Sedimentology*, Canadian. Soc. Petr. Geol. Memoir 5 (1978)

[8] A.Holmes, *Principles of Physical Geology* (Nelson 1978)

[9] C.P.Stark, Nature **352** (1991)

[10] B.B.Mandelbrot, *The Fractal Geometry of Nature* (Freeman 1982)

[11] J.Huang and D.L.Turcotte, J. Geophys. Res. **94**, 7491 (1989)

Chapter 6: Results (2)

6.1 Introduction

6.1.1 Description

The work described here is based on the same simulation results as that described in chapter 5, although chronologically separated from it by almost a year. The main problem at the time when the simulation was produced was finding a real system with enough accurate data available for accurate comparison (it was noted that rhomboid rills on beaches seemed suitable candidates). This chapter consists of a quantitative comparison of those results with a single real system produced under controlled experimental conditions and subsequently measured in detail : the work of Professor Elpidio Caroni of the University of Trieste [1].

The experiment as performed can best be summarised by the following quote from his abstract in that paper:

"... a laboratory experiment was set up consisting of an artificial plot (4 x 8 m) of uniform slope (at an angle of about 20°) filled with an homogenous mixture of sand and cohesive materials; this artificial soil was initially arranged in a plane sloping bare surface. By means of a rainfall simulating device, consisting of a set of sprinklers feeding the system the slope was left free to adjust its surface, thus producing a rill network."

Caroni allowed the experiment to proceed until a well-defined drainage network had formed, and then proceeded to map it and to measure cross-sections of it. A plan of the drainage network is reproduced from his paper in fig. 6.1, and the two cross-sections in fig. 6.2.

6.1.2 Differences and Similarities.

There are obvious similarities that make a comparison between this experiment and the simulation data appealing, but at the same time there are significant differences to be considered: primarily that the boundaries in the experiment are open. The effect of this cannot be dismissed since the removal of sediment was allowed to occur until a drainage network had

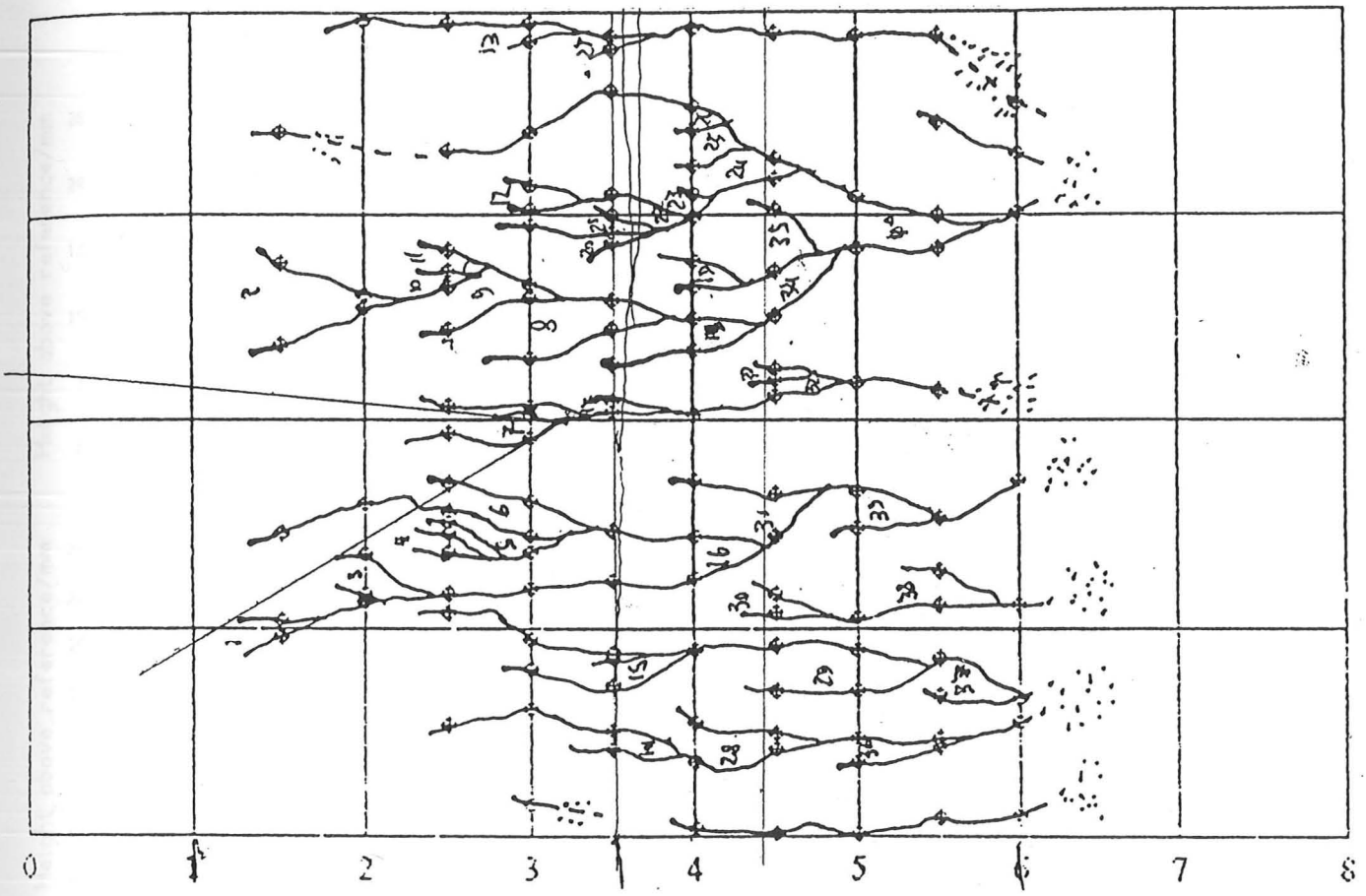

Distance downstream /m

Fig. 6.1: The drainage network resulting from Prof. Caroni's experiment (reproduced from reference 1). The numbers at the vertices were added subsequently to simplify collecting branch-angle statistics. The branch angles have a large uncertainty associated with them due to the sinuosity of the rills (the two lines superimposed at vertex 7 are approximate tangents to th two branches at the join, drawn to allow measurment of the angle).

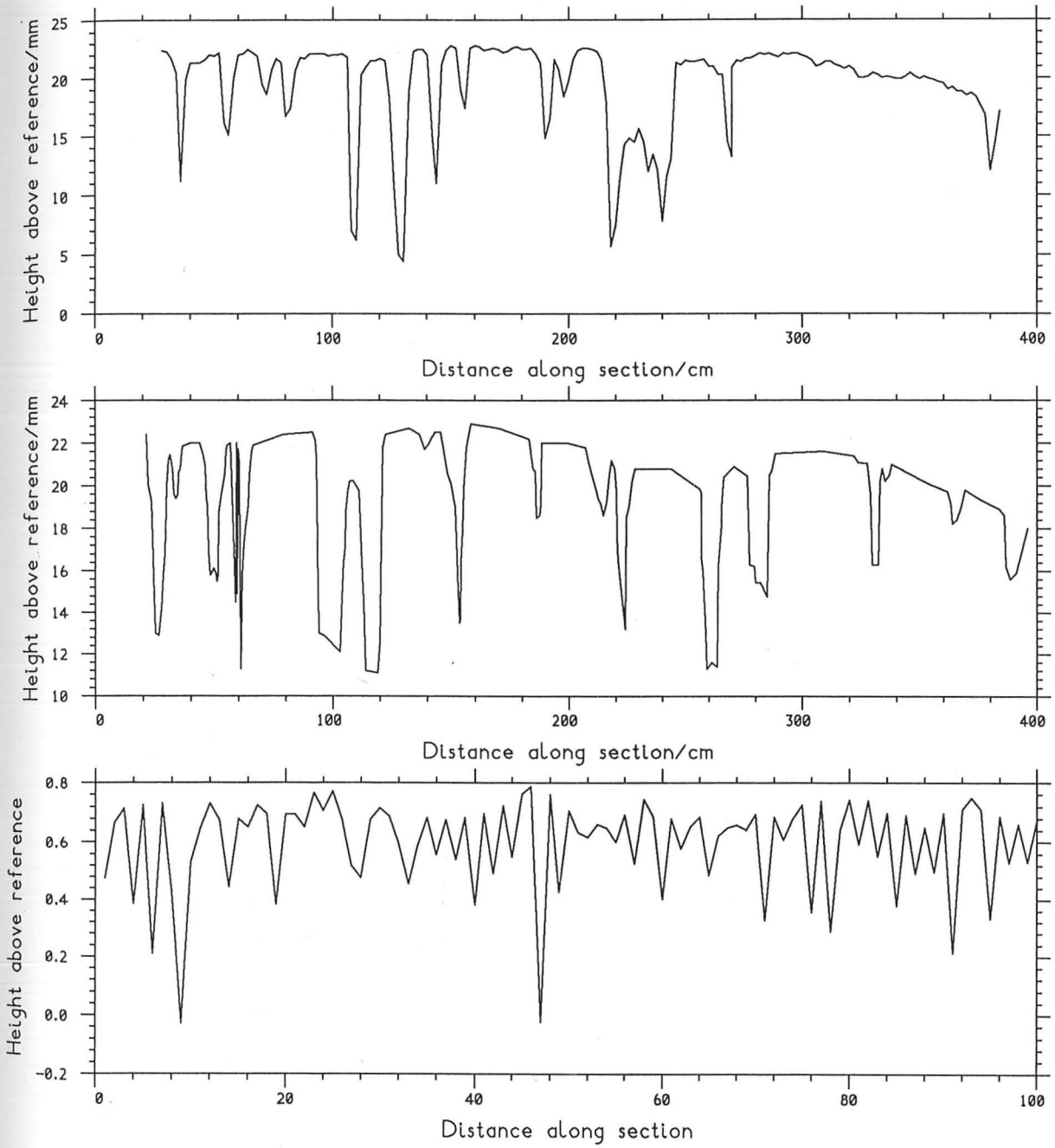

Fig. 6.2: Cross-stream sections. The top two are experimental, while the third is from the simulation. This last is significantly more jagged than the other two, but there are two points bearing on this:
(i) that the top picture (height measured at regular intervals) is noticeably rougher than the middle one (height measured at significant features).
(ii) that the top picture actually contains many small features made inconspicuous by the few that have deepened into channels, and effect that is absent in the simulated section.

been formed, by which time the importance of a sink at the lower boundary is clearly significant since without one, as discussed previously, no such network could form. Against this is the fact that the experiment involved the evolution from a uniform inclined plane of sediment under an initially uniform flow of water : Caroni used a set of sprinklers, all at the same height above the surface to provide simulated rainfall that was very nearly uniform. The stability analysis shows that adding water to the system as rainfall does not affect the qualitative behaviour, simply adding a small diffusion-like term corresponding to the tops of ridges being washed down into the channels, which will tend to lessen the importance of short wave-lengths. Clearly in its early stages the experiment would have been the direct physical counterpart of the sort of system that was being simulated in this thesis. The only question was whether the further evolution producing the drainage network had so altered the terrain produced as to make comparison unproductive.

Inspection of fig. 6.1 shows a drainage network that still has a large number of tributaries with comparatively small drainage basins flowing into larger streams whose separation is still small compared to their length. From the visual appearance, one can easily hypothesise that such a pattern could evolve from an irregular area of rhomboid rills such as some of those considered in Chapter 5, by the process of the deeper of the two outgoing channels from any vertex deepening and increasing in flow at the expense of the shallower one (since it would be evolving faster) until it eventually suppressed it completely (fig. 6.3 is a sketch of this). Subsequently one would expect the network to thin out as tributary capture proceeded, but this process does not seem to have gone particularly far in this case. The line of argument here is therefore that in the early stages of the experiment most of the sediment plane would be only very slightly affected by the presence of a sink at the lower boundary, and would evolve in a way described by the model used here. This would result in features of vertical size up to the depth of the water coverage (probably 1-2 mm. since the sprinklers are described as simulating "light" and "heavy" rainfall), and although the removal of material at the lower edge would result in down-cutting of channels, the formation of a dendritic drainage network, and (in the longer term) re-shaping of the channels themselves, it seems plausible

that much of the initially-formed structure and geometry would be preserved for a while, particularly in the upper parts where the channels are still numerous and small.

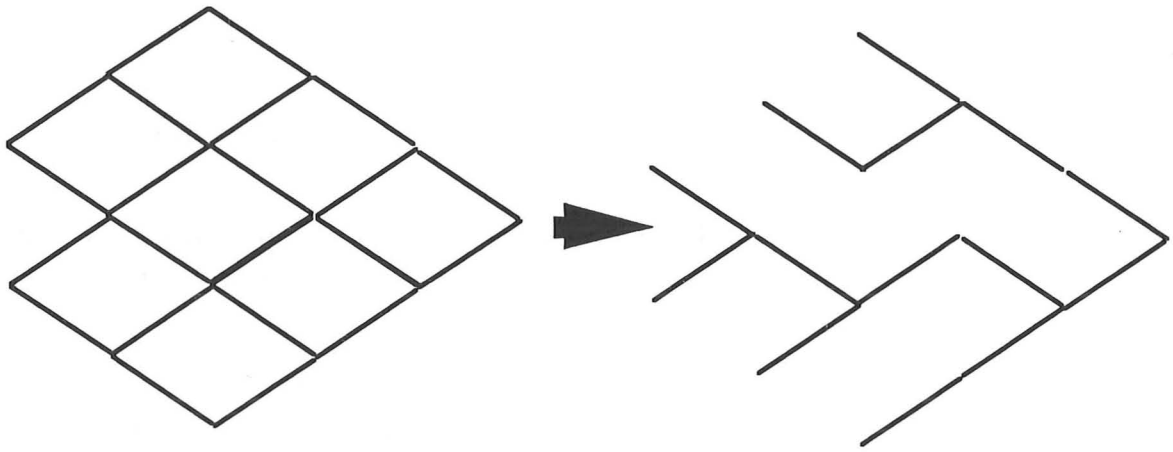

Fig.6.3: Possible evolution of a system of rhomboid rills into a dendritic drainage network by the elimination of the least active exit channel at each vertex (idealised).

6.2 Comparison

6.2.1 Appearance in plan

As remarked above, regions of the drainage network bear a plausible resemblance to a system rhomboid rills which has been pruned to ensure that each vertex has only one outgoing channel. If this were the case, one could hope that the join angle of the tributaries would preserve the preferred rill angle which was discussed in chapter 3, and this clearly invites direct comparison. For a given inclination of the plane, θ ,the other factors affecting rill angle are the depth of the water sheet and the wavelength of the rills. This poses obvious problems in that the layer of water flowing over the experiment will be deepening continually in the downstream direction. Since all that was really expected in this case was an order of magnitude comparison (as the original experiment did not include measurement of the depth), the simple solution of dividing the bed into two

sections across the direction of stream and calculating and average depth for each of these seemed sufficient. These were taken as the regions between 1.5m and 4m from the top of the experiment for the first (see fig.6.2) and 4m to 6m from the top for the second (these were chosen to give roughly equal numbers of values in each). The join angles of the stream vertices were measured for each section, averaged and divided by two to give the estimated rill angles. This procedure gave angles of 12.5+/-2.5° for the upper section and 19.4+/-5.5 for the lower.
Finally, an estimate of the feature size is needed, although since the water depth scales linearly with cut-off wavelength for fixed ϕ_{max} . Based on the cross-sections (which show all channels, and therefore tends to provide a lower bound) and drainage network (which only shows active channels, and hence can be seen as an upper bound) a value of 0.1m was chosen. Using this gives water depths of 0.4+/-0.2mm in the upper section and 1.1+/-0.6mm in the lower (the errors are much worse here because of the shape of the depth/angle curve, see fig. 6.4). The depths are consistent with Prof. Caroni's estimates of the water flow in the experiment, although not too much can be read into this since the choice of cut-off length means that the absolute depths are even more uncertain that the error bounds suggest. It is however highly encouraging that the water flow in the lower part is deeper than in the upper part. Unfortunately both the uncertainties on the depths and the physical width of the sections to which the figures apply make it impossible to say whether the depth is actually increasing as the 2/3 power of the flux, but there is no obvious inconsistency (i.e. the numbers do not warrant saying that there is a fit, but do not exclude it).

6.2.2 Cross-sections

The main qualitative work that Caroni carried out on his experimental system was the drawing of accurate cross-sections at two points along the bed, and establishing box-counting dimensions for them. This is in line with a number of observations of the fractal nature of erosion-produced topographies [3-5]. The cross-sections were taken along the two lines A and B in fig. 6.1, fortunately across regions with a large number of small tributaries, which according to the working hypothesis should be those

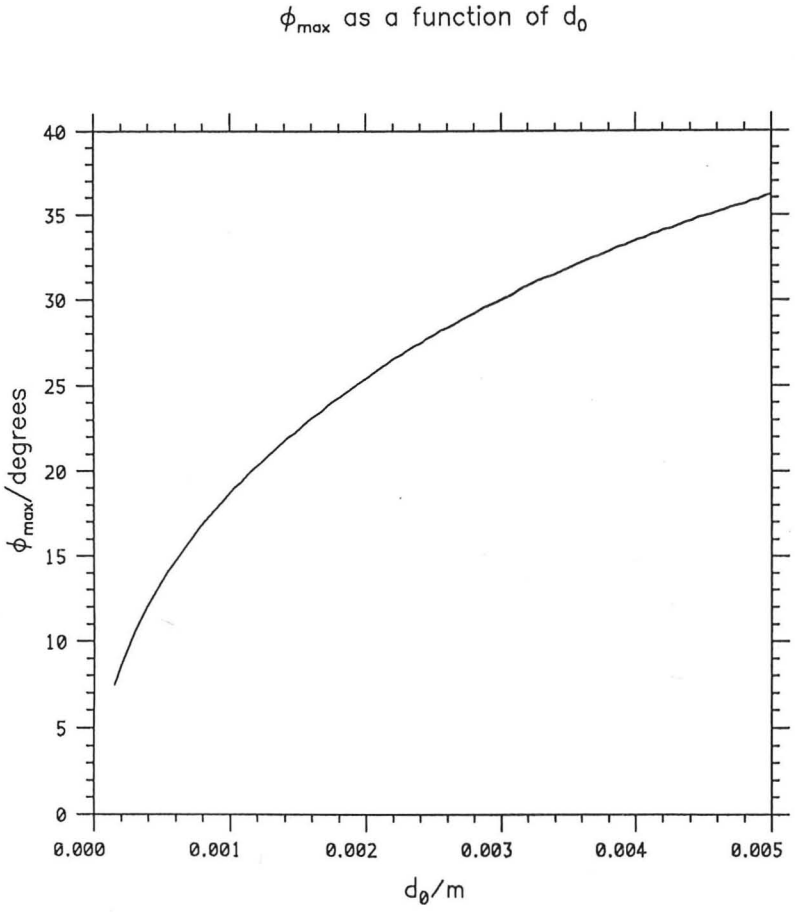

Fig. 6.4: The variation of prefered rill angle (ϕ_{max}) with water depth at constant slope and cut-off size. The graph is at its steepest near the origin, resulting in amplified uncertainties when used to convert angles into depths for small values.

most closely comparable to the simulation. The cross-sections are reproduced in fig 6.2, alongside a similar one from the simulation grid shown in fig. 5.4a. Visual comparison is not particularly rewarding: while the simulation results are clearly affected by the lattice spacing, showing many channels of the minimal width, and appear more ragged (as might be expected if the experimental cross-sections are coming to be dominated by a smaller number of channels) there are no obvious grounds for describing the two as clearly dissimilar. The next step was to compare the box-counting dimension, D_B. Box-counting is the most widely used means of quantifying fractals in science due mainly to the ease with which its measurement can be automated [6,7] (these refernces also contain a useful comparison of commonly-used fractal dimensions).

Prof. Caroni in his paper estimated D_B as 1.25 for the experimental landscape, a result in close agreement with the first estimates for the simulated one. It was possible to side-step problems of comparing the exact methods of measurement since Caroni was kind enough to supply me with the raw data of his cross-sections, so that all comparisons are in fact of values of D obtained by using the same programmes in each case (the results obtained off his data do not differ appreciably from his own estimates, but this does ensure that the comparison is not clouded by issues of method). Fig. 6.5 shows log-log plots of box-count versus box-size for both experiment and simulation (the simulation results are an average over all possible cross-sections in order to obtain as smooth a curve as possible). There is a problem with estimating a value of D off such a curve: at both high and low box sizes (i.e. larger than the rill depth, and smaller than the horizontal resolution), the relation between size and count will clearly be inverse linear and only over some intermediate range of sizes will any other power-law behaviour be detectable. Unfortunately, while at least two orders of magnitude of fractal behaviour are normally recommended for determining D_B, the best obtainable here is slightly less than one (the actual range is altered by the vertical scaling, or the aspect ratio of the boxes used. It does not affect the measured value of D_B, and was chosen here to maximise the width of the power-law region.) Furthermore, as the slope changes continually from $-D_B$ to -1, it is necessary to exclude points outside a region whose boundaries must be in some way determined.

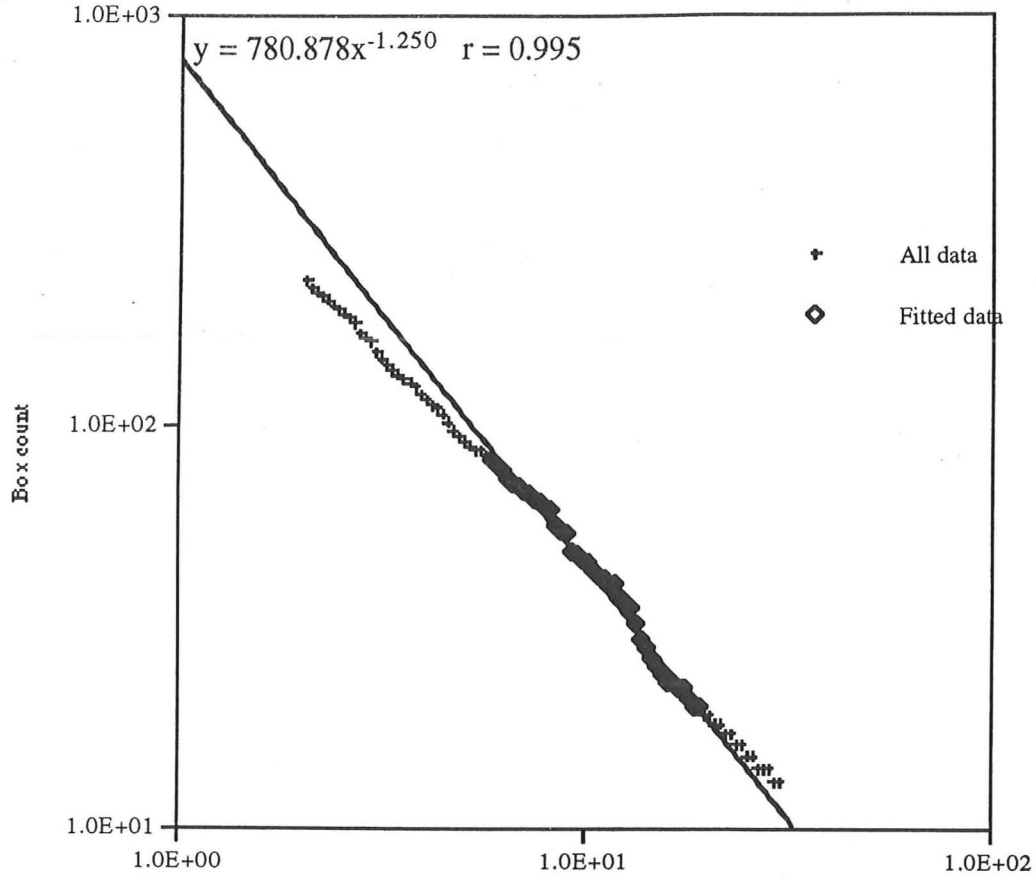

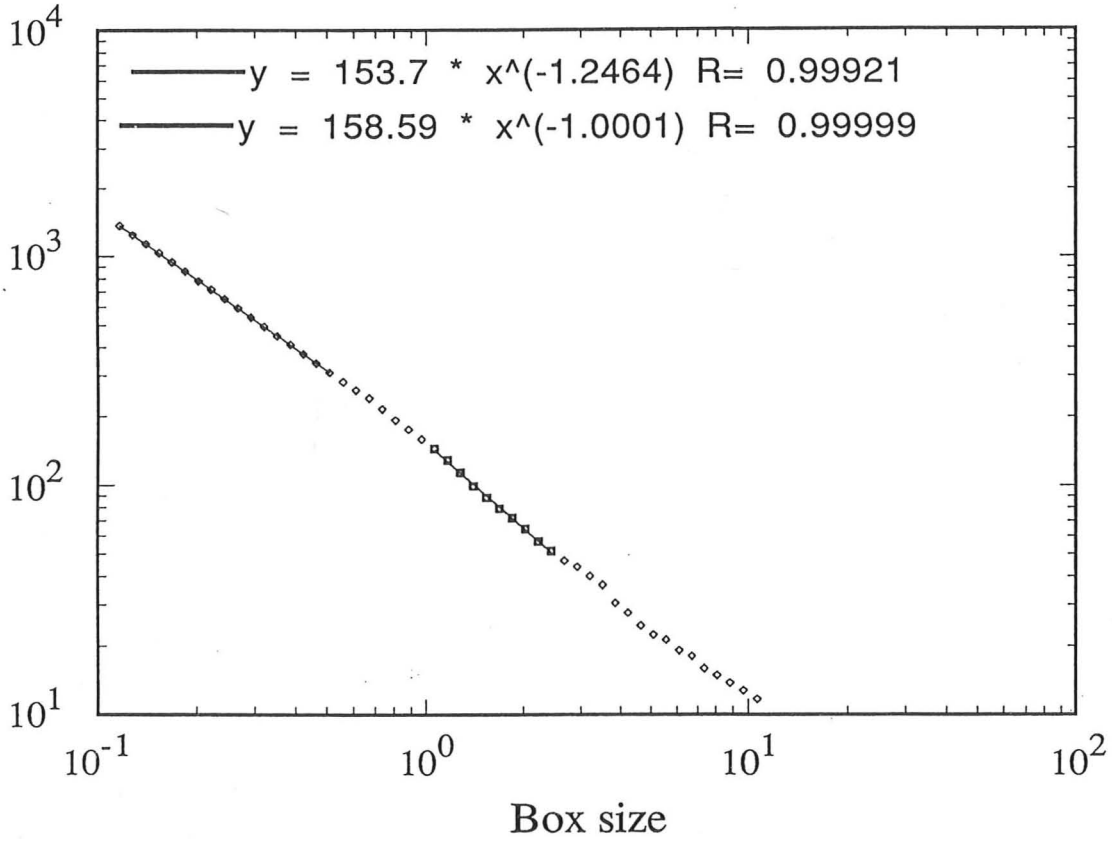

Fig. 6.5: Graphs used to estimate the box-counting dimensions of the experimental (top) and simulated (bottom) terrains. Both give exponents of approximately -1.25 in the region that is not linear, although the range of scaling behaviour is small for accurate estimation. (The figures on the graph differ slightly from those in the text as the latter are averages over measurments using boxes of different aspect ratios.)

That was resolved here by selecting the contiguous set of points that maximised the quality of fit, R. (It might be thought that the number of points available within the interval selected, and hence the accuracy of the estimate, could be increased by reducing the increments in box-size. Unfortunately, the finite horizontal resolution of the measurements defeats this.)

The outcome of these measurements was that to within the estimated error, the values of D_B for the experimental and simulated landscape cross-sections are indistinguishable at 1.26+/- 0.05 and 1.27+/-0.04 respectively.

6.3 Conclusions

Overall, this attempt to match theory and experiment is encouraging: the attempt to compare rill angles and water depths between the two, while it does not provide for firm conclusions is consistent with the two systems sharing similar behaviour. The comparison of cross-sections provides more quantitative agreement in that slices through the two topographies apparently share the same box-counting dimension.

It is important to bear in mind that different dynamics can lead to fractals of the same dimension (and that the value of D_B does not uniquely characterise a fractal) as well as the caveat in 6.1 that the experiment represents a more mature drainage system than the simulation can produce. That said, the results so far do suggest that further comparison would be rewarding if a rerun of the experiment were to make data on earlier stages and/or accurate depth measurements available.

References

[1] E.Caroni, Preprint, Hydrofractals '93 conference, Ischia

[2] E.Caroni, personal communication.

[3] J.Huang and D.L.Turcotte, J. Geophys. Res. **94**, 7491 (1989)

[4] J.Thorn, Nature **345**, 764 (1990)

[5] W.I.Newman and D.L.Turcotte, Geophys. J. **100**, 433 (1990)

[6] H.Peitgen, H.Jürgen and D.Saupe, *Chaos and Fractals* , (Springer-Verlag 1992)

[7] K.Falconer, *Fractal Geometry, mathematical Foundations and Applications* ,(Wiley 1990)

Chapter 7: Stability Analysis (2)

7.1 Limitations of the original model, and solutions

The configuration covered in chapters 3 and 4 was chosen for simplicity of analysis and simulation. It does have a number of disadvantages in terms of constraints on the terrain configurations that can possibly be produced: the fact that water and sediment are conserved and cycled round the periodic boundary conditions means for example that the formation of a proper drainage system, and hence of dry land, is not possible.

Of the ways in which this limitation can be addressed, the most physically obvious (and hence the one most easily comparable to real systems) is to redesign the boundary conditions to provide a source of water (either an inflow at the top of the grid, or rainfall, or some combination of these) and a sink for water and sediment at the bottom [1-4]. Despite the attraction of this scheme as a close approximation of real physical processes, there are a number of drawbacks: firstly, the areas close to the upper and lower boundaries must typically be discarded due to the effects of the boundary itself, which typically result in artificially accelerated erosion if no precautions are taken due to what is usually called a "waterfall effect" (this is discussed in chapter 5. of reference [1]). While it is possible to minimise the disruption due to the boundary (see the same reference), there are still computational penalties due to

(a) the need to treat the boundary grid-points specially, and

(b) the fact that a larger grid is still needed since the very edges will always be affected to some extent.

Secondly, the tendency will be to erode a profile of non-uniform slope, as do all real systems, because the edge nearest the sediment sink is eroded away first [5-6]. While this has the advantage of opening up the possibility of comparison with the source-to-sink profiles of real rivers, it has the drawback that parameters such as the ratio of erosion to deposition, which would be expected to influence the topography, will vary continuously along the stream, restricting the use of spatial averaging in any analysis to one dimension, and so again tending to require a larger simulation area. Finally, there is the consideration that the effects at the boundaries may adversely affect the performance of

the simulation code, particularly where this is not intrinsically stable, and must use an adaptive time-step to avoid numerical failure.

Due to these considerations, the decision was to attempt to reproduce some of the features of the sediment sink in a uniform manner over the area of the simulation. This was done by introducing a term corresponding to the decay of sediment in proportion to the distance it had travelled downstream. This also had the advantage of allowing the extension of the linear analysis used in chapter 3 to the new equations in a straightforward way.

7.2 Linear analysis

All the rules used in chapter 3 still apply, except for that describing conservation of sediment. The modified equation for this is given by:

$$\partial h/\partial t = -\nabla.q_s + \varepsilon|qC| \qquad (7.1)$$

where ε is the decay constant: an inverse length corresponding to the reciprocal of the distance downstream over which the sediment would be reduced to e^{-1} of its initial value in uniform flow conditions. Using the formula for the linear response of the water flow calculated previously, the growth exponent for sinusoidal perturbations is now

$$Re(p) = Kd_0^{\alpha+\beta-1/2}\theta^{\beta+3/2}\{3/2\frac{k_x^2((\alpha+\beta)k_y^2+(\alpha/2-\beta)k_x^2)}{[(1/2k_x^2+k_y^2)^2+9/4\theta^2k_x^2/d_0^2]} \qquad (7.2)$$

$$+ \varepsilon'\frac{(1/2k_x^2+k_y^2)[(\beta-\alpha/2)k_x^2 -(\alpha+\beta+3/2)k_y^2]}{[(1/2k_x^2+k_y^2)^2+9/4\theta^2k_x^2/d_0^2]}\}$$

with ε' being the dimensionless decay constant $\varepsilon d_0/\theta$. The crucial point which is visible at this stage is that for the values of α, β used here, the two terms on the RHS have different k-dependencies: the first term, corresponding to the movement of conserved sediment between ridge and trough is, as noted in chapter 3, negative for sediment ripples running at right-angles to the slope (which get washed away), and positive for channels close enough to the slope (although there is a maximum at a non-zero angle between slope and channel). The second term, due to the creation ($\varepsilon' > 0$) or destruction of sediment ($\varepsilon' < 0$) , will be positive for cross-stream ripples in the case of sediment-creation, and for down-stream channels in the erosive case. This is in line with intuitive expectation: in the limit of sediment not being conserved at all

it is clear that those channels running directly down-slope will have the highest flow-speed, and hence the greatest rate of sediment destruction, resulting in fastest deepening. The point of interest, then, is how competition between these two terms will affect the overall angular behaviour of the system as the value of ε' is varied.

7.3 Features of behaviour: the phase transition

7.3.1 Transition in ϕ_{max}

In fig.7.1, plots of Re(p) as a function of k are shown, comparable to fig 3.2, for three different values of ε', corresponding to erosion, balance, and deposition. The ridge that marks the angle of maximum growth-rate can clearly be seen to rotate in the plane. More quantitatively, fig.7.2 shows this angle, ϕ_{max}, plotted against ε' at a fixed cut-off length (the choice of the maximum value of $|\mathbf{k}|$ does not affect the result here provided that it is large in the sense that $k >> \theta/d_0$) : there is a sharp transition (but having non-zero width) from rills running straight downhill in the erosive regime (the 'channel' phase) to ones running at right angles to the slope (and the flow) in the depositional case (the 'washboard' phase).

It should be noted that the graph shows the angle of greatest instability, but not the actual maximum value of Re(p) at each point, and that this value is not everywhere positive. The behaviour of this is straightforward at large values of $|\varepsilon'|$: behaviour comes to be dominated entirely by the non-conservation of sediment, and the rate of perturbation growth increases proportionally to ε' , with either pure washboard or pure channel terrain resulting. Near the transition the sediment-conserving term from the original model becomes significant, one result being the existence of a small range of positive ε' ($2 < \varepsilon' < 3$) over which there is no actual instability: the value of ϕ_{max} is still defined, but even at this angle the rills silt up and disappear, rather than grow. This is a consequence of the fact that the sediment transport tends to favour channel-like formations (not directly downslope, but with a ϕ_{max} of less than $\pi/4$) and that there is a point where this and the sediment creation term at positive ε' (which is favouring washboard formation) interact to prevent any rill growth. The other consequence of the sediment divergence term is the non-zero width of the transition

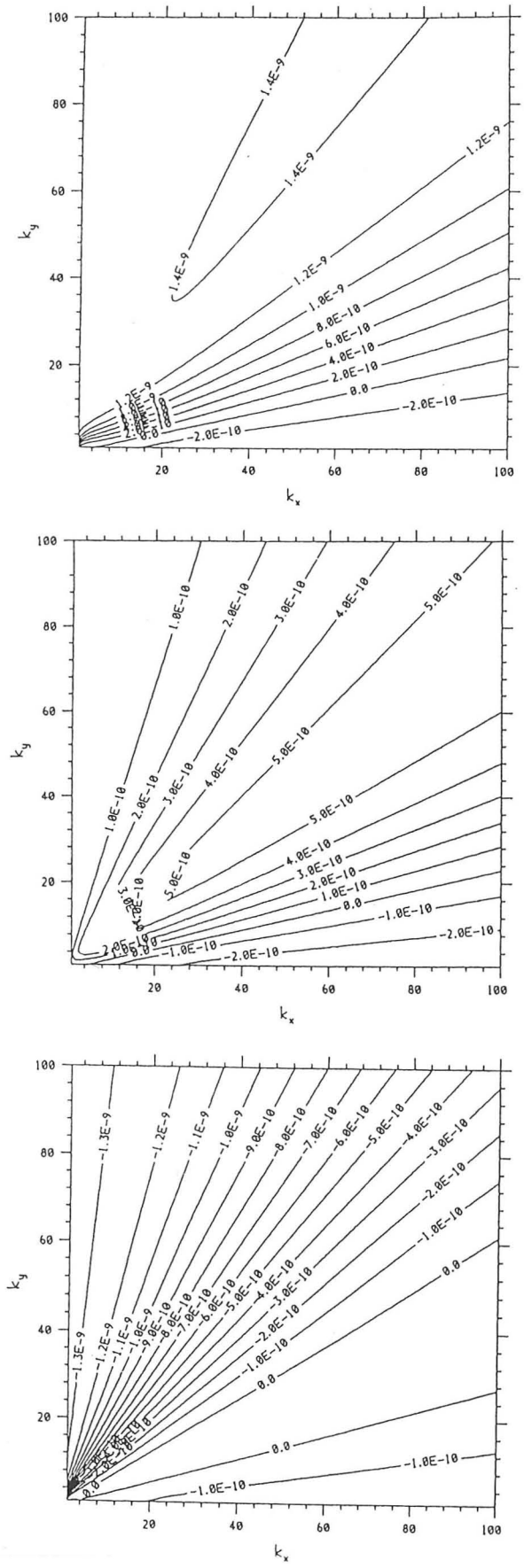

Fig. 8.1: Contour plots of the Re(P) in the **k**-plane for three different values of ε′ (-1.25 ,0, 1.25 from top to bottom), showing the rotation of the ridge of fastest growth . The plots shown use the values $d_0 = 0.1$, $\theta = 0.02$, K=1, which are typical of the simulation rather than of real systems (although the difference simply amounts to scaling the time variable), hence the small-seeming values of the exponent.

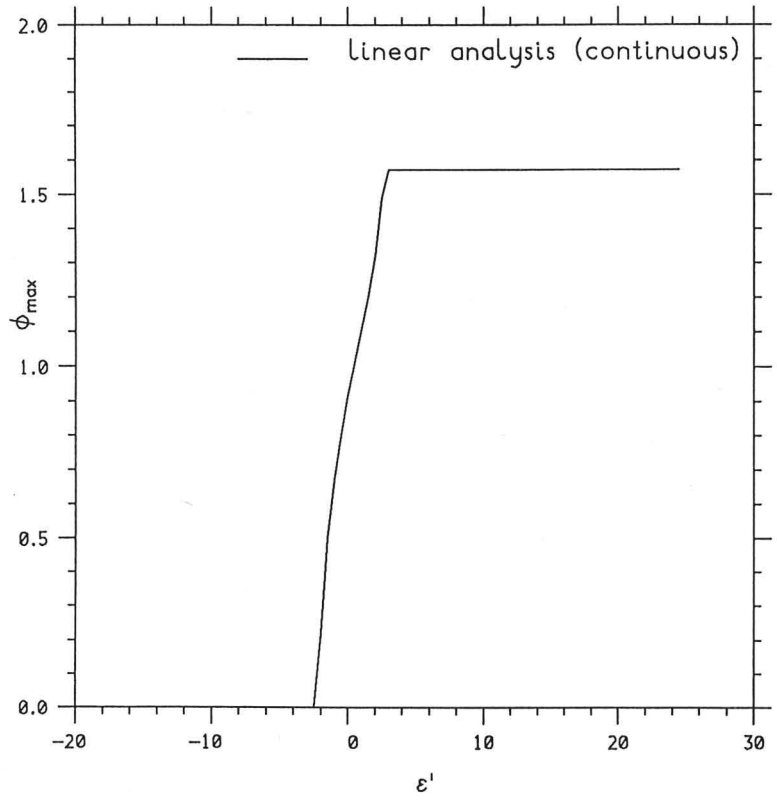

Fig. 7.2: Graph of ϕ_{max} against ε' , showing a clear (but not instantaneous) transition from 0 to $\pi/2$ centred of $\varepsilon' = 0$.

(since the erosion/deposition term on its own would result in a perfectly sharp change at $\varepsilon'=0$ from one terrain type to the other) .

7.3.2 Behaviour in the ε' - θ plane

There is also a dependence of behaviour on the slope of the sediment plane. The intuitive expectation here would be that increasing the tilting of the plane would tend to favour the channel phase, by increasing the advantage of higher flow-rates for rills running close to downstream. Fig. 7.3 bears this out: this shows a contour plot of ϕ_{max} in the ε' - θ plane, with the channel and washboard regions marked, plotted over the same range of ε' and θ/d_0 for three different values of cut-off wavelength (2, 1, 0.5): because the model has so few independent length scales, reducing the cut-off is equivalent to zooming in on the origin, and all three plots contain the same information, on different scales. It can be seen that the phase behaviour is largely what would be expected from the argument above: except for behaviour very close to the origin, , where there is an initial broadening of the transition, the onset of the pure channel moves towards higher ε' although only slightly so, remaining below $\varepsilon'=0$ at all times The formation of the washboard phase, on the other hand, is much more strongly affected by increasing slope, the value of ε' at which pure washboards ($\phi_{max} = \pi/2$) occur being proportional to θ/d_0, with a widening transitional region separating it from the channel phase.

7.4 Overview

In summary, the altered model shows a clear transition between channel formation and washboard formation, with both the direction of the transition and the way in which it is affected by slope seeming physically sensible. There is the question that while good approximations to a pure channel phase can be found on steep, easily eroded slopes, there are no obvious examples of washboards in nature that could be attributed to the mechanism considered here. There are examples such as alluvial fans that show quite large channel angles, corresponding to points well into the transitional region, which are formed under a much higher than average rate of sediment deposition[7], but there does appear to be an asymmetry between the extremes of erosion and deposition. Further investigation into the

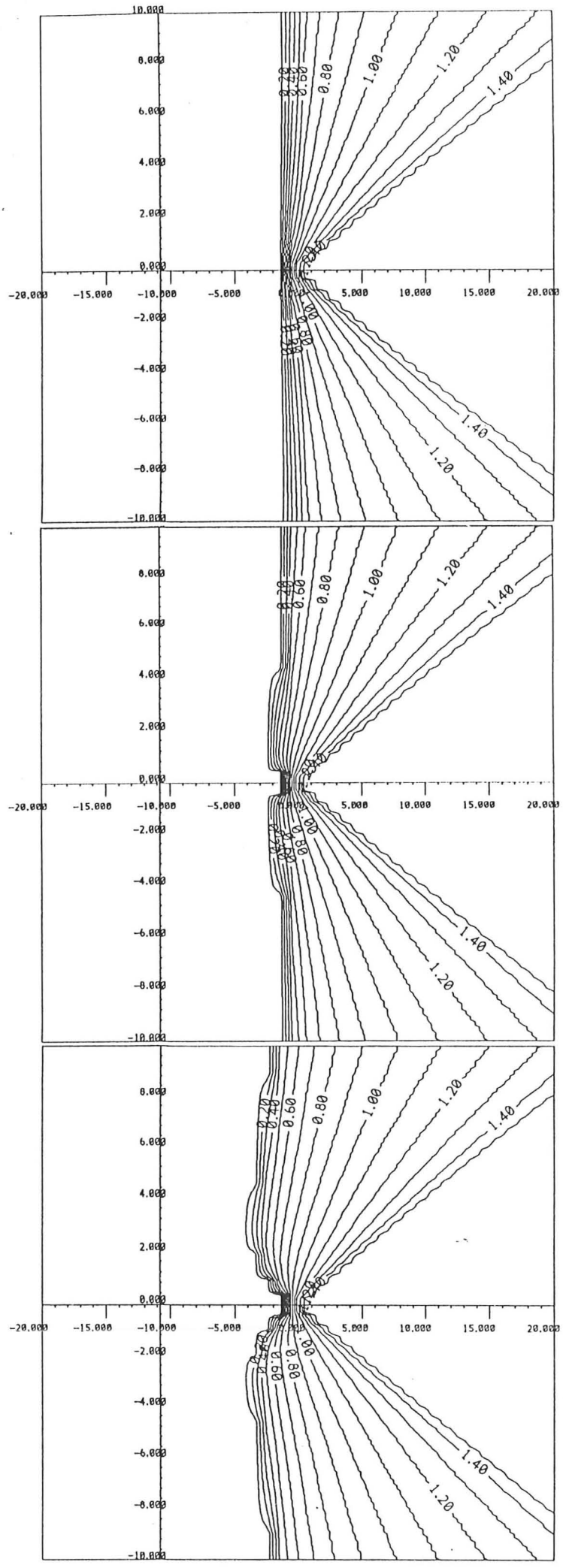

Fig. 7.3: Contour plots of ϕ_{max} against ε' (horizontal axis) and d_0/θ (vertical) for three values of the cut-off length (2, 1 and 0.5 from to to bottom). In each case there is a half-plane to the left corresponding to the channel phase, and a triangular wedge of washboard phase to the right, but the behaviour of the central region becomes more conspicuous as the cut-off is shrunk.

nature and possible realism of the terrains produced requires a return to numerical simulation, which is covered in the next chapter.

References

[1] D.M.Tetzlaff and J.W.Harbaugh, *Simulating Clastic Sedimentation* , (Van Nostrand Reinhold 1989)
[2] R.Leheny and S.Nagel, Phys. Rev. Lett. **71**, 1470 (1993)
[3] C.P.Stark, Nature **352** (1991)
[4] S.Cramer & M.Marder, Phys. Rev. Lett. **68**, 205 (1992)
[5] S.A.Schumm, *The Fluvial System*, (Wiley-Interscience 1977)
[6] K.Richards, *Rivers: Form and Process in Alluvial Channels*, (Methuen 1982)
[7] W.Nemec and R.J.Steel, *Fan Deltas: Sedimentology and Tectonic Setting* (Blackie, 1988)

Chapter 8: Results(3)

8.1 Changes to the simulator

The simple and local nature of the change made to the model in chap.7 minimised the amount of work involved in altering the simulator to fit: the code was simply altered to multiply the amount of sediment flowing out of the downstream end of each bond to be $(1+\varepsilon)$ times the amount flowing in at the upstream end , as illustrated in fig. 8.1(since it can always be removed by scaling the other parameters, the lattice space is taken throughout to have the value 1. If it is written in explicitly then the above becomes $\Delta Sediment = \varepsilon Sediment \Delta x$, which has the desired limit). This has the drawback that although very simple to code, and making practically no increase in program size, the naive implementation does inflict an appreciable performance penalty, since it is necessary to ascertain when updating each lattice-point what the direction of flow down each bond is. Since this occurs in the innermost loop, and since conditional execution often has a strong adverse effect on speed, it would in any future update to the simulator be worth finding a more efficient way round this (discussed further in Chap.9), but at the time the speedy availability of a solution which could easily be shown to do the right thing was more important.

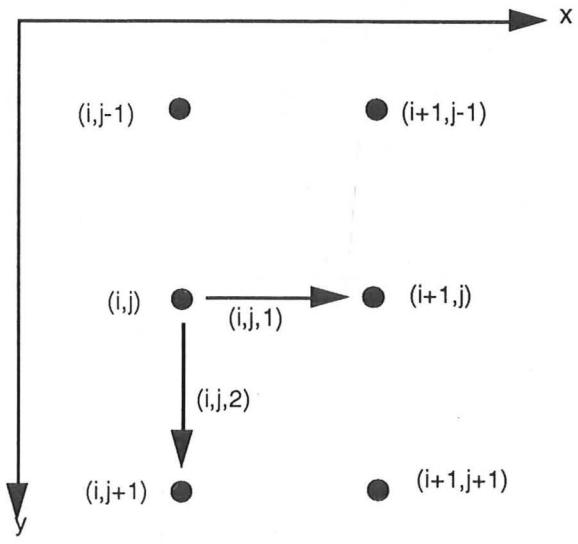

Flux along (i,j,1)=
-(d**3/2)*dx/(dx**2+dy**2)**1/4

Where: d= (d(i,j)+d(i+1,j))/2
dx=H(i+1,j)-H(i,j)
dy=(H(i+1,j-1)+H(i+1,j+1)-
H(i,j-1)-H(i,j+1))/2
H(i,j)=h(i,j)+d(i,j)

The sign of the flux is used to determine whether the flow along (i,j,1) is from (i,j) into (i+1,j) or vice-versa, and the sediment contribution *for the destination point only* is multiplied by $(1 + \varepsilon)$.

Fig.8.1 Diagram of the revised difference scheme incorporating non-conservation of sediment.

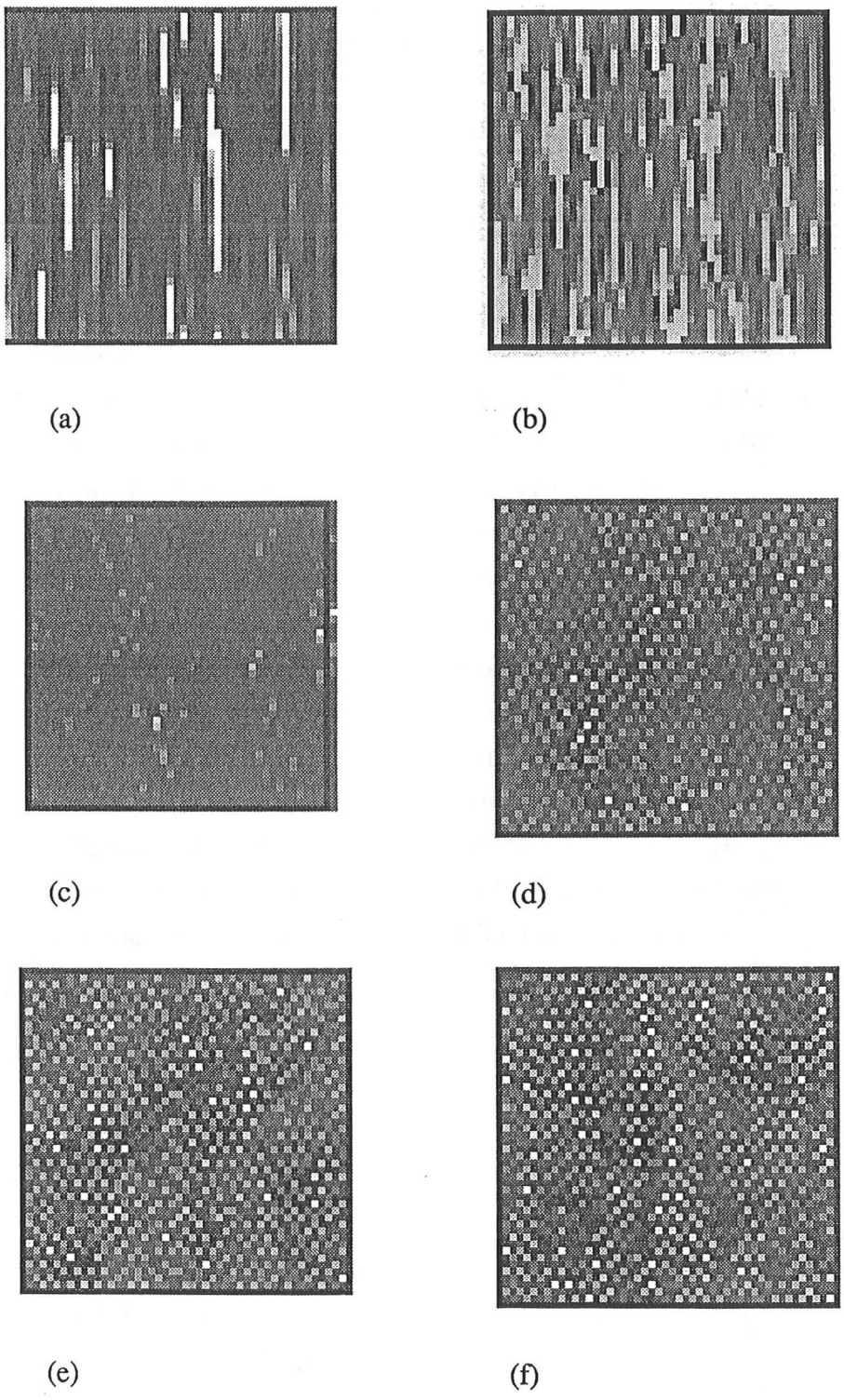

Fig. 8.2: Grey-scale elevation maps (c.f. fig.5.4) of simulation results on a 50x50 lattice for different values of ε' (other initial conditions as before).

(a) ε'=-5.0 (b) ε'=-3.5 (c) ε'=0.0 (d) ε'=3.0 (e) ε'=3.0

(f) ε'=25.0

8.2 Simulation Behaviour and Results Overview

The time-dependence of the simulation behaviour is qualitatively the same as that covered in the case of sediment-conservation in chapter 5: an initial exponential growth peaking and falling back to a value much lower than the starting point. The rate of sediment creation or removal does, however, affect the value of the plateau height. The exponent of the power-law noise produced is unchanged.

Figure 8.2 shows a collage of simulation results on 50x50 grids for different values of ε, but all at the same values of d_0, θ (i.e. along a horizontal cross-section through the surface shown in fig. 7.3). These are directly comparable with fig. 5.4, being again grey-scale representations of elevation with the mean height removed. They form a clear sequence broadly in line with the expectations from the stability analysis: under strong erosion deep channels are formed running almost directly downstream for most of the length if the grid, and as the value of ε increases, the angle to the downstream direction widens. One result of going beyond the linear regime is that dry land can now form in the erosive regime as channels deepen sufficiently to drain the rest of the simulation. Since flow-rate increases with depth, the deepest channels are dug fastest, and flow rapidly becomes dominated by a few major ones.

8.3 Analysis of Results

8.3.1 Angular behaviour

The simplest quantitative comparison to make between the simulation results and the analysis is that of the preferred growth angle as a function of ε'. This was measured on the simulation grids using a simple program that followed troughs down the slope by choosing at each point the move that leads to the lowest of the nearest neighbours of the current point. The average slope is removed so that sideways moves may be chosen (necessary in the case of washboard-like terrains) but moves that would be uphill are disallowed. The program keeps a total of the horizontal and vertical distances moved, and uses these to compute the mean angle of travel. The results of this are shown in fig. 8.3

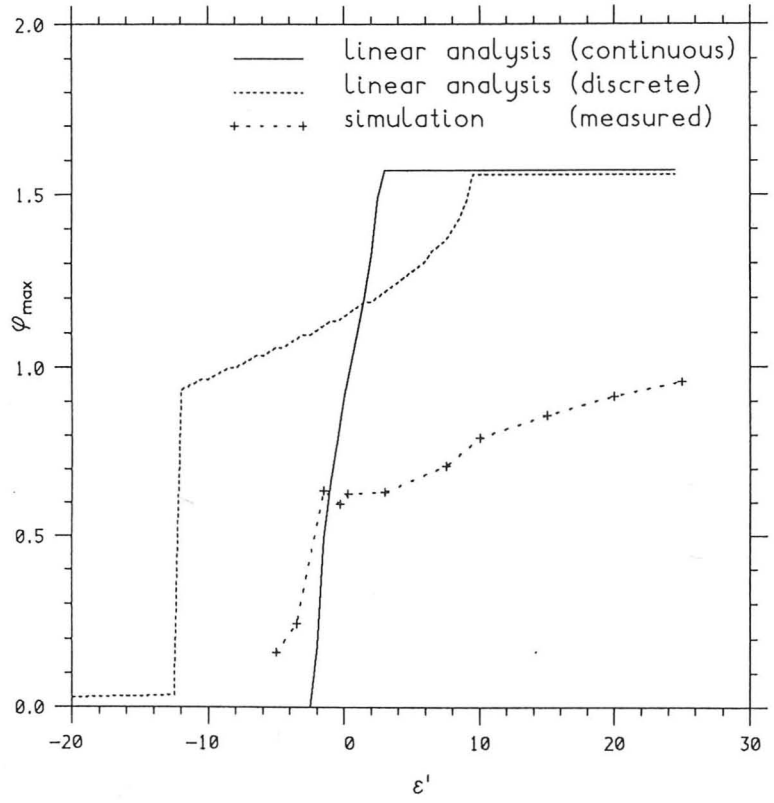

Fig. 8.3: The angle of fastest rill growth (ϕ_{max}) shown as a function of the scaled erosion parameter (ε') for the three cases of
(a) linear analysis assuming a continuum (solid line)
(b) linear analysis allowing for a non-zero lattice spacing (close-dashed line)
(c) measured simulation results (spaced dashes)

Also plotted on that figure for comparison is the predicted curve from the stability analysis. Two main points emerge:

(i) There is indeed a transition in the simulated results, and going from erosion to deposition its onset occurs quite close to the point predicted : the measured curve starts to rise sooner and more gently than the theoretical one, but from $\varepsilon'=-2$ to $\varepsilon'=0$ the two are very close together.

(ii) Once the deposition regime is entered, the behaviour in the two cases diverges. The predicted angle continues to rise sharply, reaching $\pi/2$ by $\varepsilon'=3$, while the measured value has a plateau of $\phi_{max.} \approx 0.65$, from which it then rises gradually, to nearly 0.9 by $\varepsilon'=25$ (the highest value tried). While the appearance is that the value of $\pi/2$, and hence pure washboard behaviour would eventually be reached, the transition has been broadened by about one order of magnitude, and this specifically in the region above $\varepsilon'=0$.

The two major differences between the simulation and the stability analysis are the fact that non-linear behaviour becomes significant, and the move from a continuum to a lattice. Of these, the latter seemed the most likely cause for the discrepancy: it had already been noted (chapter 5.2) that in the $\varepsilon'=0$ case changing the lattice geometry (from square to triangular in that case) significantly altered the rill angle, although the grids produced were otherwise similar. This was coupled with the expectation that if the lattice were to cause such a plateau it would be at an angle close to $\pi/4$, which was broadly consistent with observation. The next step was then to extend the stability analysis to allow for the replacement of derivatives by finite-differences on a square lattice. The working for this is essentially similar to that in the continuum case, and some details of the working, along with the result, can be found in appendix C.

The predicted angle given by this second linear analysis is also plotted on fig. 8.3. It can be seen that the correspondence between the new predictions and observation is both better in some ways and worse in others: the predicted curve now includes the feature of an initially sharp rise suddenly levelling off and then beginning to rise again, although the plateau value is higher than observed (0.95 *vs.* 0.65), and the slope in the analysis continues to increase such that $\pi/2$ is reached with the curve almost vertical again, the transition having been broadened, but less than in the simulated case. Overall these features do represent a definite improvement in the fit between theory and experiment, as expected.

What was not expected was that the prediction of the lower edge of the transition is now drastically worse: against a continuum solution value of -2.2 and an observed value for the start of the sharp rise at -3 (although the first signs of the transition are already appearing at the lowest value used of -5), the 'corrected' analysis has the steepest part of the transition occurring at -10.

One other region in which the new analysis fits the measured data better than the original is that it no longer has a region of ε' for which there are no unstable rill angles. The growth rate is still largest for large values of $|\varepsilon'|$, going through a minimum near the transition, but that minimum is now positive, a fact in line with the observation that the simulation failed to detect any region of stability. Furthermore, the region of least instability, like the transition in rill angle, has been shifted into the erosive regime, occurring now close to $\varepsilon'=-2.3$. Of the simulations, that at $\varepsilon'=-1.5$ showed the slowest growth, producing the least surface relief by the end of the run, (see the reduced contrast compared to the other parts of fig. 8.2). It seems reasonable then to hypothesise that as with the transition point, the non-linear effects in the simulation cause the range of least instability to be moved to higher ε' compared to the lattice analysis, and that this is the effect being observed. The overall conclusion thus seems to be that the real behaviour shares features of both the continuum and lattice versions of the linear analysis, with the apparent failure to fit one or the other consistently being due to the fact that the full equations being simulated are non-linear and that the effect of this on behaviour cannot be neglected.

8.3.2 Features of the Power Spectra

The other main sources of information in attempting to characterise the two phases and the changes occurring at the transition were the power spectra, both of the terrain and of the water surfaces. Figure 8.4 shows a selection of the full 2-D power spectra, for a different values of ε', along with the ratio of the water surface power to the terrain power at each point: if the results from the linear regime were applicable, this would fit $|A|^2$, with A being the linear response calculated in chapter 3. This is shown for comparison, and it can be seen that in some cases the resemblance is close. Regarding the power spectra themselves, those for the water surface are generally easier to interpret, being less noisy. The

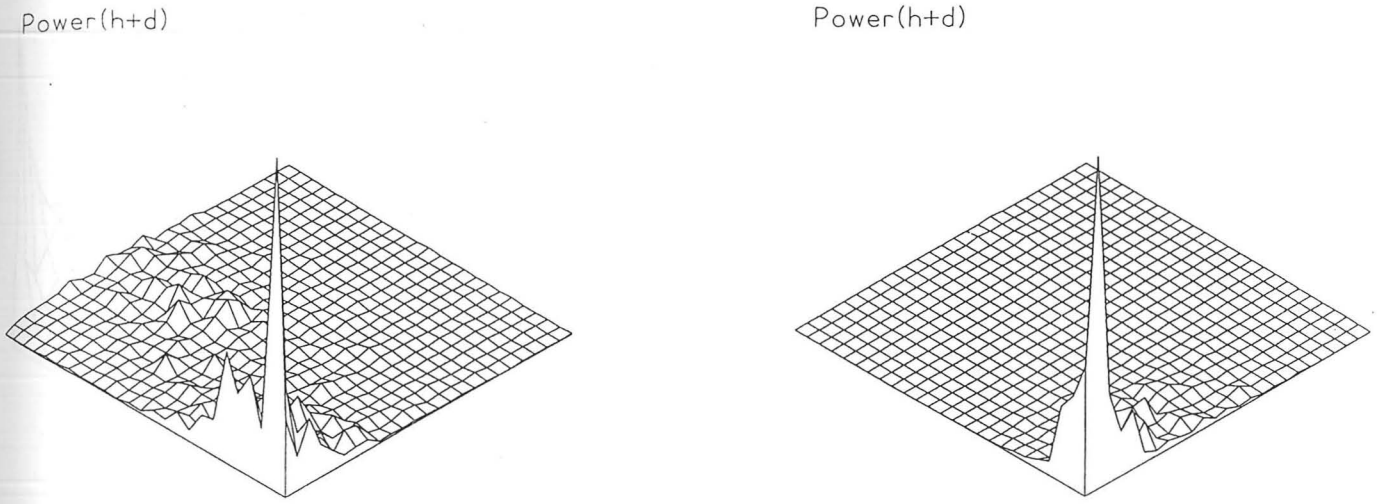

Fig. 8.4 (i): 2-D spatial power spectra for the water surface (top) and terrain surface (bottom) at $\varepsilon' = -0.3$ (left) and $\varepsilon' = 20.0$ (right).

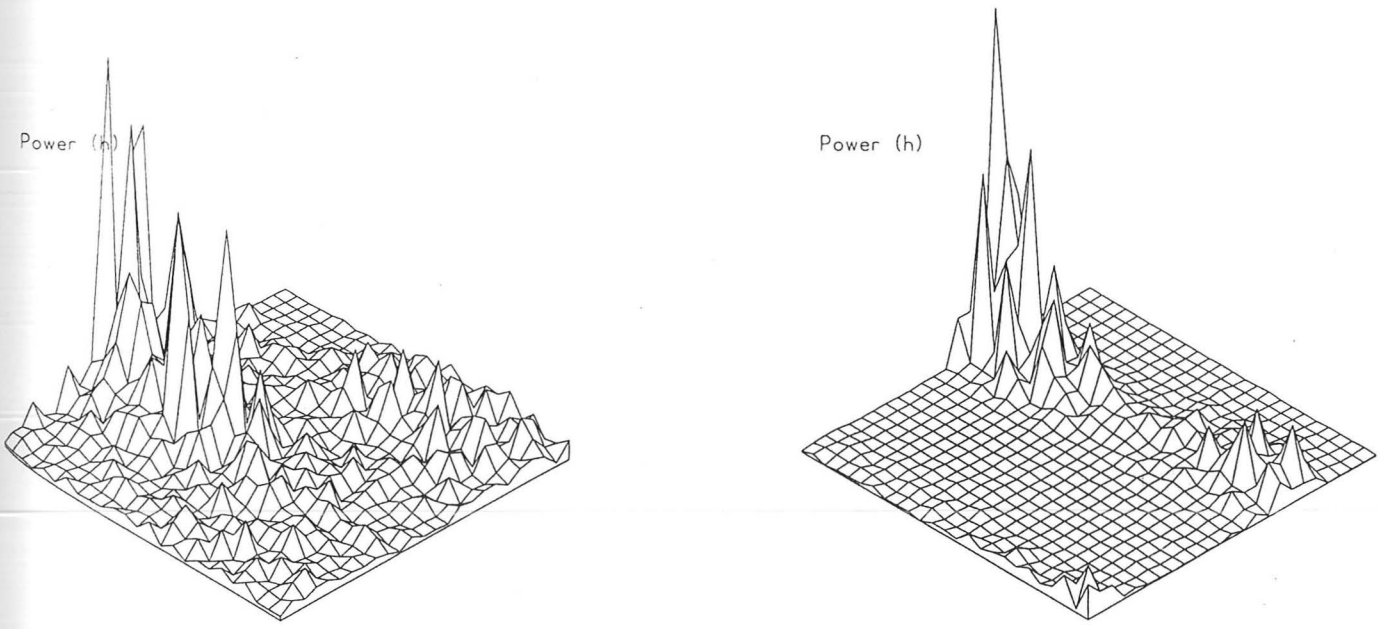

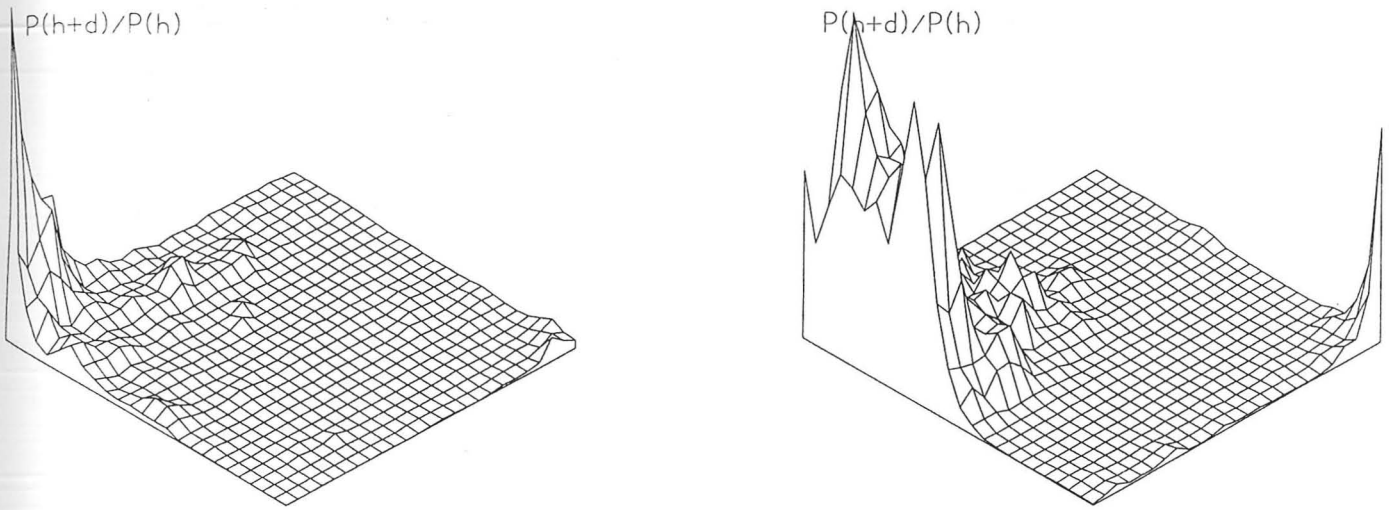

Fig. 8.4 (ii): At the top, the ratio of water:terrain power spectra for ε'= -0.3 (left) and ε'= 20.0 right. At the bottom is the linear analytic result for comparison. The fact that there is a noticeable resemblance at least for ε'= -0.3 allows interesting speculation as to whether this could be used to calculate approximate solutions in the non-linear domain.

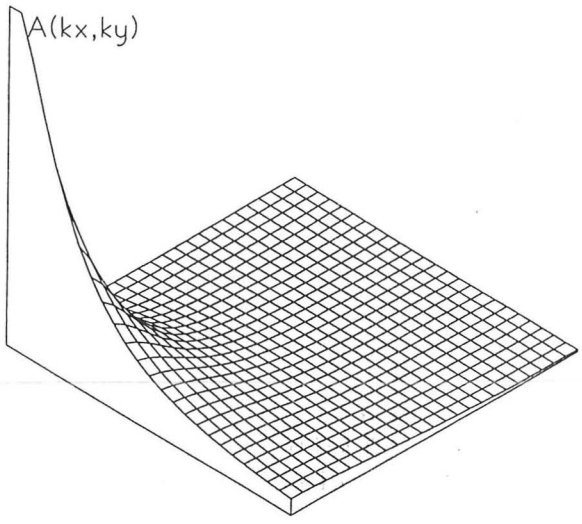

overall trend is from power spectra peaked at the origin and decaying smoothly (although not isotropically) with increasing |k|, for large positive ε', to ones covered in large amounts of noise as the erosive regime is entered.

Some features become clearer when these spectra are averaged over k_x (x being the downslope direction in all cases) and only the behaviour in k_y is considered. This is shown in fig. 8.5: one of the features now readily visible is that at high ε' the power-spectra for the water surface show a clear region of power-law decay, with an exponent of approximately -2.34 (c.f. [1-2]), the limits of this region closing in from both ends as ε' is decreased until in the channel phase the graph is close to flat. The terrain surface shows similar behaviour, although there is never clear power-law behaviour (it might seem that a small such region does exist in the topmost of the land surface power-spectra in fig.8.5, but it is too small and too noisy for any firm conclusion to be drawn). This is in line with the fact that the size of the linear response , |A| goes as $|k|^{-1}$ for large |k|, and hence that even in the non-linear regime the water surface might be expected to be smoother than the land, and hence show more power at long wavelengths. Also apparent in fig.8.5 is that in the channel phase the land and water power-spectra appear similar. This is also seen in the next figure, which shows the average value of k (defined simply as $\Sigma k_y P(k_y)/\Sigma P(k_y)$, with P being the power, and the sum over all k_y), again for both water and terrain. Here, moving from the washboard phase to the channel phase, the two curves, which for large ε' are parallel (with the terrain line being at the higher average k, as expected) move apart in the transition and then converge again, being superposed in the channel phase. Physically, this is due to the fact that in the channel phase, the removal of sediment is allowing rills to dig deep enough to drain most of the water and produce dry land. At the same time, the channels that capture most of the water deepen fast, while the others are effectively frozen when regarded on the same time-scale. The result of this is that the terrain is dominated by a few deep channels, with the rest being (by comparison) flat. Since the water drains of most of it, leaving only a very thin layer (which would ultimately drain to zero, although this can in fact take an infinite length of time, depending on the exact implementation of the water flow), the water surface becomes comparably flat in most places (where it follows the terrain surface closely), except for the deep channels, where it dips sharply as there is no longer enough water to cover them entirely. Hence

overall trend is from power spectra peaked at the origin and decaying smoothly (although not isotropically) with increasing |k|, for large positive ε', to ones covered in large amounts of noise as the erosive regime is entered.

Some features become clearer when these spectra are averaged over k_x (x being the downslope direction in all cases) and only the behaviour in k_y is considered. This is shown in fig. 8.5: one of the features now readily visible is that at high ε' the power-spectra for the water surface show a clear region of power-law decay, with an exponent of approximately -2.34 (c.f. [1-2]), the limits of this region closing in from both ends as ε' is decreased until in the channel phase the graph is close to flat. The terrain surface shows similar behaviour, although there is never clear power-law behaviour (it might seem that a small such region does exist in the topmost of the land surface power-spectra in fig.8.5, but it is too small and too noisy for any firm conclusion to be drawn). This is in line with the fact that the size of the linear response , |A| goes as $|k|^{-1}$ for large |k|, and hence that even in the non-linear regime the water surface might be expected to be smoother than the land, and hence show more power at long wavelengths. Also apparent in fig.8.5 is that in the channel phase the land and water power-spectra appear similar. This is also seen in the next figure, which shows the average value of k (defined simply as $\Sigma k_y P(k_y)/\Sigma P(k_y)$, with P being the power, and the sum over all k_y), again for both water and terrain. Here, moving from the washboard phase to the channel phase, the two curves, which for large ε' are parallel (with the terrain line being at the higher average k, as expected) move apart in the transition and then converge again, being superposed in the channel phase. Physically, this is due to the fact that in the channel phase, the removal of sediment is allowing rills to dig deep enough to drain most of the water and produce dry land. At the same time, the channels that capture most of the water deepen fast, while the others are effectively frozen when regarded on the same time-scale. The result of this is that the terrain is dominated by a few deep channels, with the rest being (by comparison) flat. Since the water drains of most of it, leaving only a very thin layer (which would ultimately drain to zero, although this can in fact take an infinite length of time, depending on the exact implementation of the water flow), the water surface becomes comparably flat in most places (where it follows the terrain surface closely), except for the deep channels, where it dips sharply as there is no longer enough water to cover them entirely. Hence

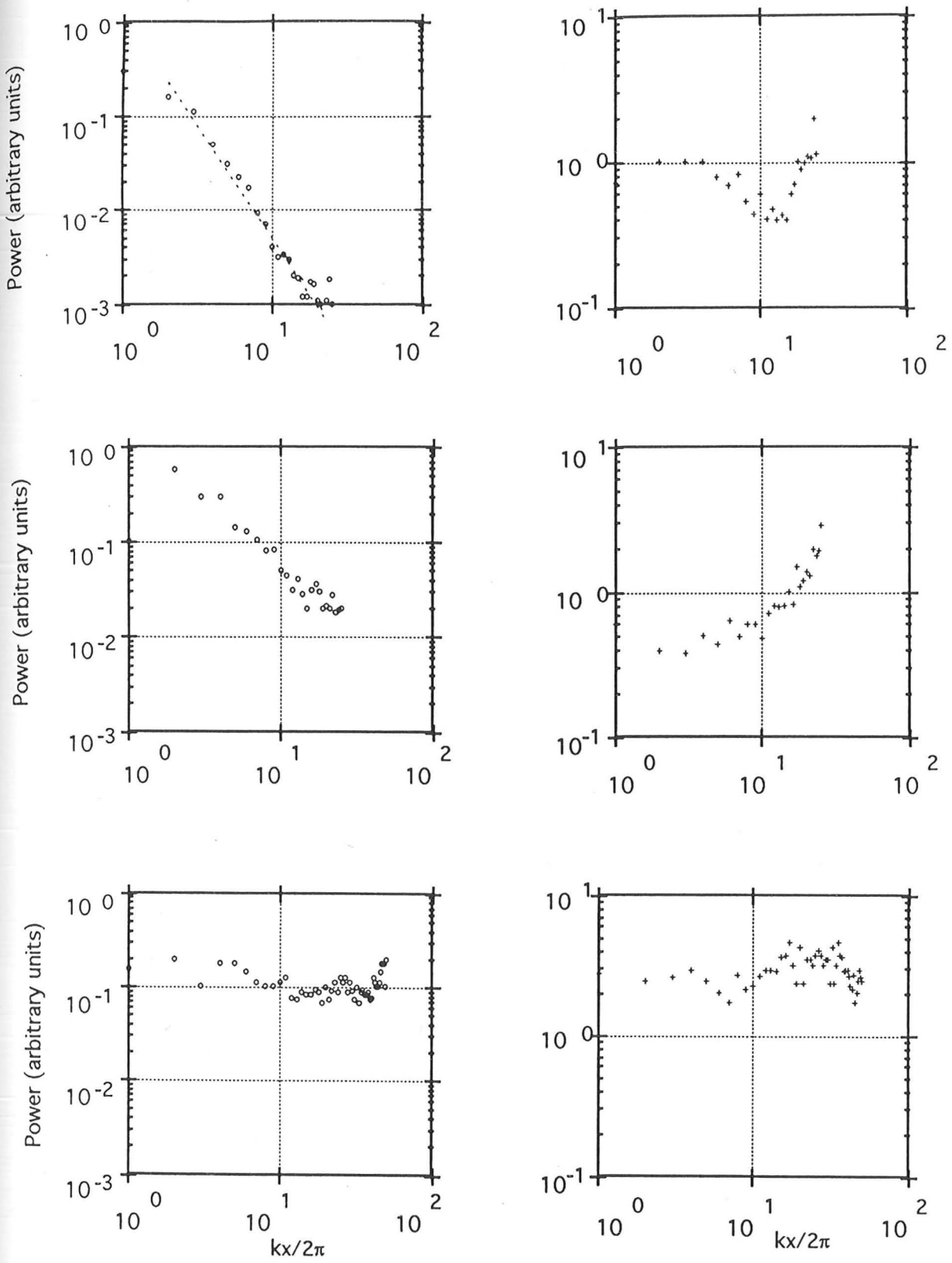

8.5: Power spectra of simulation data (averaged over y) shown for the water surface (left-hand column) and land surface (right-hand) at ε' values of 20.0, -0.3 and -1.5 (top to bottom). Noticeable features are:
(i) The clear power-law behaviour in the top-left figure, with a best-fit exponent of -2.34
(ii) The similarity between the two bottom plot, in the erosion regime where channels are starting to dominate water distibution.

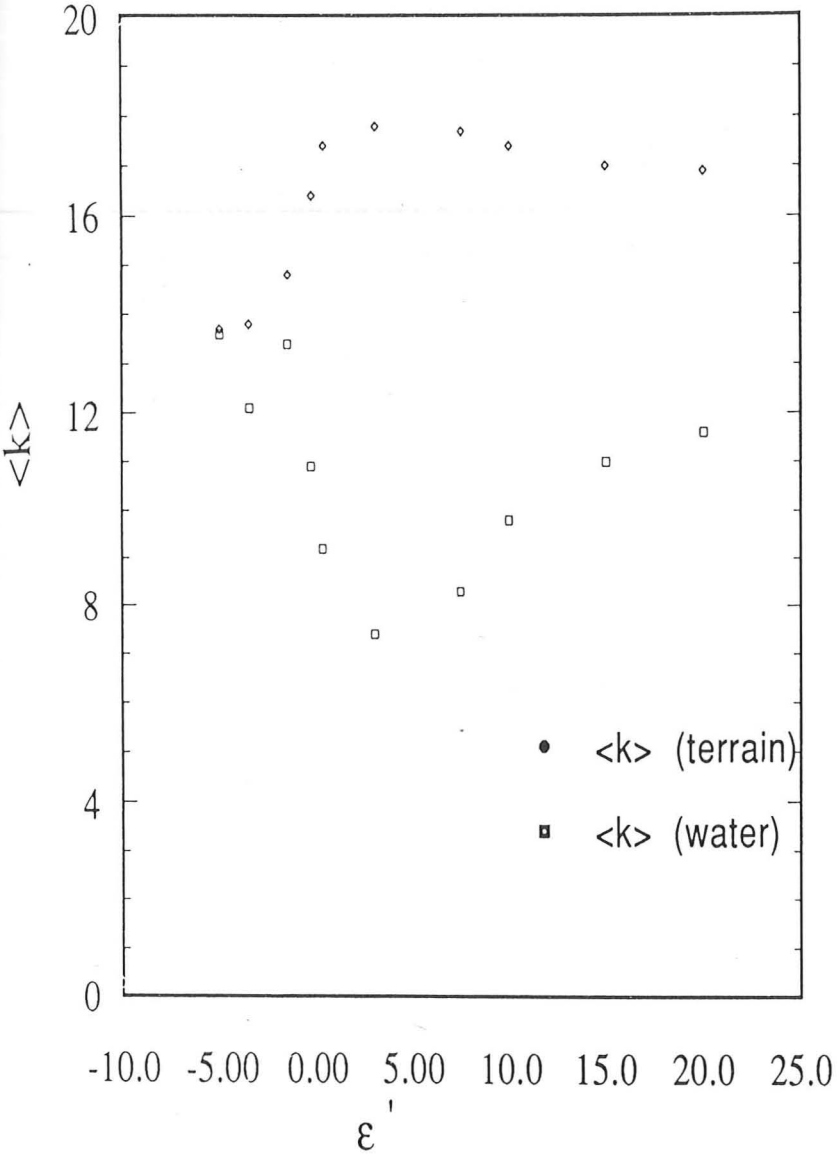

Fig. 8.6: Average wavenumber (as defined in the text) for the land surface power spectra (diamonds) and the water (squares), as a function of ε'. Both show a turning point corresponding to the transition.

the water surface, on a large scale, is forced to follow the terrain surface, and the two power spectra converge.

Another feature of figure 8.6 is that compared to the angular behaviour the transition appears to be sharper and to occur at a larger value of ε' (if the turning-points in the curves of $\langle k \rangle$ are taken to mark the point of change from sharp channel-like to washboard-like behaviour, corresponding to the switch from steep rise to plateau in the plot of angular behaviour). This is probably an effect of the fact that the angle measurements are dominated by the shortest possible wavelengths, of order the lattice vector (this is implicit in the algorithm used to measure the angle, which is entirely local, considering only nearest neighbours), while the mean wave-number plots clearly are not, since the values measured correspond to a larger lattice spacing. It was noted in the analysis in chapter 7 that reducing the cut-off wavelength simply scales the 'phase diagram' , resulting in a broadening of the transition., and this is consistent with the observed behaviour of phase transitions in general that the transition first becomes noticeable on the largest length-scales. Thus this difference is not an inconsistency, but simply the result of using two methods that probe the behaviour at two different length-scales.

8.33 Power Spectra and Roughness

The final set of measurements on the data obtained from this set of simulation runs was an attempt to measure a cross-stream coefficient of roughness. It was noted above that the power-spectra for the water-surface at large positive values of ε' showed a region of power-law behaviour. It can be shown that the power spectrum is given by the Fourier transform of the autocorrelation. From this, given the assumption that p is sufficiently negative, it can be deduced that if the power spectrum varies as

$$S(k) \sim k^p$$

, then a measurement of $\langle (H(x,y)-H(x,y+s))^2 \rangle$ would go as s^{-a} with

$$a = (p-1)/2$$

(see [1]) for a suitable range of s, dependent on the cut-off of the power-law behaviour in the spectrum (if the power-spectrum is power-law down to some cut-off k=K, then the above will hold up to $Ks \sim 1$). Figure 8.7 shows a plot of this: unfortunately, the above suggests that the power-law region would only extend to $s \sim 5$, and this is what is observed. Over this region, the fit to a straight line for the log-log plot is quite good (although it is not

obvious how meaningful this is with so few data points), and the measured exponent is 0.68, compared with a value deduced from the corresponding power-spectrum of 0.65.

8.4 Comparison with reality

The alteration of the equations to include non-conservation of sediment has clearly introduced a wide range of new behaviour, and it is natural to ask at this point to what extent these correspond to reality, and what measurements could be made. One of the comments in the previous chapter was that while the change from deep channels directly following the local gradient when sediment is being rapidly removed to shallower rills running at much larger angles where it is being added seems physically sound, there are no obvious examples in nature of a proper washboard phase. The work covered in this chapter, however, has failed to produce evidence that such a phase appears. There are strong arguments to suggest that the lattice on which the simulation is performed plays a large part in this, and the linear analysis performed with a finite grid spacing partly bears this out, but even so the simulated results remain in the plateau region far longer than that analysis predicts. While it may well be that this is purely a result of the interaction of the actual non-linearity of the model with the presence of a lattice, it seems at least possible that once the non-linear terms are taken into account the phase transition is genuinely asymmetrical even in the continuum. If it were the case that while small negative departures from exact sediment balance produced a sharp transition to channels a positive departure only gradually pushed behaviour towards the washboard phase then the behaviour of the model would seem more realistic than suggested by chapter 7. Unfortunately, without some suitable approximation to a continuum solution outside the linear limit this is speculative.

Certainly it seems to be the case that fluvial features where heavy deposition is occurring, such as deltas and outwash fans do favour numerous shallow channels with wide branch angles [3], but one of the basic problems in comparisons with real systems is determining ε' for those systems. While obviously material is conserved in such systems ε' could still be usefully defined as the ratio of the quantity of material eroded or deposited in a given area to the quantity carried through (which is what it was intended to represent) with the expectation of a meaningful

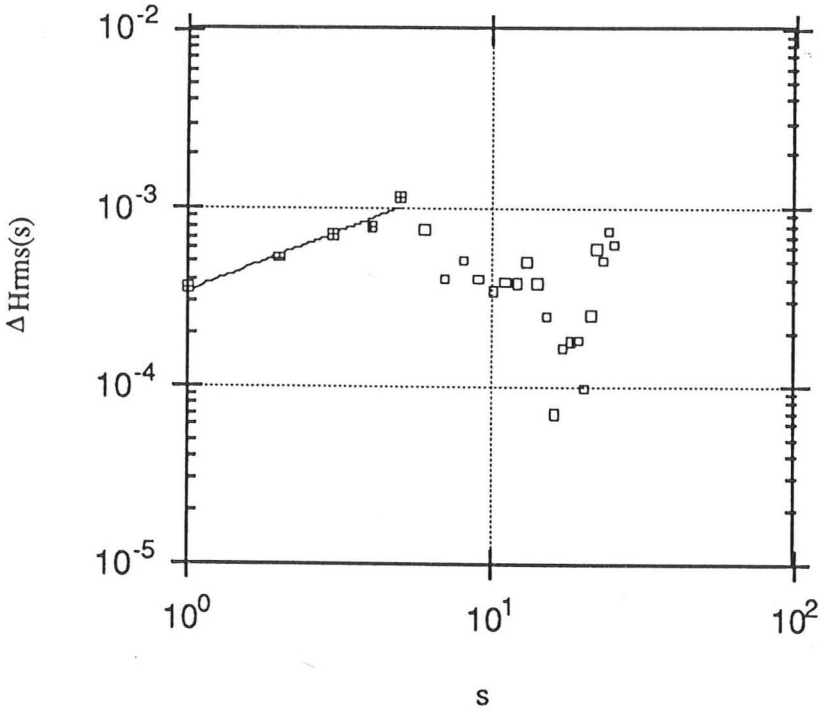

Fig. 8.7: a plot of $[H(x,y) - H(x,y+s)]_{rms}$ showing approximate power-law behaviour at low s, with an exponent of 0.69. (The failure of the power-law behaviour for s>5 here is consistent with the failure of power-law behaviour at low k in the power-spectra).

comparison, in practice the data needed to find this ratio would be unlikely to be available for natural systems (for a flume bed, on the other hand this might well be practicable).

Channel angles are appealing because they are easily measured from aerial photographs which are readily available, but most other comparisons with measurements made here would depend on digital elevation maps of suitable areas. Given such maps and the resources to process what would be very large amounts of data, a number of other possibilities would open up. One would be to remove the need for an estimate of ε' by considering two variables both dependent on it. For example, if $\langle k \rangle$ were plotted against channel angle ϕ_{max}, using the information in fig.s 8.3 and 8.6 the result should be a curve parametric in ε', and given both digital maps and photographs of a number of real systems with a suitable variety of erosion/deposition conditions it would be essentially straightforward to see if they fell onto a similar curve.

The roughness exponent estimated in 8.3.3 would likewise be highly useful were it measured for the land surface. Unfortunately, only the water surface, with its much clearer power spectra, yielded any meaningful estimate, and while elevation measurements for a suitable water may exist they would certainly be far rarer. In principle with suitable approximations a value of roughness exponent for the land surface could be estimated (since the linear response of the water surface to the land underneath is known) but this would be of uncertain validity.

Overall then, the modified model produces a range of new behaviour much of which could in principle be compared with real systems.

References

[1] J.Huang and D.L.Turcotte, J. Geophys. Res. **94**, 7491 (1989)

[2] W.I.Newman and D.L.Turcotte, Geophys. J. **100**, 433 (1990)

[3] W.Nemec and R.J.Steel, *Fan Deltas: Sedimentology and Tectonic Setting* (Blackie, 1988)

Chapter 9 : Summary and Possible Future Directions

9.1 Overview

This chapter divides naturally into two main parts: an outline of what this thesis has covered, and a review of possible directions in which this work could be taken. That in turn comes under three main headings:

(a) Practical improvements: the simulator has a number of drawbacks in its present form, and in at least some cases it is clear in principle how these might be remedied.

(b) Further work using the current model: there remain questions about the model in its present form which might usefully be answered.

(c) Extensions to the model itself.

This is in turn followed by a very brief summary of personal views on the merits of extending the current form of the model, given its performance to date.

9.2 Outline of Work

9.2.1 Chapters 1-4

After the introductory material in chapter 1, the model was introduced in chapter 2 in terms of a set of equations describing the movement of both water and sediment. The motivation behind the form of these equations being simplicity in so far as this was consistent with physical plausibility (backed by reference to empirical work). The analysis in chapter 3 showed that despite their simplicity the equations used did result in interesting behaviour, namely the instability of a flat sediment surface, that was consistent with experimental observation. The analysis also showed that further simplification of the model was possible while still retaining the essentials of this behaviour, and the simplified version was used for all subsequent work. As outlined in the next chapter, the model was then implemented as a finite-difference simulation, which despite some limitations implicit in the way it was written

was tested and shown to reflect accurately in most ways the behaviour of the analytic model in the regime where the two are comparable.

9.2.2 Chapters 5-6

Chapter 5 presented the results of these simulations, looking at the conspicuous features of the terrain produced and then considering the correspondence to real systems: the overall resemblance to beach rills (which it was argued are produced under analogous conditions) and the quantitative features of island-size distribution which was compared to that of braided rivers. It was noted that the island size generally showed a power-law distribution, and that the apparent exponent in both cases, varied as a function of the fractional water coverage of the channel. The fit here was not exact (and the number of data points not as great as would have been desirable for the comparison) but the overall proximity of the measured data points to the simulated curve of island-size exponent was encouraging.

The following chapter then focused on one particular experiment, performed by Prof. Caroni of Trieste University [1], which was in many ways a physical counterpart to the simulations performed. A number of differences were noted, due partly to the fact that the two experiments (physical and computational) were not set up to explore the same limits of behaviour, and partly because the simulation contained features such as periodic boundaries that have no counterpart in a real system. Nonetheless, some positive facts did emerge: the prediction of flow depth from rill angle based on the theoretical model gave plausible answers , and there was a qualitative resemblance between the measured and simulated terrain cross-sections. This latter was supported quantitatively by the fact that both exhibited self-similarity (albeit over a small range of length-scales), and were shown to have the same box-counting dimension to within the accuracy achievable.

9.2.3 Chapters 7-8

Chapter 7 went on to consider the limitations imposed by the periodic boundary conditions, and suggested a method of evading some of these by the selective non-conservation of sediment. The analysis of chapter 3 was extended to include this new feature, which was shown to result in the existence of two separate regions of behaviour, separated by a distinct phase transition as the parameter controlling the non-conservation (ε') was varied,

the measured change being in the angle of fastest rill-growth. Furthermore, by including the effects of depth and slope in the analysis, a two-dimensional phase diagram was produced.

The extent to which this still occurred in the simulated version (since it had been noted earlier that the use of a discrete grid in the simulation resulted in changes of behaviour that could not be ignored) was the subject of chapter 8. Here a series of simulation runs was used to explore a one-dimensional slice through the phase-diagram mentioned. It was found that he transition did still occur, although both its width and onset changed it. A number of measurements in addition to the rill angle were made on the resulting terrain surfaces, and these all showed changes over a region consistent with the position of the transition as originally located. These measurements included a tentative measure of a roughness exponent in one of the two phases.

9.3 Possible Extensions

9.3.1 Practical improvement

As stated in the overview, the simulator itself has a number of limitations which, if corrected, would make it far more efficient in use of processor time, and simpler to use. The most important issue by far is the instability inherent in the use of an explicit update scheme for the sediment. This is partly resolved by the use of an adaptive time-step, which does manage to avoid the growth of instability. The price paid for this is that the entire grid evolves at a rate limited by the least stable bond at any time, and there would be considerable speed gain if the scheme were changed so as not to suffer from numerical instability. It is worth noting that removing instability does not entirely solve the problem of some sites evolving much faster than others: in an implicit method, the answer obtained if the time-step is too large compared to the rate of change is still inaccurate, but the error will not grow without limit bringing the simulation to a stop. However, since the point of interest in these simulations is the overall nature of the terrain rather than any specific detail, such loss of accuracy would be acceptable as long as it did not statistically affect the outcome. The stability of methods for solving non-linear P.D.E.s has been widely studied [2] and a number of methods exist which are either stable or less restrictive of the time-step. Some of these are quite specialised, but a

number, of which the most obvious candidates would the hop-scotch schemes originally analysed by A.R.Gourlay [2-4], could certainly be implemented without excessively complicated alterations to the simulator. This class of schemes has the attraction of combining useful stability and efficiency with conceptual simplicity in a way that would make for a worthwhile addition to the program.

9.3.2 Further use of the existing model.

One of the limitations of the present work is that due to the time requirements of both simulation and data reduction it has explored only a limited amount of the available parameter space. Firstly, the parameters α and β original defined in equation 2.5: these were chosen to be in the centre of the range of empirically fitted values found in the literature[5]. A few runs were made at different values at the edge of the range (specifically at the highest and lowest values of α/β consistent with the references checked) in the sediment-conserving case to see whether the simulation results were sensitive to these choices, and no significant differences appeared, but a fuller investigation the effect on behaviour could be interesting. For example, equation 3.5 predicts a simple dependence of the angle of fastest growth on these values. However the simulations performed so far have shown that the agreement of the analytic and computational results on the behaviour of ϕ_{max} is only approximate, so the effect of changing the values of these parameters in the simulations is still unclear.

Similarly, the phase diagram illustrated in fig. 7.3 has only been partly explored: the results obtained correspond to a section through it at fixed θ/d_0 and variable ε'. Given the differences found between the analytically predicted cross-section and that obtained, it would be interesting to see at least one section running at right angles (i.e. constant ε') and possible several in each direction to determine how the overall shape of the phase diagram is affected.

Finally, there are a number of comparisons with existing models and real systems that would require the program to be slightly altered so as to allow use of open boundaries. This would allow more detailed assessment of the resemblance to such existing features as braided streams (chap. 5). Also, by measuring the instantaneous rate of deposition or erosion at points on the

grid, along with the sediment flux at those points, it would be possible to calculate values of ε' and, by comparing the terrain morphologies produced with those from the simulation with closed boundaries at the same values of ε', to decide on the effectiveness of using non-conservation of sediment to model varying carrying capacity. This method has, as discussed, the advantage of efficiency since it produces directly comparable erosion/deposition conditions over the entire simulation grid, and such an assessment of its validity would be useful given its potential advantages.

9.3.3 Extension to the Model

Beyond the issues of implementation, the model as it stands has what seem to be two major limitations built in to its present form. These are the dominance of high wavenumbers and the single sediment type.

The dominance of high wavenumbers is apparent from the analysis in chapter 3, where the rate of fastest growth is seen to increase monotonically with $|\mathbf{k}|$. In the simulation this was not a problem with closed boundaries as the lack of a sediment sink prevented channel deepening, and the resulting landscape cross-sections bear a plausible resemblance to real ones (chapter 6) when allowance is made for vertical scaling, including having the same box-counting dimensions to within experimental error. In the work of chapter 8, however , the 'ultraviolet' problem became a serious issue since in the channel phase the removal of sediment does allow deepening without limit. This gives the physically implausible result of a channel of which the filled part is several times deeper than it is wide, whereas in reality it would be expected to approach a well-defined shape determined by the flow conditions and maintain that profile.

In real systems three main physical effects oppose the formation of very narrow, deep rivers. The first of these is the tendency of turbulent mixing to spread the sediment load. Although in detail this effect is dependent on the full 3-dimensional flow patterns, attempts to represent it as a non-linear diffusion-like term give results that are in some ways realistic even when it is the only factor controlling the depth/width ratio [6]. The second is that even in the absence of erosion, the banks, particularly if composed of soft sediment, will tend to collapse under gravity once they exceed a critical angle. This

effect has been found to influence the resulting topography significantly[7]. The third effect is that the sides, as well as the bottom (if the channel cross-section is considered in idealised form as rectangular) produces drag forces that reduce the flow speed, so that a very narrow channel will not be favourable. This could be represented either by adding a viscosity-like term that produced momentum transport between adjacent flux lines, or in the simplest possible way by altering the flow equations originally put forward in equation 2.1 so that the flow speed is no longer controlled by the vertical distance to solid ground (the depth) but by the shortest distance, as shown in fig. 9.1. The corresponding equation for the water flux would then be

$$\mathbf{q} = -w^{1/2} d\nabla(h+d)/|\nabla(h+d)|^{1/2}$$

with w being the distance of clear water to the nearest point on the sediment surface, and d the depth as previously defined.

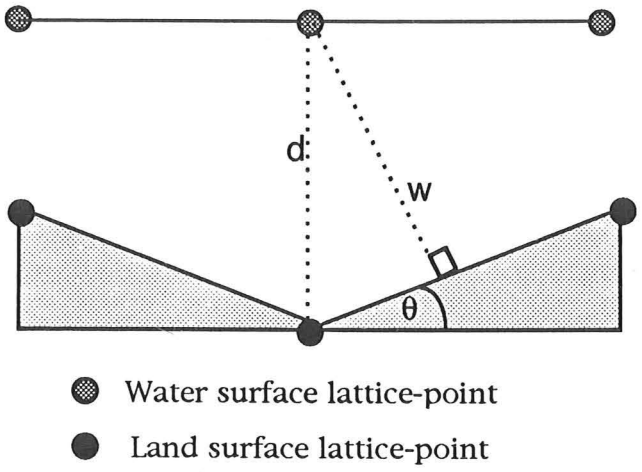

Fig. 9.1: Cross-section through a hypothetical terrain, showing suggested alteration to the flow model (flow is at right angles to the page). If the flow velocity depends on w rather than d, channels with steep slopes will deepen less rapidly. As $\theta \rightarrow \varepsilon$ the original case analysed in chapter 3 is recovered to 1st order.

Of these solutions it is this last one that seems to fit most easily into the context of the existing model. It has, for example, the same form in the limiting case of a flat sediment surface, and the entire stability analysis would remain the same since the changes would be second order (if the two halves of the channel are at an angle θ in fig. 9.1 then $w=d.\cos\theta$), and would have the

desired effect on channel profiles, as well as having a clear physical motivation. The cost in computational intensiveness of this change would, however, be considerable since w would now need to be calculated in addition to d., although the approximation that only the terrain between the point to be updated and its nearest neighbours need be considered in finding w would reduce this greatly (it is clearly possible to find cases in which this is false, see fig. 9.2, but this rule might well prove good enough to use in some cases).

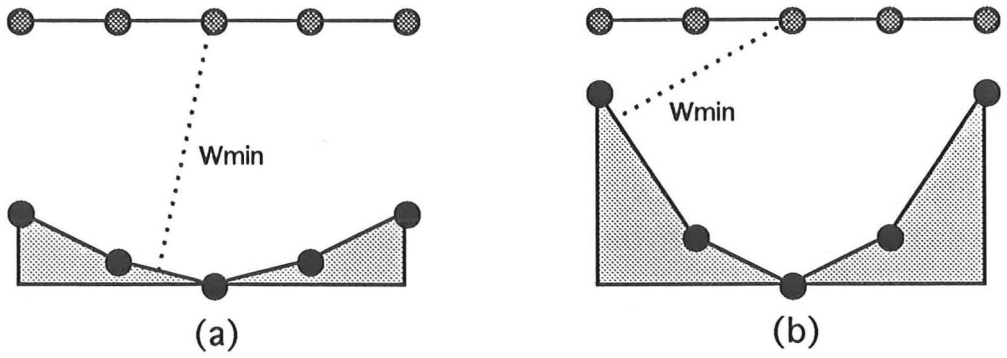

Fig.9.2 The assumption that w_{min} for a site can be found by inspecting only nearest neighbour sites will frequently hold good (a) but if the channel is too deep compared to the total water depth, it will fail (b).

While the model already appears to capture some aspects of sedimentary behaviour in, e.g. braided rivers and freshly eroded sediment surfaces, it obvious needs extending to multiple sediment types if it is to address other issues involved in river-bed evolution such as the sorting processes that occur in river bars and in during floods. It is common to restrict models to two sediment types, usually referred to as 'sands' and 'fines', but in fact the generalisation to more types would raise far fewer conceptual issues than the initial generalisation from one to two. This is due to some fundamental aspects of the model as used so far: the assumption built into it in chapter 2 is that a flux of water has a carrying capacity for sediment which is a function of flow conditions and which entirely determines the behaviour of sediment: if the load exceeds capacity at any point sediment is deposited while in the opposite

case it is eroded. This is conceptually straightforward, and lends itself easily to further simplification if the assumption is made that the adjustment is rapid (see chapter 3). The way this should be extended to two sediment types is not so obvious: the first step would be to define a carrying capacity for each sediment type (with probably the same flow dependence but different magnitudes, the expectation being that fines are more readily transported than fines). Then a number of questions need answering: do the capacities and loads of the two types interact, if so in what way, and, above all, what is the physical motivation for making them interact in this way?

To understand these problems consider a volume of water flowing down a channel that is uniform except for the composition of the bed, which consists of one stretch of pure sand, followed by another of pure fines. At the upper end of the channel the load will consist entirely of sand, exactly matching the capacity, while at the lower end the expectation (based on observation of real systems) is that if the channel is long enough the load will consist almost entirely of fines, the sand having been deposited on the way down. This is readily understood if one regards the sediment transport as a dynamic equilibrium in which sediment is continuously being eroded and deposited [8], and a balance between load and capacity corresponds to the two processes occurring at equal rates. This viewpoint works well in the example above: the material being deposited has the composition of the sediment in suspension (initially sand-rich) while that being eroded has the composition of the bed (fines-rich) and so the replacement occurs. The problem is that in the single sediment case the two viewpoints (load/capacity balance *vs.* erosion deposition balance) are clearly equivalent: if the rates of erosion and deposition are only influenced by the flow conditions then the same flow conditions will results in the same sediment transport, making the use of a flow-determined transport capacity valid. In the two sediment case this is less clear: the sediment capacities must be made to interact so that the presence of one sediment in suspension decreases the carrying capacity of the other if the results are to be made similar to those expected from the erosion/deposition argument, and further allowance must be made for the fact that one of the two sediment types may not be available in the bed material, making uptake impossible. The process for adjusting sediment load would then work as follows

(a) If the load exceeds the capacity sediment is deposited, with composition equal to that of the load, until equilibrium is reached.

(b) If capacity exceeds load then sediment is taken up with composition equal to that of the bed.

The difficulty, of course, lies in making the carrying capacities interact suitably to give plausible results, and in the question: does this have any sensible physical basis?

It is possible to argue that it has: ultimately the basis for sediment transport is the dissipation of energy by the water flow, largely in small-scale vortices that contribute to keeping sediment in suspension. The amount of work that is available at this length-scale for supporting sediment particles is limited, and hence the expectation is that the presence of one type of sediment already in suspension would limit the uptake of another, and similar arguments can be applied to bed-load sediment. That said, it would not be trivial to go from these qualitative arguments to a consistent model of the interaction of sediment loads and capacities, and it could be argued that much of the conceptual clarity that made the load/capacity scheme appealing in the single sediment case would be lost. Overall then it seems that going over to regarding the system as two reservoirs of sediment (the bed, and the suspended material) of different composition that are continually exchanging material and whose equilibrium is dynamic would be a more promising approach.

9.4 Closing Comments.

Overall, the model that has been developed and explored in this thesis shows a range of behaviour (and offers the possibility of further aspects under conditions not yet tried, but considered in 9.3.2 above) which in addition to its inherent interest as a system, does appear to capture some aspects of sedimentary behaviour with some realism, despite its deliberate simplicity.

These include some statistical properties of braided rivers (to a first approximation), as well as the early stages in the evolution of a rill network (chapter 6). There is a clear argument that the realism of certain aspects could be improved by alterations that are, at least conceptually, fairly minor (see

9.3.3 (i)). At the same time, it would seem from the preceding discussion that although the next fundamental step, that of proceeding to more than one sediment type, could be grafted onto the present model, this might well involve a loss of clarity that would make it preferable to step back and reconsider sediment transport in terms of erosion and deposition as two separate processes rather than attempt to unify them through the notion of a sediment capacity, despite the success of this approach so far.

References

[1] E.Caroni, Preprint, Hydrofractals '93 conference, Ischia

[2] L.Lapidus and G.Pinder, *Numerical Solution of Partial Differential Equations in Science and Engineering* (Wiley-Interscience 1982)

[3] A.R.Gourlay, J. Inst. Math. Appl. **6**, 375 (1970)

[4] A.R.Gourlay and G.R.McGuire, J. Inst. Math. Appl. **7** 216 (1971)

[5] D.M.Tetzlaff and J.W.Harbaugh, *Simulating Clastic Sedimentation* , (Van Nostrand Reinhold 1989)

[6] S.Cramer & M.Marder, Phys. Rev. Lett. **68**, 205 (1992)

[7] R.Leheny and S.Nagel, Phys. Rev. Lett. **71**, 1470 (1993)

[8] J.R.L.Allen, *Sedimentary Structures*, (Elsevier Scientific 1982)

Appendix A: Extracts from the Initial Testing Results

These are not meant as a comprehensive overview of the testing performed, but provide an example of the sort of testing used and the accuracy sought.

Table 1a: accuracy achieved by the water solver after 200 iterations in calculating the response of the water surface to a sinusoidal perturbation of the sediment plane, of amplitude 1% of water depth.

$25*k_x/\pi$ (k_y=1)	$A^{(1)}$	$A^{(2)}$	$A^{(3)}$
2	0.410	0.448	0.419
4	0.772	0.792	0.783
6	1.063	1.091	1.076
8	1.286	1.315	1.301
10	1.446	1.482	1.459

(1) Analytic result
(2) Water solver with initial guess at time-step
(3) Water solver with refined time-step

The fact that the accuracy is poorest at longer wavelengths is consistently reproduced across all test runs, both in the amplitude (as above) and in the phase, as below.

Table 1b: accuracy in estimating phase of response to a sinusoidal perturbation.

k_x	ky	% error in phase
0.126	0.0	12.1
0.126	0.126	4.0
0.126	0.251	0.5
0.251	0.0	0.7
0.251	0.126	2.5
0.251	0.251	0.6
0.377	0.0	0.1
0.377	0.126	0.2
0.377	0.251	0.01
0.503	0.0	0.07
0.503	0.126	0.11
0.503	0.251	0.12
0.628	0.0	0.07
0.628	0.126	0.5
0.628	0.251	0.05

It is worth noting that in IBM single-precision the depth will only be stored to a little better than 1 in 10^7, and since the perturbation only amounts to 10^{-2} of that, one would not even naively expect to obtain accuracies of better than 1 in ^{5}.

Similar testing was used for th sediment transport (although less comprehensively due to greater computational expense), and gave similar results: that performance varies with wave-vector but no examples were found for which convergence failed (provided the time-step was sufficiently cautious). Accuracies achieved were of order 1%.

Appendix B: Source Code Listing for the Simulator

```
C*************************************************************************
C*************************************************************************
C
C                 SIMULATION VERSION 2.7
C
C Device 7 is main input, device 8 is the main output, 9 is the log file.
C
C V 2.7 has: harmonic depth mean
C            sediment transport
C            sediment non-conservation  (now fixed)
C            rectangular grid.
C
C*************************************************************************
C**** MAIN CONTROL CODE *************************************************
C*************************************************************************
C ****Section%1
C*************************************************************************
      REAL H(200,200),D(200,200),ALPH,BETA,D0,THETA,EPS,T,DL,DT,DTM
      REAL DMX
      INTEGER I,N,XSIZE,YSIZE
      COMMON/PARAM/ ALPH,BETA,D0,THETA,EPS,XSIZE,YSIZE
      COMMON/TIME/T,DL,DT,DTM,DMX
C
C Open log file for current run
C
        OPEN (UNIT=7,FILE='/tmp/NUM.DAT',STATUS='OLD')
        READ(7,*) N
        CLOSE (7)
       DO 1 I=1,N
        DL=0.0
        T=0.0
        OPEN(UNIT=7,FILE='/tmp/GNB10.DT',STATUS='OLD')
        READ(7,*) DT,DTM
        CLOSE(7)
        OPEN(9,FILE='/tmp/GNB10.SIMLOG',STATUS='UNKNOWN')
C
C Load parameters
C
        CALL PARS(ALPH,BETA,D0,THETA,EPS,XSIZE,YSIZE,DMX,6)
C
C Load (or create) simulation arrays
C
        CALL LOAD(H,D,XSIZE,YSIZE)
C
C Run simulation
C
        CALL PCHECK('MAIN   ',ALPH,BETA,D0,THETA,XSIZE,YSIZE)
        CALL RUN(H,D,D0,XSIZE,YSIZE)
C
C Save results and finish
C
        CALL SAVE(H,D,XSIZE,YSIZE)
        CALL DELTAS(H,XSIZE,YSIZE)
        CLOSE(9)
        WRITE(6,*) I
1       CONTINUE
```

```
            END
C
C*********************************************************************
C**** MAIN PROCESSING CODE ***********************************
C*********************************************************************
C**** Section%2
C*********************************************************************
C*********************************************************************
C RUN  is the top level, controlling the iteration
C (diagnostic code commented out)
C
        SUBROUTINE RUN(H,D,D0,XSIZE,YSIZE)
        REAL H(200,200),D(200,200),EX(200),X(200),TOTAL,A1,A2
        REAL D0
         INTEGER I,XSIZE,YSIZE,J
         LOGICAL NEW
         COMMON /CH/ NEW
         DO 2 J=1,19
C        WRITE(6,*) J
         DO 1 I=1,60
         CALL STEP(H,D,0)
1         CONTINUE
C          WRITE(9,*) 'Total water:', TOTAL(D,XSIZE,YSIZE)
          CALL REFIL (D,D0*REAL(XSIZE)*REAL(YSIZE),
     .                TOTAL(D,XSIZE,YSIZE),XSIZE,YSIZE)
          A1=AMP(H,XSIZE,YSIZE)
C          WRITE(9,*) 'Amplitude:',A1,' Diff.:',A1-A2
C          WRITE(9,*) 'Exp:',(A1-A2)/(A1*3.0E7)
          A2=A1
          IF (J.GT.15.OR..NOT.NEW) CALL STEP (H,D,1)
2         CONTINUE
        END
C
C*********************************************************************
C*********************************************************************
C STEP  updates the flow
C  W(I,J,N) stores the weights for the relaxation as follows:W(I,J,1) is
C the bond from (I,J) to (I+1,J), W(I,J,2) is that to (I,J+1).
C +++ The depth dependence has been altered in this version
C
        SUBROUTINE STEP(H,D,FLAG)
        REAL H(200,200),D(200,200),ALPH,BETA,D0,THET,DN(10),HN(10)
        REAL W(200,200,2),TD1,TD2,Q(200,200,2),D1,D2,D3,EPS
        INTEGER FLAG,I,J,XSIZE,YSIZE
        COMMON /PARAM/ ALPH,BETA,D0,THET,EPS,XSIZE,YSIZE
C
C Main control loops...
C
        DO 1 I=1,XSIZE
          DO 1 J=1,YSIZE
C
C Get surrounding values (corrected for b.c.s)
C
           CALL FETCH(H,HN,I,J,1.0)
           CALL FETCH(D,DN,I,J,0.0)
           DX=(HN(4)+DN(4)-HN(3)-DN(3))
           DX1=(HN(4)+DN(4)-HN(2)-DN(2))/2.0
           DY=(HN(5)+DN(5)-HN(3)-DN(3))
           DY1=(HN(5)+DN(5)-HN(1)-DN(1))/2.0
C
C Depth averaging courtesy of Dr. P.King
C
```

```
            D1=DN(3)**1.5
            D2=DN(4)**1.5
            D3=DN(5)**1.5
            IF ((D1+D2).EQ.0.0.OR.(D1+D3).EQ.0.0) WRITE(6,*) 'Z:a'
             TD1=2.0*(D1*D2)/(D1+D2)
             TD2=2.0*(D1*D3)/(D1+D3)
            IF ((DX**2+DY1**2).EQ.0.0) THEN
               DX=1.0E-10
               WRITE(6,*) 'CORRECTION AT: A'
            ENDIF
            W(I,J,1)=(TD1)/((DX**2+DY1**2)**.25)
            IF ((DX1**2+DY**2).EQ.0.0) THEN
               DY=1.0E-10
               WRITE(6,*) 'CORRECTION AT: B'
            ENDIF
            W(I,J,2)=(TD2)/((DX1**2+DY**2)**.25)
C
C If sediment needs moving must calculate fluxes..
C
             IF (FLAG.EQ.1) THEN
              Q(I,J,1)=-DX*W(I,J,1)
              Q(I,J,2)=-DY*W(I,J,2)
             ENDIF
1         CONTINUE
C
C  .. and call routine.
C
          IF (FLAG.EQ.1) CALL SMOVE(Q,H,D)
         CALL UPDATE(H,D,W,XSIZE,YSIZE)
        END
C
C*********************************************************************
C NEIGHB  rteturns indices for neighbours of        ----->I
C  i,j with slope orrection if any                 !    n
C                                                  !  m   k
C                                               J(=y)!    l
       SUBROUTINE NEIGHB(I,J,K,L,M,N,M1,M2)
       REAL ALPH,BETA,D0,THET,M1,M2,EPS
       INTEGER I,J,K,L,M,N,XSIZE,YSIZE
       COMMON/PARAM/ ALPH,BETA,D0,THET,EPS,XSIZE,YSIZE
       M1=0.0
       M2=0.0
        K=I+1
        IF (K.GT.XSIZE) THEN
           K=1
           M1=THET*REAL(XSIZE)*1.0
        ENDIF
        L=J+1
        IF (L.GT.YSIZE) L=1
        M=I-1
        IF (M.EQ.0) THEN
          M=XSIZE
          M2=-THET*REAL(XSIZE)*1.0
        ENDIF
        N=J-1
        IF (N.EQ.0) N=YSIZE
      END
C
C*********************************************************************
C FETCH returns 4 nearest neighbours in form !------> x (=I)
C  corrected for slope (if FL                ! 1
C  =1.0)                                     ! 234
```

```
C                                        Y(=J)!  5
C
      SUBROUTINE FETCH(A,AN,I,J,FL)
      REAL A(200,200),AN(10),M1,M2,FL
      INTEGER I,J,K,L,M,N
         CALL NEIGHB (I,J,K,L,M,N,M1,M2)
         AN(1)=A(I,N)
         AN(2)=A(M,J) + M2*FL
         AN(3)=A(I,J)
         AN(4)=A(K,J) + M1*FL
         AN(5)=A(I,L)
       END
C
C*********************************************************************
C UPDATE
C
      SUBROUTINE UPDATE(H,D,Q,XSIZE,YSIZE)
      REAL Q(200,200,2),H(200,200),D1(200,200),D(200,200),M1,M2
      INTEGER I,J,K,L,M,N,XSIZE,YSIZE
       DO 1 I=1,XSIZE
        DO 1 J=1,YSIZE
         CALL NEIGHB(I,J,K,L,M,N,M1,M2)
         D1(I,J)= .5*D(I,J)+.5*(((D(K,J)+H(K,J)+M1)*Q(I,J,1)
     .              +(D(M,J)+H(M,J)+M2)*Q(M,J,1)
     .              +(D(I,L)+H(I,L))*Q(I,J,2)
     .              +(D(I,N)+H(I,N))*Q(I,N,2))/(Q(I,J,1)
     .              +Q(I,J,2)+Q(M,J,1)+Q(I,N,2))-H(I,J))
1      CONTINUE
       DO 2 I=1,XSIZE
         DO 2 J=1,YSIZE
          IF (D1(I,J).GT.0.0) THEN
            D(I,J)=D1(I,J)
           ELSE
            D(I,J)=1.0E-8
          ENDIF
2       CONTINUE
      END
C
C*********************************************************************
C SUBROUTINE SMOVE updates the sediment grid by one timestep
C
      SUBROUTINE SMOVE(Q,H,D)
      REAL Q(200,200,2),H(200,200),D(200,200),C(200,200),DSED(200,200)
      REAL ALPH,BETA,D0,THETA,M1,M2,DT,EPS,DF(4),T,DL,DS,DTM
      INTEGER I,J,K,L,M,N,XSIZE,YSIZE
      COMMON /PARAM/ ALPH,BETA,D0,THETA,EPS,XSIZE,YSIZE
      COMMON /TIME/ T,DL,DT,DTM
       T=T+DT
C
C Calculate C values
C
        DO 1 I=1,XSIZE
          DO 1 J=1,YSIZE
             C(I,J)=(Q(I,J,1)**2+Q(I,J,2)**2)**(ALPH/2.0)
     .            *D(I,J)**BETA
1       CONTINUE
C
C Now update
C
        DO 2 I=1,XSIZE
          DO 2 J=1,YSIZE
            CALL NEIGHB (I,J,K,L,M,N,M1,M2)
```

```
C
C To perform non-conservation of sediment correctly, need to know whcih
C  bonds are flowing into the link, and which out. Get this from Fluxes
C
            DF(1)=1.0
            DF(2)=1.0
            DF(3)=1.0
            DF(4)=1.0
             IF (Q(M,J,1).GT.0.0) DF(4)=1.0+EPS
             IF (Q(I,N,2).GT.0.0) DF(3)=1.0+EPS
             IF (Q(I,J,1).LT.0.0) DF(2)=1.0+EPS
             IF (Q(I,J,2).LT.0.0) DF(1)=1.0+EPS
            DSED(I,J)= (DF(4)*Q(M,J,1)*(C(M,J)+C(I,J))+
     .             DF(3)*Q(I,N,2)*(C(I,N)+C(I,J))-
     .             DF(2)*Q(I,J,1)*(C(I,J)+C(K,J))-
     .             DF(1)*Q(I,J,2)*(C(I,J)+C(I,L)))*DT/2.0
         DS=DSED(I,J)/8.0
          H(I,J)=H(I,J)+DSED(I,J)
C         H(M,J)=H(M,J)+DS
C         H(I,N)=H(I,N)+DS
C         H(K,J)=H(K,J)+DS
C         H(I,L)=H(I,L)+DS
         DL=DL+ABS(DSED(I,J))
2       CONTINUE
       END
C
C*************************************************************************
C**** I/O, POST-PROCESSING & STUFF ***************************
C*************************************************************************
C**** Section %3
C*************************************************************************
C*************************************************************************
C PARS opens main input to the parameters file, reads the parameters,
C and closes the device.
C
       SUBROUTINE PARS(ALPH,BETA,D0,THETA,EPS,XSIZE,YSIZE,DMX,N)
       REAL ALPH,BETA,D0,THETA,RPAR(10),EPS,DMX
       INTEGER XSIZE,YSIZE,I,N
        OPEN(7,FILE='/tmp/GNB10.SIMPAR',STATUS='OLD')
        READ(7,*) XSIZE,YSIZE
        I=0
1        READ(7,*,END=99) RPAR(I+1)
         I=I+1
        GOTO 1
99      CLOSE(7)
C
C Continue only if the parameter file was correctly configured
C
        CLOSE (7)
        IF(I.NE.N) THEN
          WRITE(9,*) '***PARAMETER READ FAILURE'
          CLOSE(9)
          STOP
         ELSE
          WRITE(9,*) 'PARAMETERS READ'
          ALPH=RPAR(1)
          BETA=RPAR(2)
          D0  =RPAR(3)
          THETA=RPAR(4)
          EPS=RPAR(5)
          DMX=RPAR(6)
         ENDIF
```

```
        END
C
C*********************************************************************
C*********************************************************************
C LOAD attempts to read the arrays from main input. If the required number
C are read, these are returned. If only one value is read, a new set of
C values is created. All other cases are errors.
C
        SUBROUTINE LOAD(H,D,XSIZE,YSIZE)
        REAL H(200,200),D(200,200)
        INTEGER I,J,N,XSIZE,YSIZE
        LOGICAL NEW
        COMMON /CH/ NEW
        OPEN (7,FILE='/tmp/INPUT.DAT',STATUS='OLD')
         N=0
         DO 1 I=1,XSIZE
          DO 1 J=1,YSIZE
            READ(7,*,END=99) H(I,J)
1           N=N+1
         DO 2 I=1,XSIZE
          DO 2 J=1,YSIZE
            READ(7,*,END=99) D(I,J)
2           N=N+1
99       WRITE(9,*) N,' VALUES READ'
         CLOSE(7)
         IF (N.EQ.2*XSIZE*YSIZE) THEN
           WRITE(9,*) 'DATA READ'
           NEW=.FALSE.
           RETURN
          ELSE
            IF(N.EQ.1) THEN
              CALL CRTE(H,D)
              NEW=.TRUE.
              RETURN
             ELSE
              WRITE(9,*) '***DATA READ FAILURE'
              STOP
            ENDIF
         ENDIF
        END
C
C*********************************************************************
C CREATE and associated subroutines set up initial values
C
        SUBROUTINE CRTE(H,D)
        REAL H(200,200),D(200,200),ALPH,BETA,D0,THET,EPS
        INTEGER XSIZE,YSIZE
        COMMON/PARAM/ALPH,BETA,D0,THET,EPS,XSIZE,YSIZE
          CALL SETUP(H,0.0,THET,XSIZE,YSIZE)
          CALL SETUP(D,D0,0.0,XSIZE,YSIZE)
          CALL PERTUR(H,XSIZE,YSIZE)
          WRITE(9,*) 'NEW VALUES CREATED'
        END
C.....................................................................
        SUBROUTINE SETUP(A,C,M,XSIZE,YSIZE)
        REAL A(200,200),C,M
        INTEGER I,J,XSIZE,YSIZE
          DO 1 I=1,XSIZE
            DO 1 J=1,YSIZE
1           A(I,J)=REAL(I)*M+C
        END
C.....................................................................
```

```
      SUBROUTINE PERTUR(T,XSIZE,YSIZE)
        REAL T(200,200),Q
        INTEGER I,J,XSIZE,YSIZE,SEED
        SEED=145321
          DO 1 I=1,XSIZE
           DO 1 J=1,YSIZE
           Q=RAN(SEED)/1.0E4
1          T(I,J)=T(I,J)+Q
       END
C
C      SUBROUTINE PERTUR(A,SIZE)
C       REAL A(200,200)
C       INTEGER I,J,SIZE
C         DO 1 I=1,SIZE
C           DO 1 J=1,SIZE
C1     A(I,J)=A(I,J)+.0001*SIN(3.141593*REAL(I)
C     .                       +3.141593*REAL(J))
C       END
C
C
C*********************************************************************
C*********************************************************************
C Save writes the result of the current run to a permanent file
C
       SUBROUTINE SAVE(H,D,XSIZE,YSIZE)
       REAL H(200,200),D(200,200)
       INTEGER I,J,XSIZE,YSIZE
       OPEN (8,FILE='/tmp/INPUT.DAT',STATUS='OLD')
        DO 1 I=1,XSIZE
          DO 1 J=1,YSIZE
1           WRITE(8,*) H(I,J)
        DO 2 I=1,XSIZE
          DO 2 J=1,YSIZE
2           WRITE(8,*) D(I,J)
         WRITE(9,*) 'OUTPUT COMPLETE'
          CLOSE(8)
       END
C
C*********************************************************************
C PLOT produces a surface plot of a 2-D square array from 1 to SIZE
C
C*********************************************************************
C REFIL replaces missing water uniformly over grid
C
      SUBROUTINE  REFIL(A,T1,T2,XSIZE,YSIZE)
      REAL A(200,200),T1,T2,DA
      INTEGER I,J,XSIZE,YSIZE
       DA=(T1-T2)/(REAL(XSIZE)*REAL(YSIZE))
       DO 1 I=1,XSIZE
        DO 1 J=1,YSIZE
        IF((A(I,J)+DA).GT.0.0) A(I,J)=A(I,J)+DA
1      CONTINUE
      END
C:::::::::::::::::::::::::::::::::::::::::::::::::::::::::::::::::::::::::
C TOTAL integrates over an XSIZE*YSIZE array
C
      FUNCTION TOTAL(A,XSIZE,YSIZE)
      REAL TOTAL,A(200,200)
      INTEGER I,J,XSIZE,YSIZE
       TOTAL=0
       DO 1 I=1,XSIZE
        DO 1 J=1,YSIZE
```

```
1         TOTAL=TOTAL+A(I,J)
        END
C:::::::::::::::::::::::::::::::::::::::::::::::::::::::::::::::::::::::::::::::
C
C
        FUNCTION AMP(A,XSIZE,YSIZE)
        REAL A(200,200),AMP,MX,MN,ALPH,BETA,D0,THETA,H,EPS
        INTEGER I,J,XSIZE,YSIZE
        COMMON /PARAM/ALPH,BETA,D0,THETA,EPS
        MX=0.0
        MN=0.0
         DO 1 I=1,XSIZE
           DO 1 J=1,YSIZE
             H=A(I,J)-REAL(I)*THETA
              IF (H.GT.MX) MX=H
              IF (H.LT.MN) MN=H
1        CONTINUE
         AMP=(MX-MN)/2.0
        END
        SUBROUTINE PCHECK(SUB,A,B,D,T,SX,SY)
        REAL A,B,D,T
        INTEGER SX,SY
        CHARACTER*7 SUB
          WRITE(9,*) 'Parameter Values at ',SUB,':'
          WRITE (9,*) 'Alpha',A,' Beta',B,' D0',D,' Theta',T,'X Size',SX
     .              ,'Y Size',SY
        END
        SUBROUTINE DELTAS(H,XSIZE,YSIZE)
        REAL H(200,200),DEL,T,T1,DL,DT,DTM,DMX
        INTEGER XSIZE,YSIZE
        COMMON/TIME/T,DL,DT,DTM,DMX
         OPEN(UNIT=7,FILE='/tmp/GNB10.DELTAS',STATUS='OLD')
9         READ(7,*,END=10) T1,DEL
         GOTO 9
10         T=T+T1
          WRITE (7,*) T,DL
          CLOSE(7)
          IF (DL.LT.DEL.AND.DT.LT.DMX) THEN
           OPEN (UNIT=7,FILE='/tmp/GNB10.DT',STATUS='OLD')
           DT=DT*DEL/DL
           IF(DT.GT.DMX) DT=DMX
           IF(DL.GT.DTM) DTM=DL
           WRITE(7,*) DT,DTM
           CLOSE(7)
          ENDIF
         END
```

Appendix C: Comments of the Lattice Version of the Stability Analysis

In trying to apply the results of Chapter 3 to simulation work, there is an implicit assumption that the lattice spacings Δx and Δy are sufficiently small for the 1st order approximations

$$\sin(k_x\Delta x)/\Delta x \approx k_x$$
$$\cos(k_x\Delta x) \approx 1 \quad \text{(and similarly for y) to be useable.}$$

If this assumption is not made, the following results are obtained:

$$A = \frac{\Delta x^{-2}(\cos(k_x\Delta x)-1) + 2\Delta y^{-2}(\cos(k_y\Delta y)-1)}{\Delta x^{-2}(\cos(k_x\Delta x)-1) + 2\Delta y^{-2}(\cos(k_y\Delta y)-1) + 3/2id_0\theta\Delta x^{-1}\sin(k_x\Delta x)}$$

which can be shown to be correct by taking the relevant limit (indeed on could in principle guess this form correctly by noting which terms would be needed to provide the relevant limit).

Similarly,

$$p = d_0^{\alpha+\beta+1/2}\theta^{\beta+1/2}\,[\,-\{(\alpha-2\beta)(e^{ikx\Delta x}-1) + 3/2\beta(e^{2ikx\Delta x}-1)\}\,\Delta x^{-1} + 2\Delta y^{-2}(\cos(k_y\Delta y)-1)$$
$$-\beta(e^{ikx\Delta x}-1)^2\Delta x^{-2}(3/2i\Delta x^{-1}\sin(k_x\Delta x))]/$$
$$[\Delta x^{-2}(\cos(k_x\Delta x)-1) + 2\Delta y^{-2}(\cos(k_y\Delta y)-1) + 3/2id_0\theta\Delta x^{-1}\sin(k_x\Delta x)]$$

$$+$$

$$d_0^{\alpha+\beta+1/2}\theta^{\beta+1/2}\varepsilon'\,[\{\alpha-2\beta) + (3/2\beta+3/4)(e^{ikx\Delta x}+1)\}(\Delta x^{-2}(\cos(k_x\Delta x)-1)$$
$$+2\Delta y^{2}(\cos(k_y\Delta y)-1)) - (1/2+\beta)(e^{ikx\Delta x}-1)\Delta x^{-1}(3/2i\Delta x^{-1}\sin(k_x\Delta x))]/$$
$$[\Delta x^{-2}(\cos(k_x\Delta x)-1) + 2\Delta y^{-2}(\cos(k_y\Delta y)-1) + 3/2id_0\theta\Delta x^{-1}\sin(k_x\Delta x)]$$

, which is the form used in chapter 8.